RESEARCH ARTICLE

A Bayesian approach to dynamic homology of morphological characters and the ancestral phenotype of jawed vertebrates

Benedict King*, Martin Rücklin

Naturalis Biodiversity Center, Leiden, Netherlands

Abstract Phylogenetic analysis of morphological data proceeds from a fixed set of primary homology statements, the character-by-taxon matrix. However, there are cases where multiple conflicting homology statements can be justified from comparative anatomy. The upper jaw bones of placoderms have traditionally been considered homologous to the palatal vomer-dermopalatine series of osteichthyans. The discovery of 'maxillate' placoderms led to the alternative hypothesis that 'core' placoderm jaw bones are premaxillae and maxillae lacking external (facial) laminae. We introduce a BEAST2 package for simultaneous inference of homology and phylogeny, and find strong evidence for the latter hypothesis. Phenetic analysis of reconstructed ancestors suggests that maxillate placoderms are the most plesiomorphic known gnathostomes, and the shared cranial architecture of arthrodire placoderms, maxillate placoderms and osteichthyans is inherited. We suggest that the gnathostome ancestor possessed maxillae and premaxillae with facial and palatal laminae, and that these bones underwent divergent evolutionary trajectories in placoderms and osteichthyans.

***For correspondence:** benking315@gmail.com

Competing interests: The authors declare that no competing interests exist.

Funding: See page 13

Received: 22 August 2020
Accepted: 03 December 2020
Published: 04 December 2020

Reviewing editor: Min Zhu, Chinese Academy of Sciences, China

Introduction

The concept of homology underpins the cladistic analysis of morphological data. Testing of homology is usually considered a two-step process (***Patterson, 1982a***; ***Pinna, 1991***). First, provisional statements of homology are made (primary homology), which are hypotheses based on comparative anatomy. Primary homologues are then subjected to cladistic analysis, and those that correspond to synapomorphies are then considered 'secondary homologues'; this term corresponds to the vernacular use of the term homology (similarity due to common ancestry). The starting point for a cladistic analysis, the character-by-taxon matrix, is a set of primary homology statements. Primary homology statements are based upon 'homology criteria' (***Patterson, 1988***; ***Rutishauser and Moline, 2005***). The first and most important criterion for primary homology is similarity: structures should correspond in position and structural details (developmental similarity is part of this criterion). Second is the test of conjunction: if two structures are found together on a single animal, they cannot be homologous (***Patterson, 1988***).

Placoderms are stem gnathostomes, and the evolution and morphology of their jaws is thus of particular interest. The upper jaw bones of placoderms present a major unresolved example of a homology problem. Arthrodiran placoderms possess two upper gnathal plates in their jaws, termed the anterior and posterior supragnathals (***Figure 1A***). These have traditionally been considered primary homologues of the vomers and dermopalatines of osteichthyans (***Stensiö, 1963a***; ***Stensiö, 1969***), which are palatal bones sitting on the roof of the mouth, inside the maxilla and premaxilla (***Figure 1C***). This proposed homology of placoderm supragnathals and osteichthyan palatal bones is based on positional criteria.

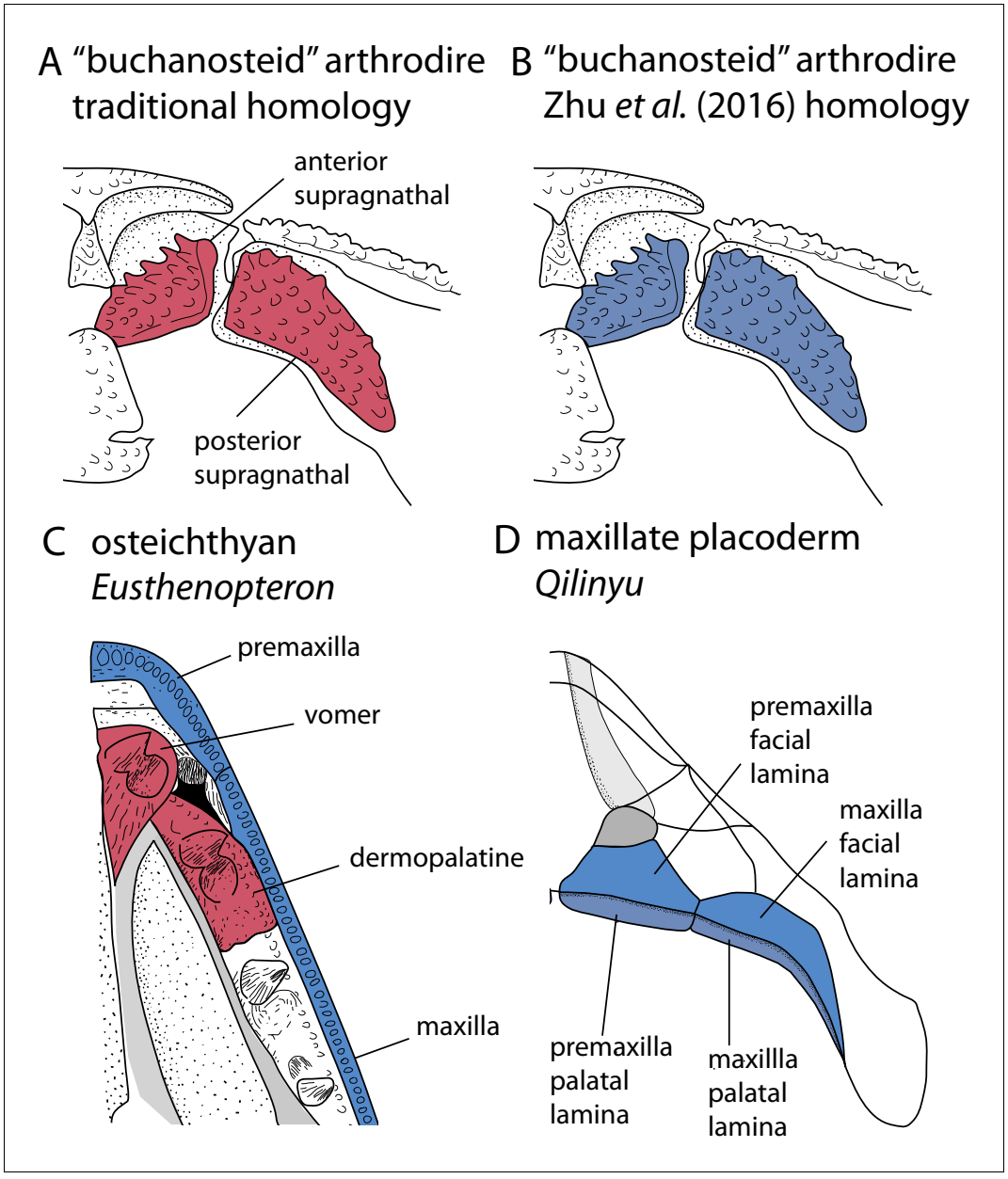

Figure 1. Upper jaw bones in arthrodire placoderms, maxillate placoderms and osteichthyans, showing alternative homology assignments for the arthrodiran supragnathals. (**A–B**) Arthrodire in palatal view, showing anterior and posterior supragnathals. Based on ***Hu et al., 2017***. (**C**) Osteichthyan *Eusthenopteron* in palatal view, based on ***Jarvik, 1980***. (**D**) Maxillate placoderm *Qilinyu* in palatal view, based on ***Zhu et al., 2016***. Blue coloration indicates the premaxilla-maxilla series, red coloration indicates the vomer-dermopalatine series. The alternative coloration of arthrodire supragnathals in A and B represents the alternative homology statements for these bones (homology states 0 and 1 respectively).

The discovery of maxillate placoderms reignited debates about the homology of placoderm and osteichthyan skull bones (***Zhu et al., 2013***; ***Zhu et al., 2016***), and a new hypothesis regarding the homology of arthrodiran gnathal plates was proposed (***Zhu et al., 2016***; ***Zhu et al., 2019***). Maxillate placoderms have premaxillae and maxillae with both palatal and facial laminae (***Figure 1D***). The palatal laminae articulate with the ventral surface of the braincase, and therefore correspond in position to arthrodiran supragnathals. The facial laminae are continuous with the external dermal bones of the skull, and are equivalent in position to osteichthyan premaxillae/maxillae. ***Zhu et al., 2016*** therefore proposed the homology of arthrodiran supragnathals with the premaxilla and maxilla of

osteichthyans. This negates a putative homology with the osteichthyan vomer-dermopalatine series, which would otherwise fail the test of conjunction (placoderm supragnathals cannot be homologous to both the premaxilla-maxilla and vomer-dermoplatine series). Nevertheless, the traditional hypothesis for the homology of arthrodiran supragnathals continues to be discussed in the literature (**Hu et al., 2017**). There are therefore two opposing possibilities for the primary homology of arthrodiran gnathal bones.

A number of approaches have been proposed to distinguish between conflicting hypotheses of primary homology. **Jardine, 1969** provided a method that selected between alternative homologies of rhipidistian skull roof bones without reference to phylogeny, based on the criterion of preservation of spatial relationship. **Lee, 1998** used parsimony to distinguish between conflicting conjectures of homology on a fixed tree topology. The latter was essentially the approach taken by **Zhu et al., 2016** to support their hypothesis regarding placoderm supragnathal bones. However, choices regarding primary homology statements necessarily restrict the search for secondary homologues: phylogenetic analyses can only find the optimal tree given the input character matrix. Indeed, it has been suggested that the two-step approach to homology entails a degree of circularity (**Rieppel, 1996**), although this is likely to only be an issue when a phylogeny is weakly supported. A solution to this issue is the simultaneous inference of primary and secondary homology, termed *dynamic homology*.

Dynamic homology of molecular sequence data in a parsimony framework has been implemented in the software POY (**Wheeler et al., 2006**; **Varón et al., 2010**). Models for dynamic homology of molecular data have also been developed (**Lunter et al., 2005**; **Redelings and Suchard, 2005**; **Wheeler, 2006**) and implemented within the phylogenetic software Bali-Phy (**Suchard and Redelings, 2006**) and POY 5.0 (**Wheeler et al., 2015**). **Agolin and D'Haese, 2009**, used the parsimony implementation in POY to analyze morphological data (specifically the setae of collembolans). However, morphological characters, with their hierarchical dependence relationships and arbitrary sequence within a data matrix, are often not amenable to models used to align molecular data. **Ramírez, 2007** presented a parsimony approach to dynamic homology, using the empirical example of sclerites on the male copulatory organs of anyphaenid spiders. In this method, multiple matrices with alternative alignments of morphological characters were analysed, and the phylogenetic tree and homology combination with the shortest tree length was selected.

Dynamic homology methods for morphological data have thus far been rarely explored, and are restricted to parsimony-based approaches. However, a Bayesian approach would confer a number of advantages. Alternative homology statements could be considered as 'nuisance parameters', such that phylogenetic trees could be estimated while accounting for uncertainty in primary homology statements. Conversely, if discovering homology is the aim, the tree topology could be considered the 'nuisance parameter'. Bayesian tip-dated analysis of morphological data allows comparative analysis (such as biogeography or ancestral state reconstruction) to occur simultaneously with tree search (e.g. **Lee et al., 2018**). Comparative analyses could therefore be performed while accounting for uncertainty in both tree topology and primary homology statements.

Here, we present an approach to dynamic homology within a Bayesian tip-dating framework, which we use to test the alternative conjectures of placoderm jaw bone homologies. The homology relations of placoderm jaw bones have implications for our understanding of character evolution in early vertebrates. In particular, homology of placoderm supragnathal bones with the marginal jaw bones of osteichthyans suggests a deep (early) origin for these bones. **Zhu et al., 2016** proposed their hypothesis within the framework of placoderm paraphyly (**Brazeau, 2009**; **Davis et al., 2012**; **Zhu et al., 2013**), but an alternative hypothesis of placoderm monophyly (excluding maxillate placoderms) is supported by an essentially equivalent amount of morphological data, and is strongly supported under Bayesian tip-dated methods (**King et al., 2017**). The implications of the hypothesis of **Zhu et al., 2016** within the framework of placoderm monophyly have not been discussed. We therefore simultaneously estimated a credible set of phenotypes for the (apomorphy-defined) gnathostome common ancestor to explore character evolution in early gnathostomes while accounting for phylogenetic uncertainty, divergence date uncertainty, and alternative placoderm jaw bone homologies.

Dynamic homology

We implemented a method for dynamic homology of morphological characters within the open source BEAST2 software package *homology* (https://github.com/king-ben/homology; ***King, 2021***; copy archived at swh:1:rev:6e6dbd77443b0d963640b3cb603c4310b5a4b47e). The method takes as inputs alternative character coding alignments, here called *homology alignments*, which are alternative character codings corresponding to alternative homology hypotheses for morphological features (for example placoderm jaw bones). Homology alignments can be included alongside fixed alignments (***Figure 2***), such that only a subset of characters has dynamic homology. During a BEAST2 MCMC run, the homology alignment used to calculate the posterior is determined by a homology state parameter, which is changed by an operator (***Figure 2***). The MCMC will spend more time in the homology state corresponding to the homology alignment that returns the highest tree likelihood.

The *homology* package contains two java classes corresponding to CalculationNodes (which calculate a part of the posterior based on inputs). These are *HomologyTreeLikelihood* and *HomologyMultiplexer* (***Figure 3***). The *HomologyTreeLikelihood* class is an extension of the core BEAST2 *TreeLikelihood* class, and differs in associating a particular homology alignment with a homology state. The *HomologyMultiplexer* takes as input two or more HomologyTreeLikelihoods and a *homology parameter*, the latter is an integer parameter with states (0, 1,. . .,N) corresponding to N homology states (one for each HomologyTreeLikelihood). During an MCMC run, the homology-multiplexer returns the value of the homology tree likelihood corresponding to the current state of the homology parameter. Due to the possibility of correlated tree- and homology-space, the package also contains two updated tree operators which simultaneously change the tree topology and homology state: *HomologySAWilsonBalding* and *HomologySAExchange*.

Results

Homoplasy-partitioned Bayesian tip-dated analysis (with dynamic homology of placoderm upper jaw bones) of the gnathostome fossil dataset results in the majority-rule consensus tree shown in ***Figure 4***. Core placoderms (placoderms excluding maxillate forms) are monophyletic (posterior probability, pp = 1.0). The maxillate placoderms *Entelognathus* and *Qilinyu* are resolved as the sister group to core placoderms, but with weak support (pp = 0.70). *Janusiscus* is resolved as a stem osteichthyan, sister to *Dialipina*, but support for this grouping is again weak (pp = 0.57).

We find strong support for homology state 1 (pp = 0.984), corresponding to the hypothesis that placoderm supragnathal bones are homologous to premaxillae and maxillae (***Zhu et al., 2016***). The mean log likelihood for homology alignment 0 is −85.099, and for homology alignment 1 –79.883. The MCMC chain therefore rarely accepts proposals for homology state 0 (***Figure 5***).

Principal coordinates (PCO) analysis of gnathostome fossils reveals chondrichthyans (including acanthodians), osteichthyans and core placoderms form three discrete and well-separated groups (***Figure 6A***), concordant with the results of ***Davis et al., 2012***. *Janusiscus* is an outlier, lying equidistant from the three groups, whereas maxillate placoderms plot close to core placoderms.

We used ancestral sequence logging in BEAST2 to reconstruct the phenotype of the gnathostome ancestor in each sample from the posterior. A sample of 90 of these reconstructed ancestors included in the PCO mostly plot close to placoderms, with a small number plotting in outlier positions closer to *Janusiscus*. A second PCO using only placoderms (maxillate and core) and the reconstructed ancestors is shown in ***Figure 6B***, with the point cloud of reconstructed ancestors converted to a 2D density plot. *Entelognathus* plots close to the center of the ancestral area, while *Qilinyu*, arthrodires, petalichthyids and acanthothoracids are equidistant. Antiarchs and ptyctodontids plot the furthest from the reconstructed ancestors. However, it should be noted that the two principal axes account for less than 10% of the total variance.

Plotting the raw distance measures shows that maxillate placoderms are the most similar taxa to the reconstructed ancestors (***Figure 6C***). The individual taxon with the lowest distance to the reconstructed ancestor (in each sample from the posterior, n = 1801) was a maxillate placoderm for 95% of the reconstructed ancestors (***Figure 6D***). This suggests that of the known gnathostome fossils, the maxillate placoderms (in particular *Entelognathus*) are the least divergent known descendants of the gnathostome common ancestor.

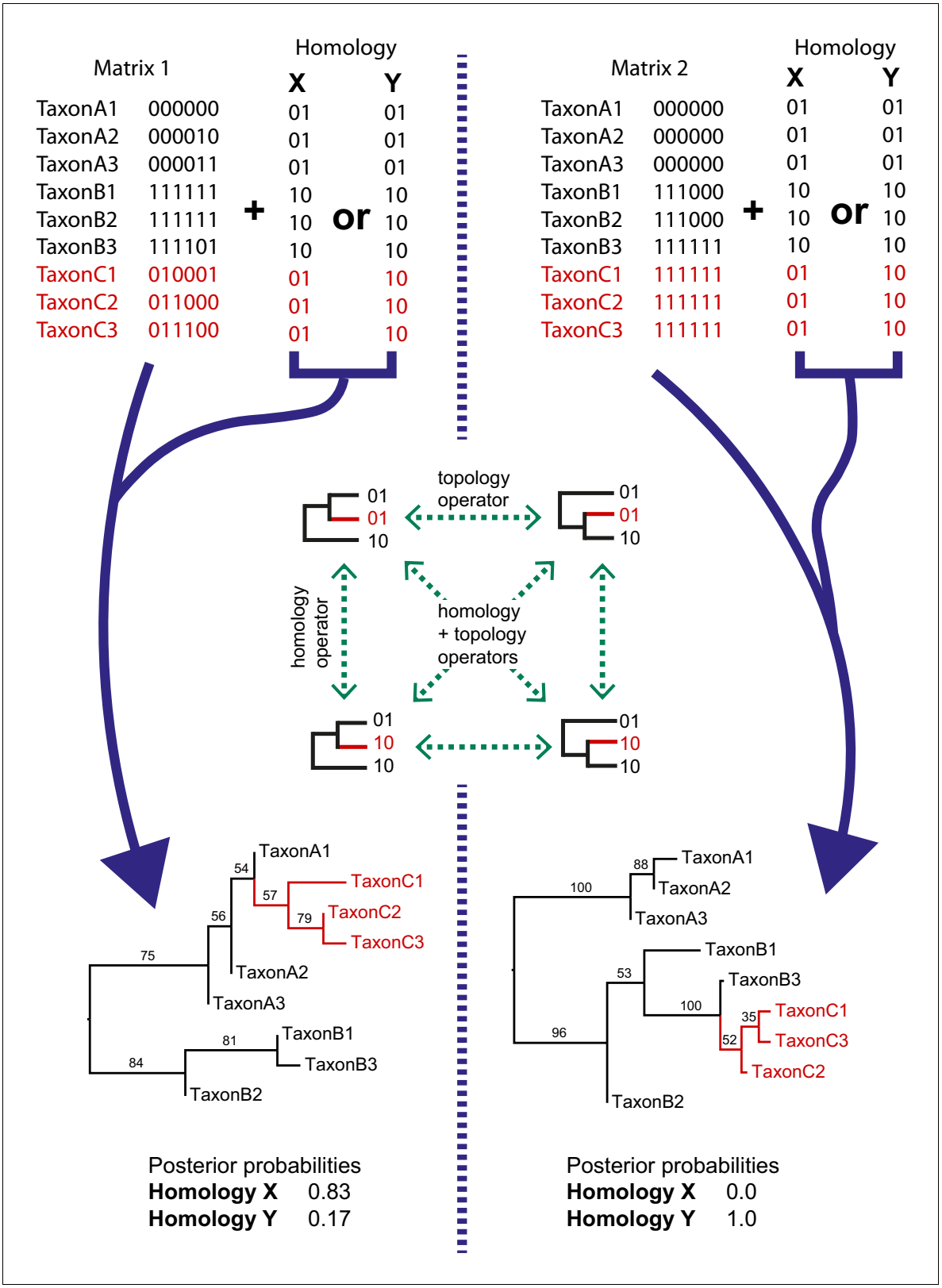

Figure 2. Simple examples of dynamic homology applied to matrices with six characters with fixed homology and two with estimated homology. Taxa C1–3 have alternative homologies (homology X and Y). For matrix1, there is moderate support for group C to fall within group A, leading to a higher posterior probability for homology X than homology Y. In matrix 2, there is strong support for taxon group C to fall within group B, leading in turn to strong support for homology Y.

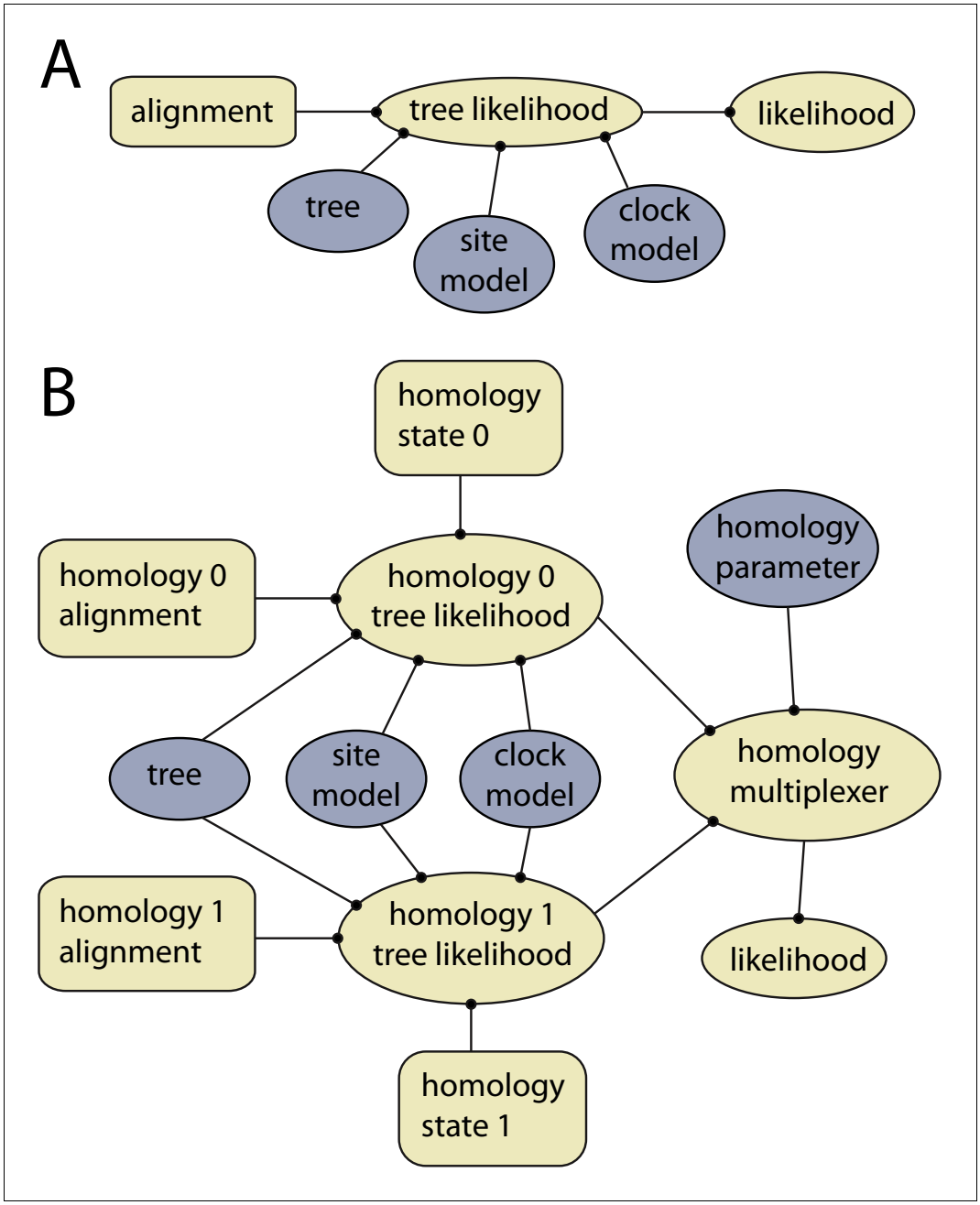

Figure 3. Example of models with and without dynamic homology of morphological characters. (**A**) Model diagram of a fixed homology partition. Tree likelihood takes as input a data alignment, tree, site model and clock model, and the calculated tree likelihood is passed to the likelihood, where it is combined with other partitions. Rectangles indicate fixed inputs, whereas ovals are model components that change during the MCMC. Blue shaded components are changed by operators, either directly (tree) or indirectly (site model, clock model). (**B**) Model diagram for a partition with dynamic homology with two homology states. The homology-multiplexer passes either the value of homology tree likelihood 0 or homology tree likelihood 1 to the likelihood, depending on the current value of the homology parameter.

The reconstructed ancestors also allow us to calculate the posterior probability of particular character states at the gnathostome node (i.e. the proportion of reconstructed ancestors with a particular character state). ***Table 1*** displays a number of characters of interest, including characters of the upper jaw bones and characters possessed by some core placoderms, argued to be retained plesiomorphies under the hypothesis of placoderm paraphyly (***Brazeau, 2009***; ***Dupret et al., 2014***).

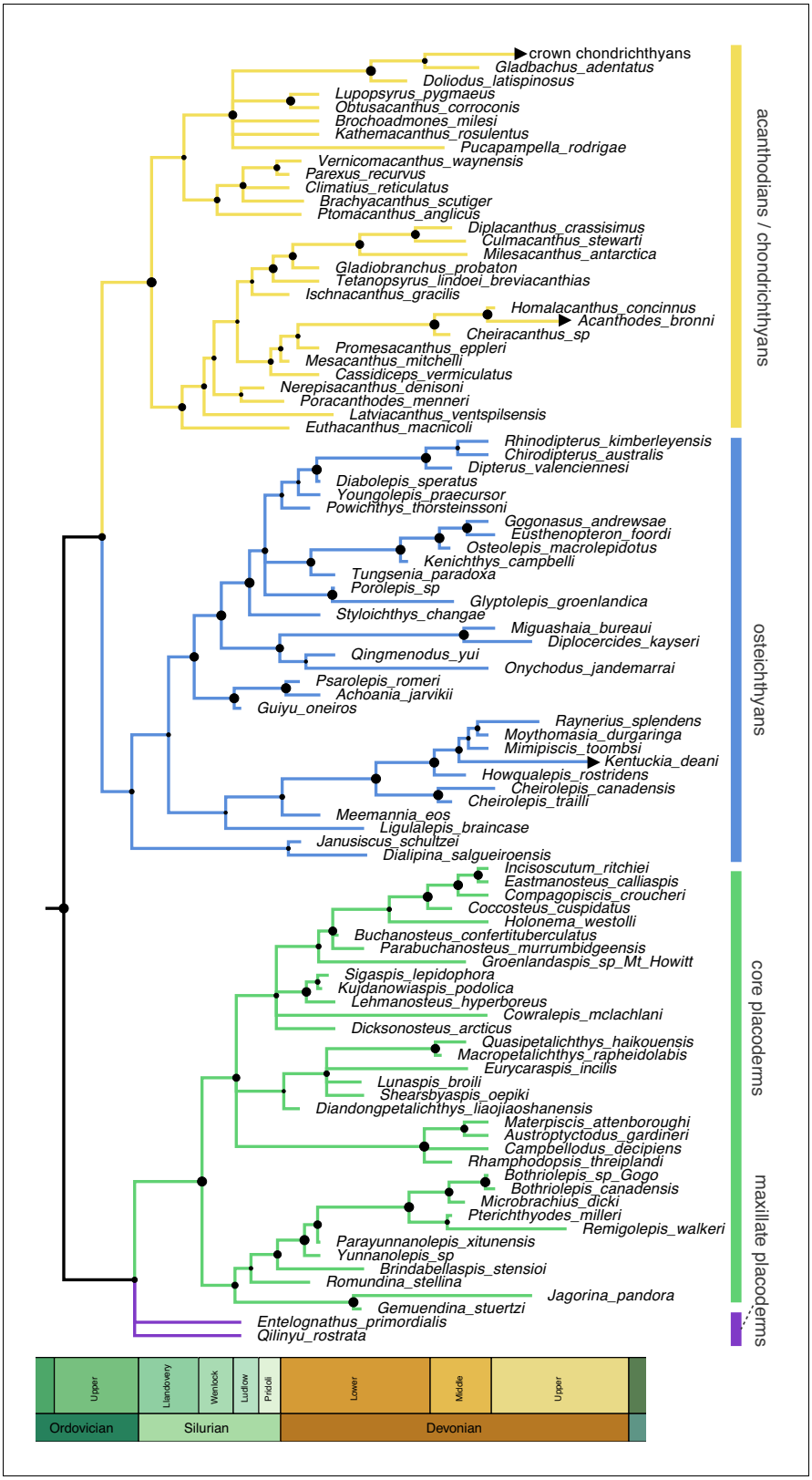

Figure 4. Time-scaled 50% majority-rule consensus tree from tip-dated homoplasy-partitioned analysis of gnathostome fossils, with dynamic homology of upper jaw bones in placoderms. Node circles indicate posterior probabilities. Branches with arrowheads (crown chondrichthyans, *Acanthodes*, *Kentuckia*) indicate tip age(s) are younger than the range displayed in the figure.

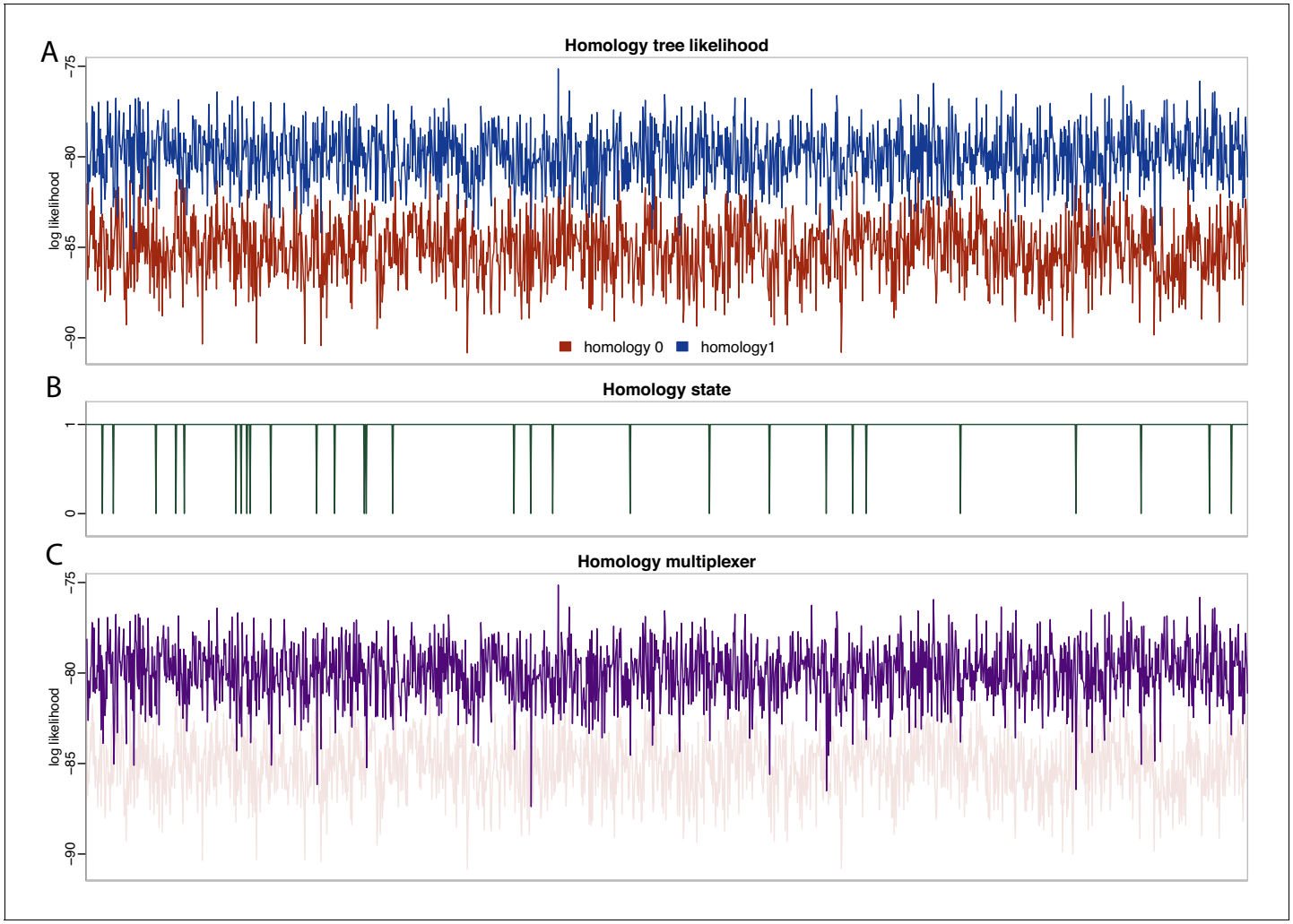

Figure 5. Likelihood and parameter traces during BEAST2 MCMC, with dynamic homology of placoderm jaw bones. (**A**) Tree likelihoods using homology alignment 0 (placoderm supragnathals are vomers/dermopalatines) are lower than those for homology alignment 1 (placoderm supragnathals are premaxillae/maxillae). (**B**) The MCMC only rarely samples homology state 0. (**C**) The homology-multiplexer therefore largely returns the tree likelihood of homology alignment 1 (homology tree likelihood 0 is replotted with transparency for reference).

Results for all characters are available in the supplementary information (***Table 1***; ***Source data 1***). Our results suggest that the gnathostome ancestor had a premaxilla and maxilla with both palatal and facial laminae, no vomer-dermopalatine series, anterior/ventral nasal capsules and lateral orbits not surrounded by neurocranium. Putative core placoderm synapomorphies (claspers, optic fissure) are reconstructed as absent at the gnathostome node with moderate support (***Table 1***). This uncertainty is likely due to the high proportion of missing data for these characters. Critically, it is unknown whether or not maxillate placoderms possessed these putative core placoderm synapomorphies.

Discussion

We find strong support for the hypothesis of ***Zhu et al., 2016***, that placoderm supragnathal bones are homologous to the maxilla and premaxilla of osteichthyans and maxillate placoderms (***Figure 5***). However, we present a distinct scenario regarding the trajectory of upper jaw bone evolution (***Figure 7***). ***Zhu et al., 2016*** proposed that the plesiomorphic states of the maxillae and premaxillae were as palatal bones, exemplified by the arthrodiran condition. Facial laminae were then gained in the common ancestor of maxillate placoderms and crown gnathostomes, and palatal laminae were

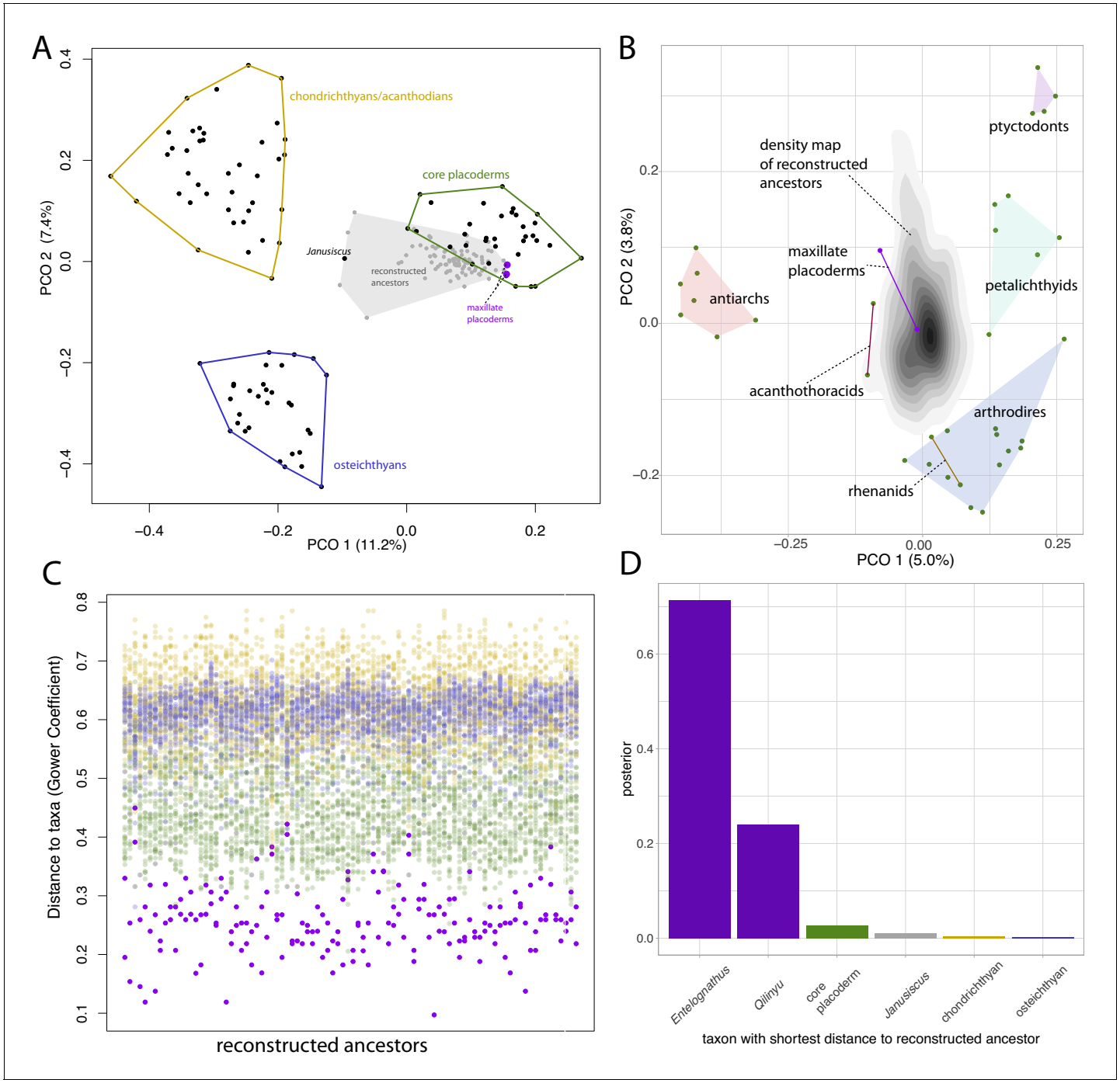

Figure 6. Distance plots suggest placoderms, and particularly maxillate placoderms are the gnathostomes least divergent from the gnathostome ancestor. (**A**) PCO plot of all gnathostome taxa in the matrix (black points) and a sample of 90 reconstructed ancestors (gray points and shaded convex hull). (**B**) PCO plot of placoderm taxa and reconstructed ancestors, with the latter point cloud converted to a density plot. (**C**) Each column represents a reconstructed ancestor (n = 90), with gnathostome fossils plotted with y-axis coordinates corresponding to distance from each reconstructed ancestor. (**D**) Frequency plot of the taxon with the shortest distance to the reconstructed ancestor across the whole posterior sample (n = 1801). Core placoderm, osteichthyan and chondrichthyan (including acanthodian) taxa are combined into single bins.

lost in osteichthyans. We instead propose that the common ancestor of (apomorphy-defined) gnathostomes possessed maxillae and premaxillae with both facial and palatal laminae. Facial laminae were subsequently lost in core placoderms and palatal laminae were lost in osteichthyans. The stem osteichthyans *Lophosteus* and *Andreolepis* show a possibly intermediate condition, in

Table 1. Character states reconstructed at the common ancestor of apomorphy-defined gnathostomes.

Character	Reconstructed ancestral state	Posterior probability
Premaxilla	Present	1.0
Maxilla	Present	0.96
Facial laminae	Present	0.96
Palatal laminae	Present	0.93
Vomer	Absent	0.93
Dermopalatine	Absent	0.95
Nasal capsules	Anterior/ventral	0.94
Orbit dorsal, surrounded by neurocranium	Absent	0.96
Claspers	Absent	0.79
Optic fissure	Absent	0.78

which the marginal jaw bones have internal (oral or palatal) laminae that are more strongly developed compared to other osteichthyans (***Botella et al., 2007***; ***Cunningham et al., 2012***; ***Chen et al., 2016***; ***Chen et al., 2020***).

In concordance with ***Zhu et al., 2016***, we find strong support for a lack of the vomer-dermopalatine series in the gnathostome ancestor. Our scenario suggests that arthrodires, for which morphological data of the jaws is best known (***Hu et al., 2017***), exhibit a specialized condition. Independent evidence for this hypothesis comes from recently described acanthothoracids (***Vaškaninová et al., 2020***), which exhibit marginal dentitions and jaw bones quite unlike those of arthrodires. In addition, the inner dental arcade of the stem osteichthyan *Lophosteus* consists of many 'tooth cushions' bearing no resemblance to arthrodire gnathal plates (***Chen et al., 2017***).

The divergent trajectories of the premaxilla and maxilla in osteichthyans and core placoderms may be associated with alternative ecological roles among their earliest members. Osteichthyans

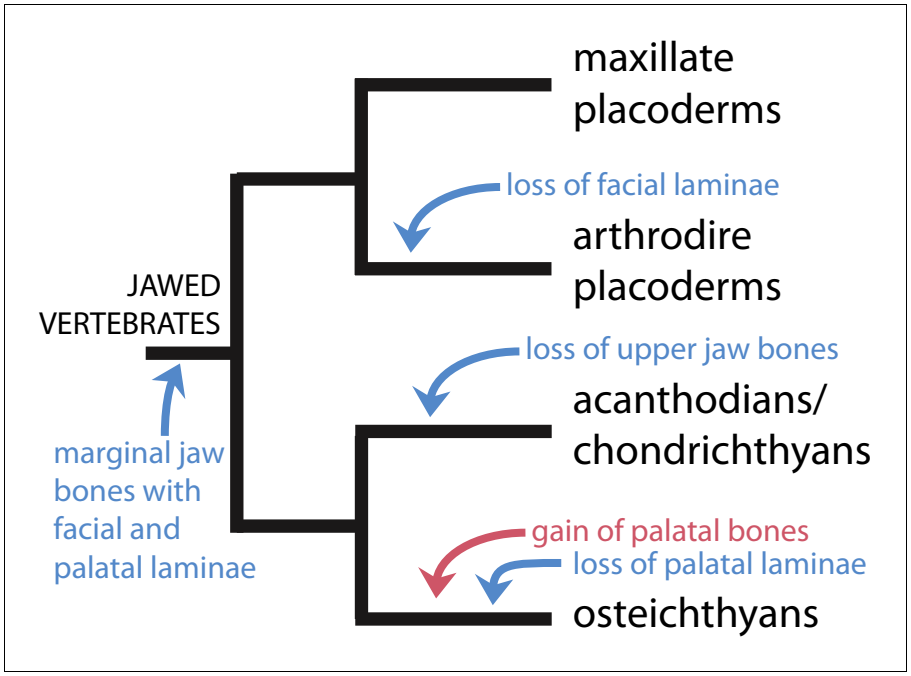

Figure 7. Scenario for the evolution of upper jaw bones in gnathostomes (jawed vertebrates). Red arrow indicates change to the palatal (vomer-dermopalatine) series of dermal jaw bones, blue arrows indicate changes to the marginal (premaxilla-maxilla) series.

from the Silurian Kuanti formation include the large *Megamastax* (**Choo et al., 2015**). The maxillate placoderms from the same formation however are clearly not apex predators, lacking large teeth on their jaw bones and in the case of *Entelognathus*, possess immovable eyes (**Zhu et al., 2013**). The loss of facial laminae in core placoderms may be associated with increased focus on crushing invertebrate prey, and may be analogous to the loss of the maxilla and specialization of the vomers in lungfishes. Conversely, the predatory osteichthyans emphasized the external tooth row and thus facial laminae.

Homology of the arthrodiran supragnathals with the premaxillae and maxillae of maxillate placoderms is consistent with observations from comparative anatomy (**Zhu et al., 2016**; **Zhu et al., 2019**). The snouts of maxillate placoderms differ from those of arthrodires mainly in the degree of dermal bone cover and are very similar in terms of their gross morphology. An early arthrodiran snout, such as that of *Kujdanowiaspis* (**Dupret, 2010**) differs from the maxillate placoderm condition by absence of facial laminae and a relatively small internasal plate compared to the large anterior premedian plate of *Entelognathus* (**Zhu et al., 2013**). **Zhu et al., 2019** suggested that the arthrodiran condition results from the inward shift of the upper jaw bones. However, the downturned, ventrally directed, snouts of maxillate placoderms means that reduction of the facial laminae and premedian plate are the only transformations required to leave the upper jaw bones separated from the dermal skull roof and in a palatal position, as in arthrodires.

The results of our phenetic analysis of reconstructed ancestors suggest maxillate-placoderm-like conditions in the last common ancestor of (apomorphy-defined) gnathostomes. Due to the nested position of acanthothoracids and antiarchs within a monophyletic core placoderms, we find strong support for anterior-ventral nasal capsules and lateral eyes in the gnathostome ancestor (**Table 1**). Under this hypothesis, the dorsal nasal capsules of antiarch, acanthothoracid and rhenanid placoderms are convergent with those of the jawless osteostracans and galeaspids, rather than representing shared plesiomophies (**King et al., 2017**). Conversely, the shared cranial architecture of arthrodires, maxillate placoderms and osteichthyans (**Dupret et al., 2014**), represent shared plesiomorphies (**Table 1**; **King et al., 2017**). Within agnathan fishes, the braincase proportions of the jawless heterostracans, which probably possess paired anterior nasal capsules (**Halstead, 1973**; **Janvier, 1996**), may represent the plesiomorphic gnathostome condition more closely than osteostracans or galeaspids.

Although our phenetic analysis suggests that maxillate placoderms are the gnathostomes morphologically closest to the ancestral condition, we are not suggesting that they are directly ancestral. The distance from each reconstructed ancestor is usually in the range 0.2–0.3, suggesting that even maxillate placoderms are highly derived from the gnathostome common ancestor. This result is not surprising given that our analysis suggests gnathostomes diverged during the Ordovician (**Figure 4**). Tentative support for this divergence might be found in the enigmatic fossils of *Skiichthys* (**Smith and Sansom, 1997**) and Mongolepidae (suggested to be early chondrichthyans, **Andreev et al., 2016**). Maxillate placoderms are never recovered as sampled ancestors in the analysis, and the fact that they are of the same age as the osteichthyan *Guiyu* (**Zhu et al., 2009**) precludes this. *Entelognathus* and *Qilinyu* are themselves quite disparate and possess their own specializations, most notably the eyes of *Entelognathus* (**Zhu et al., 2013**; **Zhu et al., 2016**).

The results of our analysis are contingent on a phylogenetic hypothesis, in particular the monophyly of core placoderms, which is only strongly supported under a Bayesian tip-dating approach. The differences between parsimony and Bayesian tip-dated trees are discussed at length in **King et al., 2017**. The hypothesis of placoderm paraphyly (**Brazeau, 2009**; **Davis et al., 2012**; **Zhu et al., 2013**), implies a radically different scenario for character evolution (**Dupret et al., 2014**), in which the maxillate placoderms are not representative of ancestral conditions.

Our study proposes the application of dynamic homology concepts to morphological characters in a Bayesian framework. In this manuscript we have applied the method to placoderm jaw bones, but it could also potentially be used to examine skull roof homologies in the future. It should be noted that the simultaneous analysis of primary and secondary homology has been criticized (**Simmons, 2004**), because adding new morphological characters to a data matrix should be a test of phylogenetic relationships, rather than simply adding further support to a given phylogenetic hypothesis. Thus, it can be argued that multiple conflicting primary homology statements should only be analysed with dynamic homology when they are equally plausible. In such cases, supporting the primary homology statement that best fits a phylogenetic hypothesis is preferable to an arbitrary

choice. There may also exist cases where alternative primary homology statements support different tree topologies, and in this case arbitrary choices of primary homology statements could lead to sub-optimal phylogenetic trees.

Materials and methods

We compiled a morphological data matrix of gnathostome fossils (**Supplementary file 1**). The matrix is based on **King et al., 2017** with a revised taxon and character matrix. The taxon list was updated with the addition of *Gladbachus adentatus*, *Milesacanthus antarctica*, *Nerepisacanthus denisoni*, *Rhinodipterus kimberleyensis*, *Chirodipterus australis*, *Dipterus valenciennesi*, *Tungsenia paradoxa*, *Diplocercides kayseri*, *Qingmenodus yui*, *Raynerius splendens*, *Lehmanosteus hyperboreus*, *Shearsbyaspis oepiki*, and *Qilinyu rostrata*. *Ramirosuarezia boliviana*, *Wuttagoonaspis fletcheri*, *Gavinaspis convergens* and *Osorioichthys marginis* were removed.

Characters concerning the premaxillae, maxillae, dermopalatines and vomers were coded into two alternative *homology alignments*. These characters included presence and absence of these bones, as well as dependent characters. One alignment (homology state 0) was coded according the traditional interpretation of placoderm jaw bones (**Figure 1A**), in which the placoderm supragnathal bones are considered primary homologues of the vomer-dermopalatine series of osteichthyans. A second alignment (homology state 1) was coded according to the alternative interpretation (**Zhu et al., 2016**), in which placoderm supragnathal bones are considered primary homologues of the premaxilla-maxilla series of osteichthyans and maxillate placoderms. In total, the matrix had 489 characters with fixed homology, and 18 with variable homology.

We analysed the matrix in BEAST2.6.2 (**Bouckaert et al., 2019**), using the beagle calculation library (**Ayres et al., 2019**). We used homoplasy-based partitioning (**Rosa et al., 2019**) to account for rate variation among characters. Homoplasy was calculated using an implied weights parsimony analysis in TNT (**Goloboff and Catalano, 2016**), with concavity constant k = 10. Characters with different homoplasy values depending on homology state were assigned the lower value. Characters were partitioned according to the number of states as well as homoplasy. Each partition was assigned a separate mutation rate parameter and was analysed using the Mk substitution model (**Lewis, 2001**). The weighted mean value of the mutation rates was fixed at one, and each individual mutation rate parameter was assigned a normal distribution prior, with mean one and standard deviation 2.

We implemented a sampled ancestor birth-death model (**Gavryushkina et al., 2014**). The birth rate was assigned a lognormal prior with mean (in real space) 0.14 and standard deviation 0.9. Extinction and sampling rates were assigned exponential priors with mean 0.1. Tip dates were assigned to fossil sites with uniform priors on fossil site ages (**King and Rücklin, 2020**). Gnathostomes, gnathostomes+osteostracans and polybranchiaspids were constrained to be monophyletic. The clock model was an uncorrelated lognormal relaxed clock (**Drummond et al., 2006**) with a lognormal prior (mean −5.5, standard deviation 2) on clock rate and an exponential prior (mean 1) on clock standard deviation. We used ancestral sequence logging to reconstruct ancestral states for all characters at the (apomorphy-defined) gnathostome node at every sampled generation of the MCMC. This leads to 1801 'reconstructed ancestors', which comprise a credible set of phenotypes at the gnathostome crown node.

We ran the analysis for 800 million generations, and for four independent runs. The MCMC chain was sampled every 400000 generations, and 10% of the run was discarded as burn-in, resulting in a posterior sample of 1801 trees. Convergence of 4 independent runs was confirmed in Tracer 1.7 (**Rambaut et al., 2018**) and RWTY (**Warren et al., 2017**). Following the recommendations of **O'Reilly and Donoghue, 2018**, we calculated the 50% majority-rule tree in the R package ape (**Paradis and Schliep, 2019**), then time-scaled and annotated this tree using TreeAnnotator 1.10.2 (**Suchard et al., 2018**). The Beast2 xml file is available in the supplementary information (**Supplementary file 2**).

We used distance-based methods to determine the similarity of known fossil taxa to the reconstructed sequences at the gnathostome node. Principal coordinates analysis was performed in the package Claddis (**Lloyd, 2016**) in R 4.0.0 'Arbor Day' (**R Development Core Team, 2018**). We used the Maximum-Observable Rescaled Distance, equivalent to the **Gower, 1971** coefficient for our dataset. First, we performed ordination using the gnathostome fossils in our dataset, and a sample

of the reconstructed ancestors from BEAST2 (***Figure 6A***). This sample consisted of 5% of the posterior sample, from which we excluded those sampled generations where the homology state was 0 (n = 1), for a total of 90 reconstructed ancestors. Homology alignment 1 was used for distance calculations. A second ordination was performed using only placoderms (both core placoderms and maxillate placoderms)(***Figure 6B***). The point cloud of reconstructed ancestors was converted to a density plot using ggplot (***Wickham, 2016***). We also plotted the raw distance measures of each gnathostome taxon to each of the 90 reconstructed ancestors (***Figure 6C***). Finally, we calculated the taxon with the shortest distance to the reconstructed ancestor for the entire posterior distribution (1801 reconstructed ancestors). These calculations used the homology alignment corresponding to the sampled homology state.

Acknowledgements

We thank John Long and Mike Lee for comments on an earlier version of the manuscript and Min Zhu and Per Ahlberg for reviews. This work is funded by NWO Vidi 864.14.009 to Martin Rücklin.

Additional information

Funding

Funder	Grant reference number	Author
Nederlandse Organisatie voor Wetenschappelijk Onderzoek	Vidi 864.14.009	Benedict King Martin Rücklin

The funders had no role in study design, data collection and interpretation, or the decision to submit the work for publication.

Author contributions

Benedict King, Conceptualization, Data curation, Software, Formal analysis, Investigation, Methodology, Writing - original draft, Writing - review and editing; Martin Rücklin, Funding acquisition, Writing - review and editing

Author ORCIDs

Benedict King https://orcid.org/0000-0002-9489-8274

Decision letter and Author response

Decision letter https://doi.org/10.7554/eLife.62374.sa1
Author response https://doi.org/10.7554/eLife.62374.sa2

Additional files

Supplementary files

- Source data 1. Character state probabilities at the (apomorphy-defined) gnathostome node for all characters.
- Supplementary file 1. Data matrix in nexus format.
- Supplementary file 2. Beast2 xml file.
- Transparent reporting form

Data availability

The data matrix in nexus format and the BEAST2 xml file are available in the supplementary information. The beast2 source code and R analysis scripts are available at https://github.com/king-ben/homology (copy archived at https://archive.softwareheritage.org/swh:1:rev:6e6dbd77443b0d963640b3cb603c4310b5a4b47e).

The following datasets were generated:

References

Agolin M, D'Haese CA. 2009. An application of dynamic homology to morphological characters: direct optimization of setae sequences and phylogeny of the family Odontellidae (Poduromorpha, Collembola). *Cladistics* **25**:353–385. DOI: https://doi.org/10.1111/j.1096-0031.2009.00272.x

Ahlberg PE. 1989. Paired fin skeletons and relationships of the fossil group Porolepiformes (Osteichthyes: Sarcopterygii). *Zoological Journal of the Linnean Society* **96**:119–166. DOI: https://doi.org/10.1111/j.1096-3642.1989.tb01824.x

Ahlberg PE. 1991. A re-examination of sarcopterygian interrelationships, with special reference to the Porolepiformes. *Zoological Journal of the Linnean Society* **103**:241–287. DOI: https://doi.org/10.1111/j.1096-3642.1991.tb00905.x

Ahlberg PE, Lukševičs E, Mark-Kurik E. 2000. A near-tetrapod from the Baltic Middle Devonian. *Palaeontology* **43**:533–548. DOI: https://doi.org/10.1111/j.0031-0239.2000.00138.x

Ahlberg PE, Smith MM, Johanson Z. 2006. Developmental plasticity and disparity in early dipnoan (lungfish) dentitions. *Evolution and Development* **8**:331–349. DOI: https://doi.org/10.1111/j.1525-142X.2006.00106.x, PMID: 16805898

Ahlberg PE, Clack JA. 1998a. Lower jaws, lower tetrapods–a review based on the Devonian genus *Acanthostega* . *Transactions of the Royal Society of Edinburgh: Earth Sciences* **89**:11–46. DOI: https://doi.org/10.1017/S0263593300002340

Ahlberg PE, Johanson Z. 1998b. Osteolepiforms and the ancestry of tetrapods. *Nature* **395**:792–794. DOI: https://doi.org/10.1038/27421

Ahlberg PE, Trewin NH. 1994. The postcranial skeleton of the Middle Devonian lungfish *Dipterus valenciennesi* . *Transactions of the Royal Society of Edinburgh: Earth Sciences* **85**:159–175. DOI: https://doi.org/10.1017/S0263593300003588

Andreev P, Coates MI, Karatajūtė-Talimaa V, Shelton RM, Cooper PR, Wang NZ, Sansom IJ. 2016. The systematics of the Mongolepidida (Chondrichthyes) and the Ordovician origins of the clade. *PeerJ* **4**:e1850. DOI: https://doi.org/10.7717/peerj.1850, PMID: 27350896

Andrews M, Long J, Ahlberg P, Barwick R, Campbell K. 2005. The structure of the sarcopterygian *Onychodus jandemarrai* n. sp. from Gogo, Western Australia: with a functional interpretation of the skeleton . *Transactions of the Royal Society of Edinburgh: Earth Sciences* **96**:197–307. DOI: https://doi.org/10.1017/S0263593300001309

Arratia G, Cloutier R. 1996. Reassessment of the morphology of *Cheirolepis canadensis* (Actinopterygii). In: Schultze H. P, Cloutier R (Eds). *Devonian Fishes and Plants of Miguasha*. Verlag Dr. F. Pfeil. p. 165–197.

Ayres DL, Cummings MP, Baele G, Darling AE, Lewis PO, Swofford DL, Huelsenbeck JP, Lemey P, Rambaut A, Suchard MA. 2019. BEAGLE 3: improved performance, scaling, and usability for a High-Performance computing library for statistical phylogenetics. *Systematic Biology* **68**:1052–1061. DOI: https://doi.org/10.1093/sysbio/syz020, PMID: 31034053

Basden AM, Young GC, Coates MI, Ritchie A. 2000. The most primitive osteichthyan braincase? *Nature* **403**:185–188. DOI: https://doi.org/10.1038/35003183, PMID: 10646601

Basden AM, Young GC. 2001. A primitive actinopterygian neurocranium from the Early Devonian of southeastern Australia. *Journal of Vertebrate Paleontology* **21**:754–766. DOI: https://doi.org/10.1671/0272-4634(2001)021[0754:APANFT]2.0.CO;2

Béchard I, Arsenault F, Cloutier R, Kerr J. 2014. The Devonian placoderm fish *Bothriolepis canadensis* revisited with three-dimensional digital imagery. *Palaeontologia Electronica* **17**:1–19. DOI: https://doi.org/10.26879/417

Bendix-Almgreen S. 1975. The paired fins and shoulder girdle in *Cladoselache*, their morphology and phyletic significance. Colloques International CNRS 111–123.

Botella H, Blom H, Dorka M, Ahlberg PE, Janvier P. 2007. Jaws and teeth of the earliest bony fishes. *Nature* **448**:583–586. DOI: https://doi.org/10.1038/nature05989, PMID: 17671501

Bouckaert R, Vaughan TG, Barido-Sottani J, Duchêne S, Fourment M, Gavryushkina A, Heled J, Jones G, Kühnert D, De Maio N, Matschiner M, Mendes FK, Müller NF, Ogilvie HA, du Plessis L, Popinga A, Rambaut A, Rasmussen D, Siveroni I, Suchard MA, et al. 2019. BEAST 2.5: An advanced software platform for Bayesian evolutionary analysis. *PLOS Computational Biology* **15**:e1006650. DOI: https://doi.org/10.1371/journal.pcbi.1006650

Brazeau MD. 2009. The braincase and jaws of a Devonian 'acanthodian' and modern gnathostome origins. *Nature* **457**:305–308. DOI: https://doi.org/10.1038/nature07436

Brazeau MD. 2012. A revision of the anatomy of the Early Devonian jawed vertebrate *Ptomacanthus anglicus* Miles. *Palaeontology* **55**:355–367. DOI: https://doi.org/10.1111/j.1475-4983.2012.01130.x

Brazeau MD, de Winter V. 2015. The hyoid arch and braincase anatomy of *Acanthodes* support chondrichthyan affinity of 'acanthodians' . *Proceedings of the Royal Society B: Biological Sciences* **282**:20152210. DOI: https://doi.org/10.1098/rspb.2015.2210

Brazeau MD, Friedman M. 2014. The characters of Palaeozoic jawed vertebrates. *Zoological Journal of the Linnean Society* **170**:779–821. DOI: https://doi.org/10.1111/zoj.12111, PMID: 25750460

Burrow CJ. 2011. A partial articulated acanthodian from the Silurian of New Brunswick, Canada. *Canadian Journal of Earth Sciences* **48**:1329–1341. DOI: https://doi.org/10.1139/e11-023

Burrow CJ, Newman MJ, Davidson RG, den Blaauwen JL. 2013. Redescription of *Parexus recurvus* , an Early Devonian acanthodian from the Midland Valley of Scotland . *Alcheringa: An Australasian Journal of Palaeontology* **37**:392–414. DOI: https://doi.org/10.1080/03115518.2013.765656

Burrow CJ, Davidson RG, Den Blaauwen JL, Newman MJ. 2015. Revision of *Climatius reticulatus* Agassiz, 1844 (Acanthodii, Climatiidae), from the Lower Devonian of Scotland, based on new histological and morphological data . *Journal of Vertebrate Paleontology* **35**:e913421. DOI: https://doi.org/10.1080/02724634.2014.913421

Burrow C, den Blaauwen J, Newman M, Davidson R. 2016. The diplacanthid fishes (Acanthodii, Diplacanthiformes, Diplacanthidae) from the Middle Devonian of Scotland. *Palaeontologia Electronica* **19**:1–83. DOI: https://doi.org/10.26879/601

Burrow CJ, Newman M, Jones R, Davidson R. 2018. The Early Devonian ischnacanthiform acanthodian *Ischnacanthus gracilis* (Egerton, 1861) from the Midland Valley of Scotland. *Acta Geologica Polonica* **68**:335–362. DOI: https://doi.org/10.1515/agp-2018-0008

Burrow CJ, Rudkin D. 2014. Oldest near-complete acanthodian: the first vertebrate from the Silurian Bertie Formation Konservat-Lagerstätte, Ontario. *PLOS ONE* **9**:e104171. DOI: https://doi.org/10.1371/journal.pone.0104171, PMID: 25093877

Burrow CJ, Turner S. 1998. Devonian placoderm scales from Australia. *Journal of Vertebrate Paleontology* **18**: 677–695. DOI: https://doi.org/10.1080/02724634.1998.10011097

Burrow CJ, Turner S. 2010. Reassessment of "*Protodus*" *scoticus* from the Early Devonian of Scotland. In: Elliot D. K, Maisey J. G, Yu X, Miao D (Eds). *Morphology Phylogeny and Paleobiogeography of Fossil Fishes*. Verlag Dr. Friedrich Pfeil. p. 123–144. DOI: https://doi.org/10.1086/665465

Carr RK, Johanson Z, Ritchie A. 2009. The phyllolepid placoderm *Cowralepis mclachlani*: insights into the evolution of feeding mechanisms in jawed vertebrates. *Journal of Morphology* **270**:775–804. DOI: https://doi.org/10.1002/jmor.10719, PMID: 19215000

Carr RK, Hlavin WJ. 2010. Two new species of *Dunkleosteus* Lehman, 1956, from the Ohio Shale Formation (USA, Famennian) and the Kettle Point Formation (Canada, Upper Devonian), and a cladistic analysis of the Eubrachythoraci (Placodermi, Arthrodira). *Zoological Journal of the Linnean Society* **159**:195–222. DOI: https://doi.org/10.1111/j.1096-3642.2009.00578.x

Castiello M, Brazeau MD. 2018. Neurocranial anatomy of the petalichthyid placoderm *Shearsbyaspis oepiki* Young revealed by X-ray computed microtomography. *Palaeontology* **61**:369–389. DOI: https://doi.org/10.1111/pala.12345, PMID: 29937580

Challands TJ. 2015. The cranial endocast of the Middle Devonian dipnoan *Dipterus valenciennesi* and a fossilized dipnoan otoconial mass . *Papers in Palaeontology* **1**:289–317. DOI: https://doi.org/10.1002/spp2.1016

Chang M-M. 1982. *The Braincase of Youngolepis, a Lower Devonian Crossopterygian From Yunnan, South-Western China*: Swedish Museum of Natural History.

Chang M-M. 1991. Head exoskeleton and shoulder girdle of *Youngolepis*. In: Chang M. M, Liu Y. H, Zhang G. R (Eds). *Early Vertebrates and Related Problems of Evolutionary Biology*. Science Press. p. 355–378.

Chang M-M. 1995. *Diabolepis* and its bearing on the relationships between porolepiforms and dipnoans. *Bulletin Du Muséum National d'histoire Naturelle Section C, Sciences De La Terre, Paléontologie, Géologie, Minéralogie* **17**:235–268.

Chang M-M, Smith MM. 1992. Is *Youngolepis* a porolepiform? *Journal of Vertebrate Paleontology* **12**:294–312. DOI: https://doi.org/10.1080/02724634.1992.10011461

Chang M-M, Yu X-B. 1984. Structure and phyogenetic significance of *Diabolepis speratus* gen. et sp. nov., a new dipnoan-like form from the Lower Devonian of eastern Yunnan, China. Proceedings of the Linnean Society of New South Wales 171–184.

Chang M-M, Zhu M. 1993. A new Middle Devonian osteolepidid from Qujing, Yunnan. Memoirs of the Association of Australasian Palaeontologists 183–198.

Chen D, Blom H, Sanchez S, Tafforeau P, Ahlberg PE. 2016. The stem osteichthyan *Andreolepis* and the origin of tooth replacement. *Nature* **539**:237–241. DOI: https://doi.org/10.1038/nature19812

Chen D, Blom H, Sanchez S, Tafforeau P, Märss T, Ahlberg PE. 2017. Development of cyclic shedding teeth from semi-shedding teeth: the inner dental arcade of the stem osteichthyan *Lophosteus* . *Royal Society Open Science* **4**:161084. DOI: https://doi.org/10.1098/rsos.161084

Chen D, Blom H, Sanchez S, Tafforeau P, Märss T, Ahlberg PE. 2020. Dental ontogeny in the most primitive bony fish *Lophosteus* reveals the developmental relationship between teeth and dermal odontodes. *bioRxiv*. DOI: https://doi.org/10.1101/2020.07.14.202234

Choo B, Zhu M, Zhao W, Jia L, Zhu Y. 2015. The largest Silurian vertebrate and its palaeoecological implications. *Scientific Reports* **4**:5242. DOI: https://doi.org/10.1038/srep05242

Clement G. 2004. Nouvelles données anatomiques et morphologie génerale des Porolepididae (Dipnomorpha, Sarcopterygii). *Revue de Paléontologie* **9**:193–211.

Clement AM. 2012. A new species of long-snouted lungfish from the late devonian of Australia, and its functional and biogeographical implications. *Palaeontology* **55**:51–71. DOI: https://doi.org/10.1111/j.1475-4983.2011.01118.x

Clement AM, King B, Giles S, Choo B, Ahlberg PE, Young GC, Long JA. 2018. Neurocranial anatomy of an enigmatic Early Devonian fish sheds light on early osteichthyan evolution. *eLife* **7**:e34349. DOI: https://doi.org/10.7554/eLife.34349

Clement AM, Ahlberg PE. 2014. The first virtual cranial endocast of a lungfish (Sarcopterygii: Dipnoi). *PLOS ONE* **9**:e113898. DOI: https://doi.org/10.1371/journal.pone.0113898, PMID: 25427173

Cloutier R. 1996. The primitive actinistian *Miguashaia bureaui* Schultze (Sarcopterygii). In: Schultze H. P, Cloutier R (Eds). *Devonian Fishes and Plants of Miguasha*. Verlag Dr. Friedrich Pfeil. p. 227–247.

Cloutier R, Ahlberg PE. 1996. Morphology, characters, and the interrelationships of basal sarcopterygians. In: Stiassny M. L. J, Parenti L. R, Johnson G. D (Eds). *Interrelationships of Fishes*. Academic Press. p. 445–479. DOI: https://doi.org/10.1016/B978-012670950-6/50018-7

Cloutier R, Arratia G. 2004. Early diversification of actinopterygians. In: Arratia G, Wilson M. V. H, Cloutier R (Eds). *Recent Advances in the Origin and Early Radiation of Vertebrates*. Verlag Dr. Friedrich Pfeil. p. 217–270.

Coates MI. 1994. The origin of vertebrate limbs. *Development* **1994**:169–180.

Coates MI, Sequeira SEK, Sansom IJ, Smith MM. 1998. Spines and tissues of ancient sharks. *Nature* **396**:729–730. DOI: https://doi.org/10.1038/25467

Coates MI. 1999. Endocranial preservation of a Carboniferous actinopterygian from Lancashire, UK, and the interrelationships of primitive actinopterygians. *Philosophical Transactions of the Royal Society of London. Series B: Biological Sciences* **354**:435–462. DOI: https://doi.org/10.1098/rstb.1999.0396

Coates MI, Finarelli JA, Sansom IJ, Andreev PS, Criswell KE, Tietjen K, Rivers ML, La Riviere PJ. 2018. An early chondrichthyan and the evolutionary assembly of a shark body plan. *Proceedings of the Royal Society B: Biological Sciences* **285**:20172418. DOI: https://doi.org/10.1098/rspb.2017.2418

Coates MI, Gess RW. 2007. A new reconstruction of *Onychoselache traquairi*, comments on early chondrichthyan pectoral girdles and hybodontiform phylogeny. *Palaeontology* **50**:1421–1446. DOI: https://doi.org/10.1111/j.1475-4983.2007.00719.x

Coates MI, Sequeira SEK. 1998. The braincase of a primitive shark. *Transactions of the Royal Society of Edinburgh: Earth Sciences* **89**:63–85. DOI: https://doi.org/10.1017/S026359330000701X

Coates MI, Sequeira SEK. 2001. A new stethacanthid chondrichthyan from the lower Carboniferous of Bearsden, Scotland. *Journal of Vertebrate Paleontology* **21**:438–459. DOI: https://doi.org/10.1671/0272-4634(2001)021[0438:ANSCFT]2.0.CO;2

Coates MI, Tietjen K. 2018. The neurocranium of the Lower Carboniferous shark *Tristychius arcuatus* (Agassiz, 1837) . *Earth and Environmental Science Transactions of the Royal Society of Edinburgh* **108**:19–35. DOI: https://doi.org/10.1017/S1755691018000130

Cunningham JA, Rücklin M, Blom H, Botella H, Donoghue PCJ. 2012. Testing models of dental development in the earliest bony vertebrates, *Andreolepis* and *Lophosteus*. *Biology Letters* **8**:833–837. DOI: https://doi.org/10.1098/rsbl.2012.0357, PMID: 22628098

Davis SP, Finarelli JA, Coates MI. 2012. *Acanthodes* and shark-like conditions in the last common ancestor of modern gnathostomes. *Nature* **486**:247–250. DOI: https://doi.org/10.1038/nature11080, PMID: 22699617

Dearden RP, Stockey C, Brazeau MD. 2019. The pharynx of the stem-chondrichthyan *Ptomacanthus* and the early evolution of the gnathostome gill skeleton. *Nature Communications* **10**:2050. DOI: https://doi.org/10.1038/s41467-019-10032-3

Denison RH. 1947. The exoskeleton of *Tremataspis*. *American Journal of Science* **245**:337–365. DOI: https://doi.org/10.2475/ajs.245.6.337

Denison RH. 1951. Evolution and classification of the Osteostraci. *Fieldania. Geology* **11**:157–196. DOI: https://doi.org/10.5962/bhl.title.3286

Dennis KIM, Miles RS. 1981. A pachyosteomorph arthrodire from Gogo, Western Australia. *Zoological Journal of the Linnean Society* **73**:213–258. DOI: https://doi.org/10.1111/j.1096-3642.1981.tb01594.x

Dennis-Bryan K. 1987. A new species of eastmanosteid arthrodire (Pisces: Placodermi) from Gogo, Western Australia. *Zoological Journal of the Linnean Society* **90**:1–64. DOI: https://doi.org/10.1111/j.1096-3642.1987.tb01347.x

Dick JRF. 1978. On the Carboniferous shark *Tristychius arcuatus* Agassiz from Scotland. *Transactions of the Royal Society of Edinburgh* **70**:63–108. DOI: https://doi.org/10.1017/S0080456800012898

Dick JRF, Maisey JG. 1980. The Scottish Lower Carboniferous shark *Onychoselache traquairi*. *Palaeontology* **23**:363–374.

Dietze K. 2000. A revision of paramblypterid and amblypterid actinopterygians from upper Carboniferous-Lower Permian lacustrine deposits of central Europe. *Palaeontology* **43**:927–966. DOI: https://doi.org/10.1111/1475-4983.00156

Donoghue PCJ, Forey PL, Aldridge RJ. 2000. Conodont affinity and chordate phylogeny. *Biological Reviews of the Cambridge Philosophical Society* **75**:191–251. DOI: https://doi.org/10.1017/S0006323199005472, PMID: 10881388

Downs JP, Donoghue PCJ. 2009. Skeletal histology of *Bothriolepis canadensis* (Placodermi, Antiarchi) and evolution of the skeleton at the origin of jawed vertebrates. *Journal of Morphology* **270**:1364–1380. DOI: https://doi.org/10.1002/jmor.10765, PMID: 19533688

Drummond AJ, Ho SY, Phillips MJ, Rambaut A. 2006. Relaxed phylogenetics and dating with confidence. *PLOS Biology* **4**:e88. DOI: https://doi.org/10.1371/journal.pbio.0040088, PMID: 16683862

Dupret V, Zhu M, Wang JQ. 2009. The morphology of *Yujiangolepis liujingensis* (Placodermi, Arthrodira) from the Pragian of Guangxi (south China) and its phylogenetic significance . *Zoological Journal of the Linnean Society* **157**:70–82. DOI: https://doi.org/10.1111/j.1096-3642.2009.00519.x

Dupret V. 2010. Revision of the genus *Kujdanowiaspis* Stensiö, 1942 (Placodermi, Arthrodira, "Actinolepida") from the Lower Devonian of Podolia (Ukraine) . *Geodiversitas* **32**:5–63. DOI: https://doi.org/10.5252/g2010n1a1

Dupret V, Sanchez S, Goujet D, Tafforeau P, Ahlberg PE. 2014. A primitive placoderm sheds light on the origin of the jawed vertebrate face. *Nature* **507**:500–503. DOI: https://doi.org/10.1038/nature12980

Dupret V, Sanchez S, Goujet D, Ahlberg PE. 2017. The internal cranial anatomy of *Romundina stellina* Ørvig, 1975 (Vertebrata, Placodermi, Acanthothoraci) and the origin of jawed vertebrates—Anatomical atlas of a

primitive gnathostome. *PLOS ONE* **12**:e0171241. DOI: https://doi.org/10.1371/journal.pone.0171241, PMID: 28170434

Finarelli JA, Coates M. 2011. First tooth-set outside the jaws in a vertebrate. *Royal Society of London B: Biological Sciences* **279**:775–779. DOI: https://doi.org/10.1098/rspb.2011.1107

Finarelli JA, Coates MI. 2014. *Chondrenchelys problematica* (Traquair, 1888) redescribed: a Lower Carboniferous, eel-like holocephalan from Scotland. *Earth and Environmental Science Transactions of the Royal Society of Edinburgh* **105**:35–59. DOI: https://doi.org/10.1017/S1755691014000139

Forey PL. 1998. *History of the Coelacanth Fishes*. Chapman and Hall.

Friedman M. 2007a. The interrelationships of Devonian lungfishes (Sarcopterygii: Dipnoi) as inferred from neurocranial evidence and new data from the genus *Soederberghia* Lehman, 1959. *Zoological Journal of the Linnean Society* **151**:115–171. DOI: https://doi.org/10.1111/j.1096-3642.2007.00320.x

Friedman M. 2007b. *Styloichthys* as the oldest coelacanth: implications for early osteichthyan interrelationships . *Journal of Systematic Palaeontology* **5**:289–343. DOI: https://doi.org/10.1017/S1477201907002052

Friedman M, Blom H. 2006. A new actinopterygian from the Famennian of east Greenland and the interrelationships of Devonian ray-finned fishes. *Journal of Paleontology* **80**:1186–1204. DOI: https://doi.org/10.1666/0022-3360(2006)80[1186:ANAFTF]2.0.CO;2

Friedman M, Brazeau MD. 2010. A reappraisal of the origin and basal radiation of the osteichthyes. *Journal of Vertebrate Paleontology* **30**:36–56. DOI: https://doi.org/10.1080/02724630903409071

Gagnier P-Y. 1996. *Acanthodii*. In: Schultze H. -P, Cloutier R (Eds). *Devonian Fishes and Plants of Miguasha, Quebec, Canada*. Freidrich Pfeil Verlag. p. 149–164.

Gagnier P-Y, Hanke G, Wilson M. 1999. *Tetanopsyrus lindoei* gen. et sp. nov., an Early Devonian acanthodian from the Northwest Territories, Canada. *Acta Geologica Polonica* **49**:81–96.

Gagnier P-Y, Wilson M. 1996. Early Devonian acanthodians from northern Canada. *Palaeontology* **39**:241–258. DOI: https://doi.org/10.1139/E08-033

Gai Z, Donoghue PCJ, Zhu M, Janvier P, Stampanoni M. 2011. Fossil jawless fish from China foreshadows early jawed vertebrate anatomy. *Nature* **476**:324–327. DOI: https://doi.org/10.1038/nature10276, PMID: 21850106

Gardiner BG. 1984. *The Relationships of the Paleoniscid Fishes. a Review Based on New Specimens of Mimia and Moythomasia From the Upper Devonian of Western Australia*. Bulletin of the British Museum (Natural History) Geology.

Gardiner BG, Bartram A. 1977. The homologies of ventral cranial fissures in osteichthyans. In: Westoll T, Andrews S, Miles R, Walker A (Eds). *Problems in Vertebrate Evolution*. Academic Press. p. 227–245. DOI: https://doi.org/10.1111/j.1558-5646.1978.tb01120.x

Gardiner BG, Miles RS. 1994. Eubrachythoracid arthrodires from Gogo, Western Australia. *Zoological Journal of the Linnean Society* **112**:443–477. DOI: https://doi.org/10.1111/j.1096-3642.1994.tb00331.x

Gardiner BG, Schaeffer B. 1989. Interrelationships of lower actinopterygian fishes. *Zoological Journal of the Linnean Society* **97**:135–187. DOI: https://doi.org/10.1111/j.1096-3642.1989.tb00550.x

Gavryushkina A, Welch D, Stadler T, Drummond AJ. 2014. Bayesian inference of sampled ancestor trees for epidemiology and fossil calibration. *PLOS Computational Biology* **10**:e1003919. DOI: https://doi.org/10.1371/journal.pcbi.1003919, PMID: 25474353

Giles S, Rücklin M, Donoghue PCJ. 2013. Histology of "placoderm" dermal skeletons: implications for the nature of the ancestral gnathostome. *Journal of Morphology* **274**:627–644. DOI: https://doi.org/10.1002/jmor.20119, PMID: 23378262

Giles S, Coates MI, Garwood RJ, Brazeau MD, Atwood R, Johanson Z, Friedman M. 2015a. Endoskeletal structure in *Cheirolepis* (Osteichthyes, Actinopterygii), An early ray-finned fish. *Palaeontology* **58**:849–870. DOI: https://doi.org/10.1111/pala.12182, PMID: 27478252

Giles S, Darras L, Clément G, Blieck A, Friedman M. 2015b. An exceptionally preserved Late Devonian actinopterygian provides a new model for primitive cranial anatomy in ray-finned fishes. *Proceedings of the Royal Society B: Biological Sciences* **282**:20151485. DOI: https://doi.org/10.1098/rspb.2015.1485

Giles S, Friedman M, Brazeau MD. 2015c. Osteichthyan-like cranial conditions in an Early Devonian stem gnathostome. *Nature* **520**:82–85. DOI: https://doi.org/10.1038/nature14065, PMID: 25581798

Giles S, Friedman M. 2014. Virtual reconstruction of endocast anatomy in early ray-finned fishes (Osteichthyes, Actinopterygii). *Journal of Paleontology* **88**:636–651. DOI: https://doi.org/10.1666/13-094

Goloboff PA, Catalano SA. 2016. TNT version 1.5, including a full implementation of phylogenetic morphometrics. *Cladistics* **32**:221–238. DOI: https://doi.org/10.1111/cla.12160

Goujet D. 1973. *Sigaspis*, un nouvel arthrodire du Dévonien Inférieur du Spitsberg. *Palaeontographica Abteilung A* **143**:73–88.

Goujet D. 1975. *Dicksonosteus*, un nouvel arthrodire du Dévonien du Spitsberg—Remarques sur le squelette viscéral des Dolichothoraci. *Colloques Internationaux du Centre National de la Recherche Scientifique* **218**:81–99.

Goujet D. 1984a. *Les Poissons Placodermes du Spitzberg: Arthrodires Dolichothoraci de la Formation de Wood Bay (Dévonien Inférieur)*: Cahiers de Paléontologie, Section Vertebrés.

Goujet D. 1984b. Placoderm interrelationships: a new interpretation, with a short review of placoderm classifications. *Proceedings of the Linnean Society of New South Wales* **107**:211–243.

Goujet D, Young GC. 1995. Interrelationships of placoderms revisited. *Geobios* **28**:89–95. DOI: https://doi.org/10.1016/S0016-6995(95)80093-X

Gower JC. 1971. A general coefficient of similarity and some of its properties. *Biometrics* **27**:857–871. DOI: https://doi.org/10.2307/2528823

Grogan ED, Lund R. 2000. *Debeerius ellefseni* (Fam. Nov., Gen. Nov., Spec. Nov.), an autodiastylic chondrichthyan from the Mississippian Bear Gulch Limestone of Montana (USA), the relationships of the Chondrichthyes, and comments on gnathostome evolution. *Journal of Morphology* **243**:219–245. DOI: https://doi.org/10.1002/(SICI)1097-4687(200003)243:3<219::AID-JMOR1>3.0.CO;2-1, PMID: 10681469

Gross W. 1935. Histologische studien am aussenskelett fossiler agnathen und fische. *Palaeontographica Abteilung A* **83**:1–60.

Gross W. 1961. *Lunaspis broilii* und *Lunaspis heroldi* aus dem Hunsrückschiefer (Unterdevons, Rheinland). *Notizblatt Hessisches Landesamtes Für Bodenforschung Zu Wiesbaden* **89**:17–43.

Gross W. 1963. *Gemuendina stuertzi* Traquair. Neuuntersuchung. *Sonderdruck aus dem Notizblatt des Hessischen Landesamtes für Bodenforschung zu Wiesbaden* **91**:36–73.

Halstead LB. 1973. The heterostracan fishes. *Biological Reviews* **48**:279–332. DOI: https://doi.org/10.1111/j.1469-185X.1973.tb01005.x

Hanke GF, Davis SP, Wilson MVH. 2001. New species of the acanthodian genus *Tetanopsyrus* from northern Canada, and comments on related taxa . *Journal of Vertebrate Paleontology* **21**:740–753. DOI: https://doi.org/10.1671/0272-4634(2001)021[0740:NSOTAG]2.0.CO;2

Hanke GF. 2008. *Promesacanthus eppleri* n. gen., n. sp., a mesacanthid (Acanthodii, Acanthodiformes) from the Lower Devonian of northern Canada. *Geodiversitas* **30**:287–302.

Hanke GF, Davis SP. 2008. Redescription of the acanthodian *Gladiobranchus probaton* Bernacsek & Dineley, 1977, and comments on diplacanthid relationships. *Geodiversitas* **30**:303–330.

Hanke GF, Davis SP. 2012. A re-examination of *Lupopsyrus pygmaeus* Bernacsek & Dineley, 1977 (Pisces, Acanthodii). *Geodiversitas* **34**:469–487. DOI: https://doi.org/10.5252/g2012n3a1

Hanke GF, Wilson MVH. 2004. New teleostome fishes and acanthodian systematics. In: Arratia G, Wilson M. V. H, Cloutier R (Eds). *Recent Advances in the Origin and Early Radiation of Vertebrates*. Verlag Dr. Friedrich Pfeil. p. 189–216.

Hanke GF, Wilson MVH. 2006. Anatomy of the Early Devonian acanthodian *Brochoadmones milesi* based on nearly complete body fossils, with comments on the evolution and development of paired fins . *Journal of Vertebrate Paleontology* **26**:526–537. DOI: https://doi.org/10.1671/0272-4634(2006)26[526:AOTEDA]2.0.CO;2

Hanke GF, Wilson MVH. 2010. The putative stem-group chondrichthyans *Kathemacanthus* and *Seretolepis* from the Lower Devonian MOTH locality, Mackenzie Mountains, Canada. In: Elliott D. K, Maisey J. G, Yu X, Miao D (Eds). *Morphology Phylogeny, and Paleobiogeography of Fossil Fishes, Honoring Meemann Chang*. Verlag Dr. Friedrich. p. 159–182.

Harris JE. 1938. The dorsal spine of *Cladoselache*. *Scientific Publications of the Cleveland Museum of Natural History* **8**:1–6.

Hemmings SK. 1978. The Old Red Sandstone antiarchs of Scotland: *Pterichthyodes* and *Microbrachius*. *Palaeontographical Society Monographs* **48**:13–45. DOI: https://doi.org/10.1016/S0016-7878(37)80021-8

Henderson SAC, Challands TJ. 2018. The cranial endocast of the Upper Devonian dipnoan '*Chirodipterus*' *australis*. *PeerJ* **6**:e5148. DOI: https://doi.org/10.7717/peerj.5148, PMID: 30002977

Holland T. 2013. Pectoral girdle and fin anatomy of *Gogonasus andrewsae* Long, 1985: implications for tetrapodomorph limb evolution. *Journal of Morphology* **274**:147–164. DOI: https://doi.org/10.1002/jmor.20078, PMID: 23023825

Holland T. 2014. The endocranial anatomy of *Gogonasus andrewsae* Long, 1985 revealed through micro CT-scanning . *Earth and Environmental Science Transactions of the Royal Society of Edinburgh* **105**:9–34. DOI: https://doi.org/10.1017/S1755691014000164

Hu Y, Lu J, Young GC. 2017. New findings in a 400 million-year-old devonian placoderm shed light on jaw structure and function in basal gnathostomes. *Scientific Reports* **7**:7813. DOI: https://doi.org/10.1038/s41598-017-07674-y, PMID: 28798392

Janvier P. 1981. *Norselaspis glacialis* ng, n. sp. et les relations phylogénétiques entre les kiaeraspidiens (Osteostraci) du Dévonien Inférieur du Spitsberg. *Palaeovertebrata* **11**:19–131.

Janvier P. 1985a. *Les Céphalaspides du Spitsberg. Anatomie, Phylogénie et Systématique des Ostéostracés Siluro-Dévoniens Révision des Ostéostracés de la Formation de Wood Bay (Dévonien Inférieur du Spitsberg)*: Cahiers de Paléontologie, Section Vertebrés. CNRS.

Janvier P. 1985b. Les thyestidiens (Osteostraci) du Silurien de Saaremaa (Estonie). *Annales De Paleontologie* **71**:83–147.

Janvier P, Thanh TD, Phuong TH. 1993. A new Early Devonian galeaspid from Bac Thai Province, Vietnam. *Palaeontology* **36**:297.

Janvier P. 1996. *Early Vertebrates*. Oxford: Clarendon Press.

Janvier P, Arsenault M, Desbiens S. 2004. Calcified cartilage in the paired fins of the osteostracan *Escuminaspis laticeps* (Traquair 1880), from the Late Devonian of Miguasha (Québec, Canada), with a consideration of the early evolution of the pectoral fin endoskeleton in vertebrates . *Journal of Vertebrate Paleontology* **24**:773–779. DOI: https://doi.org/10.1671/0272-4634(2004)024[0773:CCITPF]2.0.CO;2

Jardine N. 1969. The observational and theoretical components of homology: a study based on the morphology of the dermal skull-roofs of rhipidistian fishes. *Biological Journal of the Linnean Society* **1**:327–361. DOI: https://doi.org/10.1111/j.1095-8312.1969.tb00125.x

Jarvik E. 1972. Middle and Upper Devonian Porolepiformes from east Greenland with special reference to *Glyptolepis groenlandica* N. Sp.: and a discussion on the structure of the head in the Porolepiformes. *Palaeontographica Abteilung a Palaeozoologie-Stratigraphie* **167**:180–214.

Jarvik E. 1980. *Basic Structure and Evolution of Vertebrates*. London: Academic Press. DOI: https://doi.org/10.1080/02724634.1981.10011908
Jessen H. 1975. A new choanate fish, *Powichthys thorsteinssoni* n.g., n. sp., from the early Lower Devonian of the Canadian Arctic Archipelago. *Colloques Internationaux du Centre National de la Recherche Scientifique* **218**: 214–222.
Jessen H. 1980. Lower Devonian Porolepiformes from the Canadian Arctic with special reference to *Powichthys thorsteinssoni* Jessen. *Palaeontographica Abteilung A* **4**:180–214.
Jia L-T, Zhu M, Zhao W-J. 2010. A new antiarch fish from the Upper Devonian Zhongning Formation of Ningxia, China. *Palaeoworld* **19**:136–145. DOI: https://doi.org/10.1016/j.palwor.2010.02.002
Johanson Z. 1997. New *Remigolepis* (Placodermi; Antiarchi) from Canowindra, New South Wales, Australia. *Geological Magazine* **134**:813–846. DOI: https://doi.org/10.1016/S0016-6995(95)80095-6
King B, Qiao T, Lee MSY, Zhu M, Long JA. 2017. Bayesian morphological clock methods resurrect placoderm monophyly and reveal rapid early evolution in jawed vertebrates. *Systematic Biology* **66**:499–516. DOI: https://doi.org/10.1093/sysbio/syw107, PMID: 27920231
King B, Young GC, Long JA. 2018. New information on *Brindabellaspis stensioi* Young, 1980, highlights morphological disparity in Early Devonian placoderms. *Royal Society Open Science* **5**:180094. DOI: https://doi.org/10.1098/rsos.180094, PMID: 30110452
King B. 2021. homology. *Software Heritage*. swh:1:rev:6e6dbd77443b0d963640b3cb603c4310b5a4b47e. https://archive.softwareheritage.org/swh:1:dir:0a689658a1eb95a5a1aeea6641428d55e38c404d;origin=https://github.com/king-ben/homology;visit=swh:1:snp:81d92a9131fe80f0b445db1e3f836465ee977fff;anchor=swh:1:rev:6e6dbd77443b0d963640b3cb603c4310b5a4b47e/
King B, Rücklin M. 2020. Tip dating with fossil sites and stratigraphic sequences. *PeerJ* **8**:e9368. DOI: https://doi.org/10.7717/peerj.9368, PMID: 32617191
Lee MSY. 1998. Similarity, parsimony and conjectures of homology: the chelonian shoulder girdle revisited. *Journal of Evolutionary Biology* **11**:379–387.
Lee MSY, Baron MG, Norman DB, Barrett PM. 2018. Dynamic biogeographic models and dinosaur origins. *Earth and Environmental Science Transactions of the Royal Society of Edinburgh* **109**:325–332. DOI: https://doi.org/10.1017/S1755691018000920
Lewis PO. 2001. A likelihood approach to estimating phylogeny from discrete morphological character data. *Systematic Biology* **50**:913–925. DOI: https://doi.org/10.1080/106351501753462876, PMID: 12116640
Liu Y. 1965. New Devonian agnathans of Yunnan. *Vertebrata PalAsiatica* **9**:125–134.
Liu Y. 1975. Lower Devonian agnathans of Yunnan and Sichuan. *Vertebrata PalAsiatica* **13**:202–216.
Liu Y-H. 1991. On a new petalichthyid, *Eurycaraspis incilis* gen. et sp. nov., from the Middle Devonian of Zhanyi, Yunnan. In: Chang M. M, Liu Y. H, Zhang G. R (Eds). *Early Vertebrates and Related Problems of Evolutionary Biology*. Science Press. p. 139–177.
Lloyd GT. 2016. Estimating morphological diversity and tempo with discrete character-taxon matrices: implementation, challenges, progress, and future directions. *Biological Journal of the Linnean Society* **118**:131–151. DOI: https://doi.org/10.1111/bij.12746
Long JA. 1983. A new diplacanthoid acanthodian from the Late Devonian of Victoria. *Memoirs of the Association of Australasian Palaeontologists* **1**:51–65.
Long JA. 1985. A new osteolepidid fish from the Upper Devonian Gogo Formation, Western Australia. *Records of the Western Australian Museum* **12**:361–377.
Long JA. 1988. New palaeoniscoid fishes from the Late Devonian and Early Carboniferous of Victoria. *Memoirs of the Association of Australasian Palaeontologists* **7**:1–64.
Long JA. 1997. Ptyctodontid fishes (Vertebrata, Placodermi) from the Late Devonian Gogo Formation, Western Australia, with a revision of the European genus *Ctenurella* Ørvig, 1960. *Geodiversitas* **19**:515–555.
Long JA, Barwick RE, Campbell KSW. 1997. Osteology and functional morphology of the osteolepiform fish *Gogonasus andrewsae* Long, 1985, from the Upper Devonian Gogo Formation, Western Australia. *Records of the Western Australian Museum Supplement* **53**:1–89.
Long JA, Young GC, Holland T, Senden TJ, Fitzgerald EMG. 2006. An exceptional Devonian fish from Australia sheds light on tetrapod origins. *Nature* **444**:199–202. DOI: https://doi.org/10.1038/nature05243
Long JA, Trinajstic K, Young GC, Senden T. 2008. Live birth in the Devonian period. *Nature* **453**:650–652. DOI: https://doi.org/10.1038/nature06966
Long JA, Mark-Kurik E, Young GC. 2014. Taxonomic revision of buchanosteoid placoderms (Arthrodira) from the Early Devonian of south-eastern Australia and Arctic Russia. *Australian Journal of Zoology* **62**:26–43. DOI: https://doi.org/10.1071/ZO13081
Long JA, Mark-Kurik E, Johanson Z, Lee MS, Young GC, Min Z, Ahlberg PE, Newman M, Jones R, den Blaauwen J, Choo B, Trinajstic K. 2015. Copulation in antiarch placoderms and the origin of gnathostome internal fertilization. *Nature* **517**:196–199. DOI: https://doi.org/10.1038/nature13825, PMID: 25327249
Lu J, Zhu M, Long JA, Zhao W, Senden TJ, Jia L, Qiao T. 2012. The earliest known stem-tetrapod from the Lower Devonian of China. *Nature Communications* **3**:1160. DOI: https://doi.org/10.1038/ncomms2170, PMID: 23093197
Lu J, Giles S, Friedman M, den Blaauwen JL, Zhu M. 2016a. The oldest actinopterygian highlights the cryptic early history of the hyperdiverse ray-finned fishes. *Current Biology* **26**:1602–1608. DOI: https://doi.org/10.1016/j.cub.2016.04.045, PMID: 27212403

Lu J, Zhu M, Ahlberg PE, Qiao T, Zhu Y, Zhao W, Jia L. 2016b. A Devonian predatory fish provides insights into the early evolution of modern sarcopterygians. *Science Advances* **2**:e1600154. DOI: https://doi.org/10.1126/sciadv.1600154, PMID: 27386576

Lu J, Giles S, Friedman M, Zhu M. 2017. A new stem sarcopterygian illuminates patterns of character evolution in early bony fishes. *Nature Communications* **8**:1932. DOI: https://doi.org/10.1038/s41467-017-01801-z, PMID: 29203766

Lu J, Young G, Hu Y-Z, Qiao T, Zhu M. 2019. The posterior cranial portion of the earliest known tetrapodomorph *Tungsenia paradoxa* and the early evolution of tetrapodomorph endocrania. *Vertebrata PalAsiatica* **57**:93–104.

Lu J, Zhu M. 2009. An onychodont fish (Osteichthyes, Sarcopterygii) from the Early Devonian of China, and the evolution of the Onychodontiformes. *Proceedings of the Royal Society B: Biological Sciences* **277**:293–299. DOI: https://doi.org/10.1098/rspb.2009.0708

Lund R, Poplin C, McCarthy K. 1995. Preliminary analysis of the interrelationships of some Paleozoic Actinopterygii. *Geobios* **28**:215–220. DOI: https://doi.org/10.1016/S0016-6995(95)80117-0

Lunter G, Miklós I, Drummond A, Jensen J, Hein J. 2005. Bayesian coestimation of phylogeny and sequence alignment. *BMC Bioinformatics* **6**:83. DOI: https://doi.org/10.1186/1471-2105-6-83

Maisey JG. 1989. *Hamiltonichthys mapesi, g. & sp. nov. (Chondrichthyes, Elasmobranchii), from the Upper Pennsylvanian of Kansas*: American Museum Novitates.

Maisey JG. 2001. A primitive chondrichthyan braincase from the Middle Devonian of Bolivia. In: Ahlberg PE (Ed). *Major Events in Early Vertebrate Evolution*. Taylor and Francis. p. 263–288.

Maisey JG. 2005. Braincase of the Upper Devonian shark *Cladodoides wildungensis* (Chondrichthyes, Elasmobranchii), with observations on the braincase in early chondrichthyans. *Bulletin of the American Museum of Natural History* **288**:1–103. DOI: https://doi.org/10.1206/0003-0090(2005)288<0001:BOTUDS>2.0.CO;2

Maisey JG. 2007. The braincase in Paleozoic symmoriiform and cladoselachian sharks. *Bulletin of the American Museum of Natural History* **307**:1–122. DOI: https://doi.org/10.1206/0003-0090(2007)307[1:TBIPSA]2.0.CO;2

Maisey JG, Miller R, Turner S. 2009. The braincase of the chondrichthyan *Doliodus* from the Lower Devonian Campbellton Formation of New Brunswick, Canada. *Acta Zoologica* **90**:109–122. DOI: https://doi.org/10.1111/j.1463-6395.2008.00330.x

Maisey JG, Turner S, Naylor GJ, Miller RF. 2014. Dental patterning in the earliest sharks: implications for tooth evolution. *Journal of Morphology* **275**:586–596. DOI: https://doi.org/10.1002/jmor.20242, PMID: 24347366

Maisey JG, Miller R, Pradel A, Denton JSS, Bronson A, Janvier P. 2017. Pectoral morphology in *Doliodus*: bridging the 'acanthodian'-chondrichthyan divide. *American Museum Novitates* **2017**:1–15.

Maisey JG, Janvier P, Pradel A, Denton JSS, Bronson A, Miller R, Burrow CJ. 2018. *Doliodus* and pucapampellids: contrasting perspectives on stem chondrichthyan morphology. In: Johanson Z, Underwood C. J, Richter M (Eds). *Evolution and Development of Fishes*. Cambridge University Press. p. 87–109.

Miles RS. 1967. Observations on the ptyctodont fish, *Rhamphodopsis* Watson. *Journal of the Linnean Society of London, Zoology* **47**:99–120. DOI: https://doi.org/10.1111/j.1096-3642.1967.tb01398.x

Miles RS. 1971. The Holonematidae (placoderm fishes), a review based on new specimens of *Holonema* from the Upper Devonian of Western Australia. *Philosophical Transactions of the Royal Society of London. B* **263**:101–234.

Miles RS. 1973a. *Articulated Acanthodian Fishes from the Old Red Sandstone of England, with a Review of the Structure and Evolution of the Acanthodian Shoulder-Girdle*. Bulletin of the British Museum (Natural History) Geology.

Miles RS. 1973b. Relationships of acanthodians. In: Greenwood P. H, Miles R. S (Eds). *Interrelationships of Fishes*. Zoological Journal of the Linnean Society. p. 63–103.

Miles RS. 1977. Dipnoan (lungfish) skulls and the relationships of the group: a study based on new species from the Devonian of Australia. *Zoological Journal of the Linnean Society* **61**:1–328. DOI: https://doi.org/10.1111/j.1096-3642.1977.tb01031.x

Miles RS, Dennis K. 1979. A primitive eubrachythoracid arthrodire from Gogo, Western Australia. *Zoological Journal of the Linnean Society* **66**:31–62. DOI: https://doi.org/10.1111/j.1096-3642.1979.tb01900.x

Miles RS, Westoll TS. 1968. IX.—The placoderm fish *Coccosteus cuspidatus* Miller ex Agassiz from the Middle Old Red Sandstone of Scotland. Part I. descriptive morphology . *Transactions of the Royal Society of Edinburgh* **67**:373–476. DOI: https://doi.org/10.1017/S0080456800024078

Miller RF, Cloutier R, Turner S. 2003. The oldest articulated chondrichthyan from the Early Devonian period. *Nature* **425**:501–504. DOI: https://doi.org/10.1038/nature02001

Moy-Thomas JA. 1935. The structure and affinities of *Chondrenchelys problematica* Tr. Proceedings of the Zoological Society of London p. 391–404.

Moy-Thomas JA. 1936. On the structure and affinities of the Carboniferous cochliodont *Helodus simplex* . *Geological Magazine* **73**:488–503. DOI: https://doi.org/10.1017/S0016756800095212

Newman MJ, Burrow CJ, Den Blaauwen JL, Davidson RG. 2014. The Early Devonian acanthodian *Euthacanthus macnicoli* Powrie, 1864 from the Midland Valley of Scotland. *Geodiversitas* **36**:321–348. DOI: https://doi.org/10.5252/g2014n3a1

O'Reilly JE, Donoghue PCJ. 2018. The efficacy of consensus tree methods for summarizing phylogenetic relationships from a posterior sample of trees estimated from morphological data. *Systematic Biology* **67**:354–362. DOI: https://doi.org/10.1093/sysbio/syx086, PMID: 29106675

O'Reilly JE, Donoghue PCJ. 2020. The effect of fossil sampling on the estimation of divergence times with the fossilized birth-death process. *Systematic Biology* **69**:124–138. DOI: https://doi.org/10.1093/sysbio/syz037, PMID: 31127936

Ørvig T. 1975. Description, with special reference to the dermal skeleton, of a new radotinid arthrodire from the Gedinnian of Arctic Canada. *Colloques Internationaux du Centre National de la Recherche Scientifique* **218** 43–71.
Pan Z, Zhu M, Zhu Y, Jia L. 2015. A new petalichthyid placoderm from the Early Devonian of Yunnan, China. *Comptes Rendus Palevol* **14**:125–137. DOI: https://doi.org/10.1016/j.crpv.2014.10.006
Paradis E, Schliep K. 2019. Ape 5.0: an environment for modern phylogenetics and evolutionary analyses in R. *Bioinformatics* **35**:526–528. DOI: https://doi.org/10.1093/bioinformatics/bty633, PMID: 30016406
Parrington FR. 1950. The skull of *Dipterus*. *Journal of Natural History* **3**:534–547.
Patterson C. 1982a. Morphological characters and homology. In: Joysey K. A, Friday A. F (Eds). *Problems of Phylogenetic Reconstruction*. Academic Press. p. 21–74.
Patterson C. 1982b. Morphology and interrelationships of primitive actinopterygian fishes. *American Zoologist* **22**:241–259. DOI: https://doi.org/10.1093/icb/22.2.241
Patterson C. 1988. Homology in classical and molecular biology. *Molecular Biology and Evolution* **5**:603–625. DOI: https://doi.org/10.1093/oxfordjournals.molbev.a040523, PMID: 3065587
Pearson DM, Westoll TS. 1979. The Devonian actinopterygian *Cheirolepis* Agassiz. *Earth and Environmental Science Transactions of the Royal Society of Edinburgh* **70**:337–399. DOI: https://doi.org/10.1017/S0080456800012850
Pinna MCC. 1991. Concepts and tests of homology in the cladistic paradigm. *Cladistics* **7**:367–394. DOI: https://doi.org/10.1111/j.1096-0031.1991.tb00045.x
Porro LB, Rayfield EJ, Clack JA. 2015. Computed tomography, anatomical description and three-dimensional reconstruction of the lower jaw of *Eusthenopteron foordi* Whiteaves, 1881 from the Upper Devonian of Canada. *Palaeontology* **58**:1031–1047. DOI: https://doi.org/10.1111/pala.12192
Pradel A, Maisey JG, Tafforeau P, Janvier P. 2009. An enigmatic gnathostome vertebrate skull from the Middle Devonian of Bolivia. *Acta Zoologica* **90**:123–133. DOI: https://doi.org/10.1111/j.1463-6395.2008.00350.x
Pradel A, Tafforeau P, Maisey JG, Janvier P. 2011. A new Paleozoic Symmoriiformes (Chondrichthyes) from the Late Carboniferous of Kansas (USA) and cladistic analysis of early chondrichthyans. *PLOS ONE* **6**:e24938. DOI: https://doi.org/10.1371/journal.pone.0024938, PMID: 21980367
Qiao T, King B, Long JA, Ahlberg PE, Zhu M. 2016. Early gnathostome phylogeny revisited: multiple method consensus. *PLOS ONE* **11**:e0163157. DOI: https://doi.org/10.1371/journal.pone.0163157, PMID: 27649538
Qiao T, Zhu M. 2010. Cranial morphology of the Silurian sarcopterygian *Guiyu oneiros* (Gnathostomata: Osteichthyes). *Science China Earth Sciences* **53**:1836–1848. DOI: https://doi.org/10.1007/s11430-010-4089-6
R Development Core Team. 2018. R: A language and environment for statistical computing. Vienna, Austria, R foundation for Statistical Computing. https://www.R-project.org/
Rambaut A, Drummond AJ, Xie D, Baele G, Suchard MA. 2018. Posterior summarization in Bayesian phylogenetics using Tracer 1.7. *Systematic Biology* **67**:901–904. DOI: https://doi.org/10.1093/sysbio/syy032, PMID: 29718447
Ramírez MJ. 2007. Homology as a parsimony problem: a dynamic homology approach for morphological data. *Cladistics* **23**:588–612. DOI: https://doi.org/10.1111/j.1096-0031.2007.00162.x
Rayner DH. 1952. III.—On the cranial structure of an early palæoniscid, *Kentuckia*, gen. nov. *Transactions of the Royal Society of Edinburgh* **62**:53–83. DOI: https://doi.org/10.1017/S0080456800009248
Redelings BD, Suchard MA. 2005. Joint bayesian estimation of alignment and phylogeny. *Systematic Biology* **54**:401–418. DOI: https://doi.org/10.1080/10635150590947041, PMID: 16012107
Rieppel O. 1996. Testing homology by congruence: the pectoral girdle of turtles. *Proceedings of the Royal Society of London. Series B, Biological Sciences* **263**:1395–1398. DOI: https://doi.org/10.1098/rspb.1996.0204
Ritchie A. 1973. Wuttagoonaspis gen. nov., an unusual arthrodire from the devonian of western new South Wales, Australia. *Palaeontographica Abteilung a Palaeozoologie-Stratigraphie* **143**:58–72.
Ritchie A. 2005. *Cowralepis*, a new genus of phyllolepid fish (Pisces, Placodermi) from the late Middle Devonian of New South Wales, Australia. Proceedings of the Linnean Society of New South Wales 215–259.
Robertson GM. 1938a. The Trematraspidae; Part I. *American Journal of Science* **s5-35**:172–206. DOI: https://doi.org/10.2475/ajs.s5-35.207.172
Robertson GM. 1938b. The Trematraspidae; Part II. *American Journal of Science* **s5-35**:273–296. DOI: https://doi.org/10.2475/ajs.s5-35.208.273
Robertson GM. 1939. An upper Silurian vertebrate horizon, with description of a new species, *Cephalaspis oeselensis*. Transactions of the Kansas Academy of Science 357–363.
Rosa BB, Melo GAR, Barbeitos MS. 2019. Homoplasy-based partitioning outperforms alternatives in Bayesian analysis of discrete morphological data. *Systematic Biology* **68**:657–671. DOI: https://doi.org/10.1093/sysbio/syz001, PMID: 30649562
Rutishauser R, Moline P. 2005. Evo-devo and the search for homology ("sameness") in biological systems. *Theory in Biosciences* **124**:213–241. DOI: https://doi.org/10.1007/BF02814485, PMID: 17046357
Sallan L, Friedman M, Sansom RS, Bird CM, Sansom IJ. 2018. The nearshore cradle of early vertebrate diversification. *Science* **362**:460–464. DOI: https://doi.org/10.1126/science.aar3689, PMID: 30361374
Sansom RS. 2009. Phylogeny, classification and character polarity of the Osteostraci (Vertebrata). *Journal of Systematic Palaeontology* **7**:95–115. DOI: https://doi.org/10.1017/S1477201908002551
Schaeffer B. 1981. The xenacanth shark neurocranium, with comments on elasmobranch monophyly. *Bulletin of the American Museum of Natural History* **169**:3–66.
Schultze H-P. 1968. *Palaeoniscoidea-Schuppen aus dem Unterdevon Australiens und Kanadas und aus dem Mitteldevon Spitzbergens*. Bulletin of the British Museum (Natural History) Geology.

Schultze H-P. 2001. *Melanognathus* , a primitive dipnoan from the Lower Devonian of the Canadian Arctic and the interrelationships of Devonian dipnoans . *Journal of Vertebrate Paleontology* **21**:781–794. DOI: https://doi.org/10.1671/0272-4634(2001)021[0781:MAPDFT]2.0.CO;2

Schultze H-P, Cumbaa SL. 2001. *Dialipina* and the characters of basal actinopterygians. In: Ahlberg P (Ed). *Major Events in Early Vertebrate Evolution*. Taylor and Francis. p. 315–332.

Schultze H-P, Zidek J. 1982. Ein primitiver acanthodier (Pisces) aus dem Unterdevon Lettlands. *Paläontologische Zeitschrift* **56**:95–105.

Simmons MP. 2004. Independence of alignment and tree search. *Molecular Phylogenetics and Evolution* **31**:874–879. DOI: https://doi.org/10.1016/j.ympev.2003.10.008, PMID: 15120385

Smith MM, Chang M-M. 1990. The dentition of *Diabolepis speratus* Chang and Yu, with further consideration of its relationships and the primitive dipnoan dentition . *Journal of Vertebrate Paleontology* **10**:420–433. DOI: https://doi.org/10.1080/02724634.1990.10011826

Smith MM, Sansom IJ. 1997. Exoskeletal micro-remains of an Ordovician fish from the Harding Sandstone of Colorado. *Palaeontology* **40**:645–658.

Stensiö EA. 1922. Über zwei Coelacanthiden aus dem Oberdevon von Wildungen. *Paläontologische Zeitschrift* **4**:167–210.

Stensiö EA. 1925. On the Head of the macropetalichthyids with certain remarks on the head of the other arthrodires. *Field Museum of Natural History Publications* **232**:89–198.

Stensiö EA. 1932. *The Cephalaspids of Great Britain*: British Museum.

Stensiö EA. 1963a. *Anatomical Studies on the Arthrodiran Head*: Almqvist & Wiksell.

Stensiö EA. 1963b. *The Brain and the Cranial Nerves in Fossil, Lower Craniate Vertebrates*: Universitetsforlaget.

Stensiö EA. 1969. Elasmobranchiomorphi Placodermata Arthrodires. In: Piveteau J (Ed). *Traité de Paléontologie*. Masson. p. 71–692.

Suchard MA, Lemey P, Baele G, Ayres DL, Drummond AJ, Rambaut A. 2018. Bayesian phylogenetic and phylodynamic data integration using BEAST 1.10. *Virus Evolution* **4**:vey016. DOI: https://doi.org/10.1093/ve/vey016, PMID: 29942656

Suchard MA, Redelings BD. 2006. BAli-Phy: simultaneous Bayesian inference of alignment and phylogeny. *Bioinformatics* **22**:2047–2048. DOI: https://doi.org/10.1093/bioinformatics/btl175, PMID: 16679334

Swartz BA. 2009. Devonian actinopterygian phylogeny and evolution based on a redescription of *Stegotrachelus finlayi* . *Zoological Journal of the Linnean Society* **156**:750–784. DOI: https://doi.org/10.1111/j.1096-3642.2009.00505.x

Thomson KS. 1965. The endocranium and associated structures in the Middle Devonian rhipidistian fish *Osteolepis*. *Proceedings of the Linnean Society of London* **176**:181–195. DOI: https://doi.org/10.1111/j.1095-8312.1965.tb00943.x

Trinajstic K, Long JA, Johanson Z, Young G, Senden T. 2012. New morphological information on the ptyctodontid fishes (Placodermi, Ptyctodontida) from Western Australia. *Journal of Vertebrate Paleontology* **32**:757–780. DOI: https://doi.org/10.1080/02724634.2012.661379

Trinajstic K, Boisvert C, Long J, Maksimenko A, Johanson Z. 2015. Pelvic and reproductive structures in placoderms (stem gnathostomes). *Biological Reviews* **90**:467–501. DOI: https://doi.org/10.1111/brv.12118, PMID: 24889865

Trinajstic K, Long JA. 2009. A new genus and species of ptyctodont (Placodermi) from the Late Devonian Gneudna Formation, Western Australia, and an analysis of ptyctodont phylogeny. *Geological Magazine* **146**:743–760. DOI: https://doi.org/10.1017/S001675680900644X

Valiukevicius J. 1992. First articulated *Poracanthodes* from the Lower Devonian of Severnaya Zemlya. In: Mark-Kurik E (Ed). *Fossil Fishes as Living Animals*. Academy of Sciences of Estonia. p. 193–214.

Varón A, Vinh LS, Wheeler WC. 2010. POY version 4: phylogenetic analysis using dynamic homologies. *Cladistics* **26**:72–85. DOI: https://doi.org/10.1111/j.1096-0031.2009.00282.x

Vaškaninová V, Chen D, Tafforeau P, Johanson Z, Ekrt B, Blom H, Ahlberg PE. 2020. Marginal dentition and multiple dermal jawbones as the ancestral condition of jawed vertebrates. *Science* **369**:211–216. DOI: https://doi.org/10.1126/science.aaz9431, PMID: 32647004

Wang N-Z, Donoghue PC, Smith MM, Sansom IJ. 2005. Histology of the galeaspid dermoskeleton and endoskeleton, and the origin and early evolution of the vertebrate cranial endoskeleton. *Journal of Vertebrate Paleontology* **25**:745–756. DOI: https://doi.org/10.1671/0272-4634(2005)025[0745:HOTGDA]2.0.CO;2

Wängsjö G. 1952. The Downtonian and Devonian vertebrates of Spitsbergen. IX, morphologic and systematic studies of the Spitsbergen cephalaspids. *Norsk Polarinstitutt Skrifter* **97**:1–611.

Warren DL, Geneva AJ, Lanfear R. 2017. RWTY (R We There Yet): An R package for examining convergence of Bayesian phylogenetic analyses. *Molecular Biology and Evolution* **34**:1016–1020. DOI: https://doi.org/10.1093/molbev/msw279, PMID: 28087773

Watson DMS. 1937. The acanthodian fishes. *Philosophical Transactions of the Royal Society of London. Series B, Biological Sciences* **228**:49–146.

Westoll TS. 1936. On the structures of the dermal ethmoid shield of *Osteolepis*. *Geological Magazine* **73**:157–171. DOI: https://doi.org/10.1017/S0016756800097296

Wheeler WC. 2006. Dynamic homology and the likelihood criterion. *Cladistics* **22**:157–170. DOI: https://doi.org/10.1111/j.1096-0031.2006.00096.x

Wheeler WC, Aagesen L, Arango CP, Faivovich J, Grant T, D'Haese C, Janies D, Smith WL, Varón A, Giribet G. 2006. *Dynamic Homology and Phylogenetic Systematics: A Unified Approach Using POY*: American Museum of Natural History.

Wheeler WC, Lucaroni N, Hong L, Crowley LM, Varón A. 2015. POY version 5: phylogenetic analysis using dynamic homologies under multiple optimality criteria. *Cladistics* **31**:189–196. DOI: https://doi.org/10.1111/cla.12083
White E. 1958. On *Cephalaspis lyelli* Agassiz. *Palaeontology* **1**:99–105.
White E. 1965. *The Head of Dipterus Valenciennesi*. Bulletin of the British Museum.
White E, Toombs HA. 1972. *The Buchanosteid Arthrodires of Australia*. Bulletin of the British Museum (Natural History) Geology.
Wickham H. 2016. *Ggplot2: Elegant Graphics for Data Analysis*. Springer. DOI: https://doi.org/10.1007/978-0-387-98141-3
Williams ME. 1998. A new specimen of *Tamiobatis vetustus* (Chondrichthyes, Ctenacanthoidea) from the Late Devonian Cleveland Shale of Ohio . *Journal of Vertebrate Paleontology* **18**:251–260. DOI: https://doi.org/10.1080/02724634.1998.10011054
Young GC. 1979. New information on the structure and relationships of *Buchanosteus* (Placodermi: Euarthrodira) from the Early Devonian of New South Wales. *Zoological Journal of the Linnean Society* **66**:309–352. DOI: https://doi.org/10.1111/j.1096-3642.1979.tb01912.x
Young GC. 1980. A New Early Devonian placoderm from New South Wales, Australia, with a discussion of placoderm phylogeny. *Palaeontographica Abteilung A Palaeozoologie-Stratigraphie* **167** 10 –76.
Young GC. 1984. Reconstruction of the jaws and braincase in the Devonian placoderm fish *Bothriolepis*. *Palaeontology* **27**:635–661.
Young GC. 1985. Further petalichthyid remains (placoderm fishes, Early Devonian) from the Taemas-Wee Jasper region, New South Wales. *Bureau of Mineral Resources Journal of Australian Geology and Geophysics* **9**:121–131.
Young GC. 1986. The relationships of placoderm fishes. *Zoological Journal of the Linnean Society* **88**:1–57. DOI: https://doi.org/10.1111/j.1096-3642.1986.tb00876.x
Young GC, Burrow CJ. 2004. Diplacanthid acanthodians from the Aztec Siltstone (late Middle Devonian) of southern Victoria Land, Antarctica. *Fossils and Strata* **50**:23–43. DOI: https://doi.org/10.1017/S0954102008001521
Yu X. 1998. A new porolepiform-like fish, *Psarolepis romeri* , gen. et sp. nov. (Sarcopterygii, Osteichthyes) from the Lower Devonian of Yunnan, China . *Journal of Vertebrate Paleontology* **18**:261–274. DOI: https://doi.org/10.1080/02724634.1998.10011055
Zhang M-M. 1980. Preliminary note on a Lower Devonian antiarch from Yunnan, China. *Vertebrata PalAsiatica* **18**:179–180.
Zhang G-R, Wang J-Q, Wang N-Z. 2001. The structure of pectoral fin and tail of Yunnanolepidoidei, with a discussion of the pectoral fin of chuchinolepids. *Vertebrata PalAsiatica* **39**:9–19.
Zhang M-M, Yu X-B. 1981. A new crossopterygian, *Youngolepis praecursor*, gen. et sp. nov., from Lower Devonian of east Yunnan, China. *Scientia Sinica* **24**:89–99. DOI: https://doi.org/10.1360/ya1981-24-1-89
Zhao W-J, Zhu M, Jia L-T. 2001. New discovery of galeaspids from Early Devonian of Wenshan, Southeastern Yunnan, China. *Vertebrata Pal Asiatica* **40**:97–113.
Zhu M. 1991. New information on *Diandongpetalichthys* (Placodermi: Petalichthyida). In: Chang M. M, Liu Y. H, Zhang G. R (Eds). *Early Vertebrates and Related Problems of Evolutionary Biology*. Science Press. p. 171–194.
Zhu M. 1996. The phylogeny of the Antiarcha (Placodermi, Pisces), with the description of Early Devonian antiarchs from Qujing, Yunnan, China. Bulletin Du Muséum National d'histoire Naturelle Section C, Sciences De La Terre, Paléontologie, Géologie, Minéralogie 233–347.
Zhu M, Yu X, Janvier P. 1999. A primitive fossil fish sheds light on the origin of bony fishes. *Nature* **397**:607–610. DOI: https://doi.org/10.1038/17594
Zhu M, Yu X, Ahlberg PE. 2001. A primitive sarcopterygian fish with an eyestalk. *Nature* **410**:81–84. DOI: https://doi.org/10.1038/35065078
Zhu M, Yu X, Wang W, Zhao W, Jia L. 2006. A primitive fish provides key characters bearing on deep osteichthyan phylogeny. *Nature* **441**:77–80. DOI: https://doi.org/10.1038/nature04563, PMID: 16672968
Zhu M, Zhao W, Jia L, Lu J, Qiao T, Qu Q. 2009. The oldest articulated osteichthyan reveals mosaic gnathostome characters. *Nature* **458**:469–474. DOI: https://doi.org/10.1038/nature07855, PMID: 19325627
Zhu M, Wang W, Yu X. 2010. *Meemannia eos*, a basal sarcopterygian fish from the Lower Devonian of China–expanded description and significance. In: Elliot D, Maisey J, Yu X, Miao D (Eds). *Morphology Phylogeny and Paleobiogeography of Fossil Fishes*. Verlag Dr. Friedrich Pfeil. p. 199–214.
Zhu M, Yu X, Choo B, Wang J, Jia L. 2012. An antiarch placoderm shows that pelvic girdles arose at the root of jawed vertebrates. *Biology Letters* **8**:453–456. DOI: https://doi.org/10.1098/rsbl.2011.1033, PMID: 22219394
Zhu M, Yu X, Ahlberg PE, Choo B, Lu J, Qiao T, Qu Q, Zhao W, Jia L, Blom H, Zhu Y. 2013. A Silurian placoderm with osteichthyan-like marginal jaw bones. *Nature* **502**:188–193. DOI: https://doi.org/10.1038/nature12617, PMID: 24067611
Zhu M, Ahlberg PE, Pan Z, Zhu Y, Qiao T, Zhao W, Jia L, Lu J. 2016. A Silurian maxillate placoderm illuminates jaw evolution. *Science* **354**:334–336. DOI: https://doi.org/10.1126/science.aah3764, PMID: 27846567
Zhu Y-A, Ahlberg PE, Zhu M. 2019. The evolution of vertebrate dermal jaw bones in the light of maxillate placoderms. *Evolution and Development of Fishes* **1**:71–86. DOI: https://doi.org/10.1017/9781316832172.005
Zhu M, Ahlberg PE. 2004. The origin of the internal nostril of tetrapods. *Nature* **432**:94–97. DOI: https://doi.org/10.1038/nature02843, PMID: 15525987
Zhu M, Gai Z. 2007. Phylogenetic relationships of galeaspids (Agnatha). *Frontiers of Biology in China* **2**:151–169. DOI: https://doi.org/10.1007/s11515-007-0022-6

Zhu M, Schultze HP. 2001. Interrelationships of basal osteichthyans. In: Ahlberg P. E (Ed). *Major Events in Early Vertebrate Evolution*. Taylor and Francis. p. 289–314.

Zhu M, Yu X. 2002. A primitive fish close to the common ancestor of tetrapods and lungfish. *Nature* **418**:767–770. DOI: https://doi.org/10.1038/nature00871, PMID: 12181564

Zhu M, Yu X. 2004. Lower jaw character transitions among major sarcopterygian groups—a survey based on new materials from Yunnan, China. In: Arratia G, Wilson M. V. H, Cloutier R (Eds). *Recent Advances in the Origin and Early Radiation of Vertebrates*. Verlag Dr. Friedrich Pfeil. p. 271–286.

Zhu M, Yu X. 2009. Stem sarcopterygians have primitive polybasal fin articulation. *Biology Letters* **5**:372–375. DOI: https://doi.org/10.1098/rsbl.2008.0784, PMID: 19324642

Appendix 1

Sensitivity analysis

Bayesian tip-dated analysis may be sensitive to incomplete taxon sampling (***O'Reilly and Donoghue, 2020***). The fossil record of early gnathostomes may be biased by the nearshore origination of the major groups (***Sallan et al., 2018***). One example of a possible bias are the antiarchs. The earliest antiarch included in our dataset is the Lochkovian *Yunnanolepis*. However, the antiarch *Shimenolepis* is known from the Silurian (Ludlow) of China, although its fragmentary remains provide few characters for phylogenetic analysis.

To test the effect of Silurian antiarchs on our results we reanalyzed the data with a Ludlow age assigned to *Yunnanolepis*. The major results of the analysis were unchanged, although there was a slight increase in uncertainty. Core placoderm monophyly was supported (pp = 0.98, down from 1.0), with maxillate placoderms as sister group to core placoderms (pp = 0.52, down from 0.70). Homology of arthrodire gnathal plates and the premaxilla/maxilla was supported (pp = 0.98, down from 0.984). Phenetic analysis supported maxillate placoderms as the least diverged known gnathostomes (pp = 0.87, down from 0.95). There was increased support for a member of the core placoderms being the least diverged gnathostome (***Appendix 1—figure 1***), with *Diandongpetalichthys* accounting for most of that probability. Support for key character states at the gnathostome node was slightly reduced (***Appendix 1—table 1***). Overall, this sensitivity shows that our conclusions are robust to at least some issues regarding fossil sampling. However, future studies should aim to further explore the effect of taxon sampling on results.

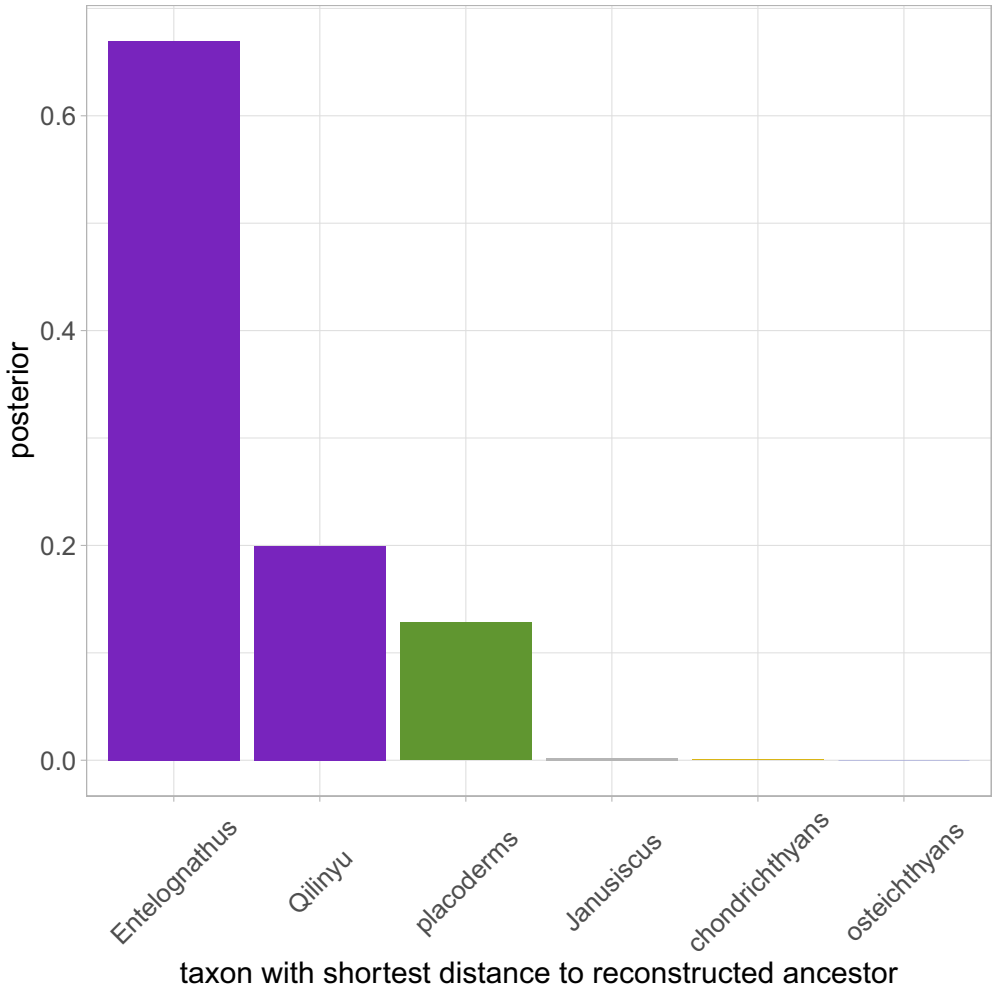

Appendix 1—figure 1. Frequency plot of the taxon with the shortest distance to the reconstructed

Appendix 1—figure 1 continued on next page

Appendix 1—figure 1 continued

ancestor across the whole posterior sample (n = 1801), when data is analysed with a Silurian age for *Yunnanolepis*.

Appendix 1—table 1. Probabilities of key character states at the gnathostome node, when data is analysed with a Silurian age for *Yunnanolepis*.

Character	Reconstructed ancestral state	Posterior probability
Premaxilla	Present	0.97
Maxilla	Present	0.92
Facial laminae	Present	0.89
Palatal laminae	Present	0.97
Vomer	Absent	0.96
Dermopalatine	Absent	0.88
Nasal capsules	Anterior/ventral	0.85
Orbit dorsal, surrounded by neurocranium	Absent	0.96
Claspers	Absent	0.76
Optic fissure	Absent	0.69

Appendix 2

Sources for taxa and age ranges

Hemicyclaspis murchisoni

Stensiö, 1932

Shropshire Downtownian. Pridoli, 423–419.2 Ma.

Cephalaspis lyelli

Stensiö, 1932; **White, 1958**

Lower Old Red Sandstone, Glammis. Lochkovian, 419.2–410.8 Ma.

Zenaspis salweyi

Stensiö, 1932

Lower Old Red Sandstone. Skirrid Fawr, Senni/St Maughans Formation. Lochkovian, 419.2–410.8 Ma.

Benneviaspis holtedahli

Janvier, 1985a

Ben Nevis Formation, Red bBay Group. Late Lochkovian, 413.6–410.8 Ma.

Boreaspis macrorhynchus

Janvier, 1985a

Wood Bay Formation. Early Pragian, 410.8–409.7 Ma.

Norselaspis glacialis

Janvier, 1981

Wood Bay Formation. Early Pragian, 410.8–409.7 Ma.

Nectaspis areolate

Wängsjö, 1952, (**Janvier, 1981**)

Wood Bay Formation. Late Pragian, 408.7–407.6 Ma.

Procephalaspis oeselensis

Robertson, 1939; **Denison, 1951**; **Janvier, 1985b**

Saaremaa. Ludlow, 427.4–423 Ma.

Trematapis mammillata

Robertson, 1938a; **Robertson, 1938b**; **Denison, 1947**; **Denison, 1951**; **Janvier, 1985b**

Saaremaa. Ludlow, 427.4–423 Ma.

Waengsjoeaspis excellens

Wängsjö, 1952; **Janvier, 1985a**

Fraenkelryggen Formation. Late Lochkovian, 413.6–410.8 Ma.

Escuminaspis laticeps

Janvier et al., 2004

Escuminac Formation. Early Frasnian, 382.7–379.2 Ma.

Eugaleaspis changi

Liu, 1965; **Zhu and Gai, 2007**

Xitun Formation, Liaojaoshan. Late Lochkovian, 413.6–410.8 Ma.

Hanyangaspis guodingshanensis

Zhu and Gai, 2007

Guodingshan Formation. Telychian, 438.5–433.4 Ma.

Polybranchiaspis liaojiaoshanensis

Liu, 1965; **Liu, 1975**

Xishancun and Xitun Formations. Lochkovian, 419.2–410.8 Ma.

Bannhuanaspis vukhuci

Janvier et al., 1993

Bac Bun Formation. Late Lochkovian–early Pragian, 413.6–409.7 Ma.

Wenshanaspis zhichangensis

Zhao et al., 2001

Posongchong Formation, Wenshan. Pragian, 410.8–407.6 Ma.

Shuyu zhejiangensis

Gai et al., 2011

Maoshan Formation. Late Telychian–early Wenlock, 435.1–431.4 Ma.

Polybranchiaspid sp histological samples

Wang et al., 2005

Xishancun and Xitun Formations. Lochkovian, 419.2–410.8 Ma.

Yunnanolepis sp

Zhang, 1980; **Zhu, 1996**

Xishancun and Xitun Formations. Lochkovian, 419.2–410.8 Ma.

Parayunnanolepis xitunensis

Zhang et al., 2001; **Zhu et al., 2012**

Xitun Formation. Late Lochkovian, 413.6–410.8 Ma.

Microbrachius dicki

Hemmings, 1978; **Long et al., 2015**

Eday Flagstone and John O'Groats Sandstone. Lower–middle Givetian, 387.7–384.4 Ma.

Bothriolepis sp Gogo

Young, 1984

Gogo Formation. Early Frasnian, 382.7–379.2 Ma.

Bothriolepis canadensis

Downs and Donoghue, 2009; **Béchard et al., 2014**

Escuminac Formation. Early Frasnian, 382.7–379.2 Ma.

Pterichthyodes milleri

Hemmings, 1978

Achanarras Horizon. Late Eifelian, 389.6–387.7 Ma.

Remigolepis walkeri

Johanson, 1997

Canowindra. Famennian, 372.2–358.9 Ma.

Diandongpetalichthys liaojiaoshanensis

Zhu, 1991

Xishancun Formation. Lochkovian, 419.2–410.8 Ma.

Quasipetalichthys haikouensis

Liu, 1991

Shixiagou Formation, Ninxia. Givetian, 387.7–382.7 Ma.

Eurycaraspis incilis

(**Liu, 1991**)

Haikou Formation. Givetian, 387.7–382.7 Ma.

Lunaspis broili

Gross, 1961

Hunsrueck Slate. Late Pragian–early Emsian, 408.7–402.8 Ma.

Shearsbyaspis oepiki

Young, 1985; **Castiello and Brazeau, 2018**

Taemas-Wee Jasper. Emsian, 407.6–393.3 Ma.

Macropetalichthys rapheidolabis

Stensiö, 1925; **Stensiö, 1963b**; **Stensiö, 1969**

Onondaga Limetone. Eifelian, 393.3–387.7 Ma.

Cowralepis mclachlani

Ritchie, 2005; **Carr et al., 2009**

Merriganowry Shale. Late Givetian–early Frasnian, 384.4–379.2 Ma.

Sigaspis lepidophora

Goujet, 1973

Wood Bay Formation. Early Pragian, 410.8–409.7 Ma.

Kujdanowiaspis podolica

Stensiö, 1963a; **Dupret, 2010**

Dnister Series, Podolia. Late Lockhovian–lower Pragian, 413.6–409.7 Ma.

Lehmanosteus hyperboreus

Goujet, 1984a

Wood Bay Formation. Early Pragian, 410.8–409.7 Ma.

Dicksonosteus arcticus

Goujet, 1975; **Goujet, 1984b**

Wood Bay Formation. Early Pragian, 410.8–409.7 Ma.

Groenlandaspis sp Mt Howitt

Specimens listed in **King et al., 2017**

Mt. Howitt. Givetian, 387.7–382.7 Ma.

Buchanosteus confertituberculatus

Burrow and Turner, 1998; **Long et al., 2014**

Buchan. Middle–late Pragian, 409.7–407.6 Ma.

Parabuchanosteus murrumbidgeensis

White and Toombs, 1972; **Young, 1979**; **Burrow and Turner, 1998**

Taemas-Wee Jasper. Emsian, 407.6–393.3 Ma.

Holonema westolli

Miles, 1971

Gogo Formation. Early Frasnian, 382.7–379.2 Ma.

Coccosteus cuspidatus

Miles and Westoll, 1968

Achanarras and Edderton fish bed. Eifelian-Givetian boundary, 394.5–392.1 Ma.

Incisoscutum ritchiei

Dennis and Miles, 1981; **Giles et al., 2013**

Gogo Formation. Early Frasnian, 382.7–379.2 Ma.

Eastmanosteus calliaspis

Dennis-Bryan, 1987

Gogo Formation. Early Frasnian, 382.7–379.2 Ma.

Compagopiscis croucheri

Gardiner and Miles, 1994

Gogo Formation. Early Frasnian, 382.7–379.2 Ma.

Materpiscis attenboroughi

Long et al., 2008; **Trinajstic et al., 2012**

Gogo Formation. Early Frasnian, 382.7–379.2 Ma.

Austroptyctodus gardineri

Long, 1997

Gogo Formation. Early Frasnian, 382.7–379.2 Ma.

Campbellodus decipiens

Long, 1997

Gogo Formation. Early Frasnian, 382.7–379.2 Ma.

Rhamphodopsis threiplandi

Miles, 1967; (**Long, 1997**)

Edderton Fish Beds. Eifelian-Givetian boundary, 394.5–392.1 Ma.

Brindabellaspis stensioi

Young, 1980; **King et al., 2018**

Taemas-Wee Jasper. Emsian, 407.6–393.3 Ma.

Romundina stellina

Ørvig, 1975; **Dupret et al., 2014**; **Dupret et al., 2017**

Prince of Wales Island. Lochkovian, 419.2–410.8 Ma.

Jagorina pandora

Stensiö, 1969; **Young, 1986**

Kellwasserkalk, Bad Wildungen. Late Frasnian, 375.7–372.2 Ma.

Gemuendina stuertzi

Gross, 1963

Hunsrueck Slate. Late Pragian–early Emsian, 408.7–402.8 Ma.

Entelognathus primordialis

Zhu et al., 2013

Kuanti Formation. Ludlow, 427.4–423 Ma.

Qilinyu rostrata

Zhu et al., 2016

Kuanti Formation. Ludlow, 427.4–423 Ma.

Janusiscus schultzei

Giles et al., 2015c

Lower Member, Kureika Formation. Middle Lockhovian, 416.4–413.6 Ma.

Nerepisacanthus denisoni

Burrow, 2011; **Burrow and Rudkin, 2014**

Bertie Formation. Ludlow–Pridoli, 427.4–419.2 Ma.

Poracanthodes menneri

Valiukevicius, 1992

Severnaya Zemlya Formation. Early Lockhovian, 419.2–416.4 Ma.

Ischnacanthus gracilis

Watson, 1937; **Miles, 1973a**; **Burrow et al., 2018**

'Turin Hill'. Lochkovian, 419.2–410.8 Ma.

Tetanopsyrus lindoei/breviacanthias

Gagnier et al., 1999; **Hanke et al., 2001**

MOTH. Lochkovian, 419.2–410.8 Ma.

Diplacanthus crassisimus

Watson, 1937; **Miles, 1973a**; **Burrow et al., 2016**

Moray Firth and Achanarras. Eifelian-Givetian boundary, 394.5–392.1 Ma.

Milesacanthus antarctica

Young and Burrow, 2004

Aztec Siltstone. Givetian, 387.7–382.7 Ma.

Culmacanthus stewarti

Long, 1983

Mt Howitt. Givetian, 387.7–382.7 Ma.

Euthacanthus macnicoli

Watson, 1937; **Miles, 1973a**; **Newman et al., 2014**

'Turin Hill'. Lockhovian, 419.2–410.8 Ma.

Cassidiceps vermiculatus

Gagnier and Wilson, 1996

MOTH. Lockhovian, 419.2–410.8 Ma.

Promesacanthus eppleri

Hanke, 2008

MOTH. Lochkovian, 419.2–410.8 Ma.

Mesacanthus mitchelli

Watson, 1937; **Miles, 1973a**

'Turin Hill' and Farnell. Lochkovian, 419.2–410.8 Ma.

Cheiracanthus sp

Watson, 1937; **Miles, 1973a**

Middle Old Red Sandstone, Moray Firth. Nodular Fish Beds. Eifelian–Givetian, 393.3–382.7 Ma.

Homalacanthus concinnus

Gagnier, 1996

Escuminac Formation. Early Frasnian, 382.7–379.2 Ma.

Acanthodes bronni

Gross, 1935; **Watson, 1937**; **Miles, 1973a**; **Miles, 1973b**; **Coates, 1994**; **Davis et al., 2012**; **Brazeau and de Winter, 2015**

Lebach ilronstone. Asselian, 298.9–293.5 Ma.

Ptomacanthus anglicus

Miles, 1973a; **Brazeau, 2009**; **Brazeau, 2012**; **Dearden et al., 2019**

Wayne Herbert Quarry. Lochkovian, 419.2–410.8 Ma.

Climatius reticulatus

Watson, 1937; **Miles, 1973a**; **Burrow et al., 2015**

'Turin Hill'. Lockhovian, 419.2–410.8 Ma.

Vernicomacanthus waynensis

Miles, 1973a

Wayne Herbert Quarry. Lochkovian, 419.2–410.8 Ma.

Parexus recurvus

Watson, 1937; **Miles, 1973a**; **Burrow et al., 2013**

'Turin Hill'. Lochkovian, 419.2–410.8 Ma.

Latviacanthus ventspilsensis

Schultze and Zidek, 1982

Ventspils. Kemeri stage. Pragian, 410.8–407.6 Ma.

Brachyacanthus scutiger

Watson, 1937

Lower Old Red Sandstone, Farnell. Lockhovian, 419.2–410.8 Ma.

Brochoadmones milesi

Hanke and Wilson, 2006

MOTH. Lockhovian, 419.2–410.8 Ma.

Gladiobranchus probaton

Hanke and Davis, 2008

MOTH. Lochkovian, 419.2–410.8 Ma.

Kathemacanthus rosulentus

Gagnier and Wilson, 1996; **Hanke and Wilson, 2010**

MOTH. Lochkovian, 419.2–410.8 Ma.

Lupopsyrus pygmaeus

Hanke and Davis, 2012

MOTH. Lochkovian, 419.2–410.8 Ma.

Obtusacanthus corroconis

Hanke and Wilson, 2004

MOTH. Lochkovian, 419.2–410.8 Ma.

Gladbachus adentatus

Coates et al., 2018

Lower Plattenkalk. Late Givetian, 382.7–384.4 Ma.

Cladodoides wildungensis

Maisey, 2005

Wildungen Limestone. Late Frasnian, 375.7–372.2 Ma.

Akmonistion zangerli

Coates and Sequeira, 1998; **Coates et al., 1998**; **Coates and Sequeira, 2001**

Manse Burn Formation, Bearsden. Serpukhovian, 330.9–323.2 Ma.

Cobelodus braincase

Maisey, 2007

Fayetteville Formation. Chesterian, 333–318.1 Ma.

Cladoselache kepleri/fyleri

Harris, 1938; **Bendix-Almgreen, 1975**; **Schaeffer, 1981**; **Maisey, 2007**

Cleveland Member of Ohio Shale. Late Famennian, 363.3–358.9 Ma.

Chondrenchelys problematica

Moy-Thomas, 1935; **Finarelli and Coates, 2011**; **Finarelli and Coates, 2014**

Glencartholm Volcanic Beds. Holkerian, 339–337.5 Ma.

Helodus simplex

Moy-Thomas, 1936

Fenton, Staffordshire. Moscovian, 315.2–307 Ma.

Debeerius ellefseni

Grogan and Lund, 2000

Bear Gulch Limestone. Upper Chesterian, 323.1–318.1 Ma.

Doliodus latispinosus

Miller et al., 2003; **Maisey et al., 2009**; **Maisey et al., 2014**; **Maisey et al., 2017**; **Maisey et al., 2018**

'Atholville Beds', Campbellton Formation. Emsian–Eifelian, 407.6–391.4 Ma.

Hamiltonichthys mapesi

Maisey, 1989

Hartford Limetone, Hamilton Quarry. Middle Virgilian, 303.7–298.9 Ma.

Onychoselache traquari

Dick and Maisey, 1980; **Coates and Gess, 2007**

Glencartholm Volcanic Beds and Wardie Shales. Holkerian-Asbian, 339–333 Ma.

Orthacanthus sp

Schaeffer, 1981

Admiral fFormation. Wolfcampian, 299–280 Ma.

Pucapampella rodrigae

Maisey, 2001; **Maisey et al., 2018**

Sica Sica Formation. Eifelian–Givetian, 393.3–382.7 Ma.

Tamiobatis vetustus

Schaeffer, 1981; **Williams, 1998**

Cleveland Shale and Salem lLimestone. Famennian, Early Visean, 372.2–358.9 Ma.

Tristychius arcuatus

Dick, 1978; **Coates and Gess, 2007**; **Coates and Tietjen, 2018**

Wardie Shales and Manse Burn Formation, Bearsden. Late Visean–lower Serpukhovian, 336.2–328.3 Ma.

Dialipina salgueiroensis

Schultze, 1968; **Schultze and Cumbaa, 2001**

Bear Rock Formation. Emsian, 407.6–393.3 Ma.

Ligulalepis braincase

Basden et al., 2000; **Basden and Young, 2001**; **Clement et al., 2018**

Taemas-Wee Jasper. Emsian, 407.6–393.3 Ma.

Cheirolepis canadensis

Pearson and Westoll, 1979; **Arratia and Cloutier, 1996**

Escuminac Formation. Early Frasnian, 382.7–379.2 Ma.

Cheirolepis trailli

Pearson and Westoll, 1979; **Giles et al., 2015a**

Achanarras Limestone, Tynet Burn and Gamrie. Late Eifelian, 389.6–387.7 Ma.

Howqualepis rostridens

Long, 1988

Mt. Howitt. Givetian, 387.7–382.7 Ma.

Raynerius splendens

Giles et al., 2015b

Upper part of the Grey Member, Ferques Formation. Conodont zone, 373.5–372.5 Ma.

Mimipiscis toombsi

Gardiner and Bartram, 1977; **Gardiner, 1984**; **Giles and Friedman, 2014**
Gogo Formation. Early Frasnian, 382.7–379.2 Ma.

Moythomasia durgaringa

Gardiner, 1984
Gogo Formation. Early Frasnian, 382.7–379.2 Ma.

Kentuckia deani

Rayner, 1952; **Giles and Friedman, 2014**
New Providence Shale Member, Stockdale Formation. Tournasian-Visean boundary, 347.1–346.3 Ma.

Meemannia eos

Zhu et al., 2006; **Zhu et al., 2010**; **Lu et al., 2016a**
Xitun Formation. Late Lochkovian, 413.6–410.8 Ma.

Guiyu oneiros

Zhu et al., 2009; **Qiao and Zhu, 2010**

Psarolepis romeri

Yu, 1998; **Zhu et al., 1999**; **Zhu and Yu, 2004**; **Zhu and Yu, 2009**
Xishancun Formation. Lochkovian, 419.2–410.8 Ma.

Achoania jarvikii

Zhu et al., 2001; **Zhu and Ahlberg, 2004**; **Zhu and Yu, 2009**
Xitun Formation. Late Lochkovian, 413.6–410.8 Ma.

Qingmenodus yui

Lu and Zhu, 2009; **Lu et al., 2016b**
Posongchong Formation, Wenshan. Pragian, 410.8–407.6 Ma.

Onychodus jandemarrai

Andrews et al., 2005
Gogo Formation, Saddler Formation. Early Frasnian, 382.7–379.2 Ma.

Miguashaia bureaui

Cloutier, 1996; **Forey, 1998**
Escuminac Formation. Early Frasnian, 382.7–379.2 Ma.

Diplocercides kayseri

Stensiö, 1922; **Jarvik, 1980**; **Forey, 1998**
Wildungen Limestone. Late Frasnian, 375.7–372.2 Ma.

Styloichthys changae

Zhu and Yu, 2002; **Friedman, 2007b**

Xitun Formation. Late Lochkovian, 413.6–410.8 Ma.

Youngolepis praecursor

Zhang and Yu, 1981; **Chang, 1982**; **Chang, 1991**; **Chang and Smith, 1992**
Xitun Formation. Late Lochkovian, 413.6–410.8 Ma.

Powichthys thorsteinssoni

Jessen, 1975; **Jessen, 1980**; **Chang and Smith, 1992**
Prince of Wales Island. Late Lockhovian–early Pragian, 413.6–409.7 Ma.

Diabolepis speratus

Chang and Yu, 1984; **Smith and Chang, 1990**; **Chang, 1995**
Xitun Formation. Late Lochkovian, 413.6–410.8 Ma.

Dipterus valenciennesi

Parrington, 1950; **White, 1965**; **Ahlberg and Trewin, 1994**; **Challands, 2015**
Achanarras Limestone. Late Eifelian, 389.6–387.7 Ma.

Rhinodipterus kimberleyensis

Clement, 2012; **Clement and Ahlberg, 2014**
Gogo Formation. Early Frasnian, 382.7–379.2 Ma.

'Chirodipterus' australis

Miles, 1977; **Henderson and Challands, 2018**
Gogo fFormation. Early Frasnian, 382.7–379.2 Ma.

Porolepis sp

Jarvik, 1972; **Clement, 2004**
Wood Bay Formation. Early Pragian, 410.8–409.7 Ma.

Glyptolepis groenlandica

Jarvik, 1972; **Ahlberg, 1989**
Red Siltstone Member of the Nathorst Fjord group. Late Eifelian–early Givetian, 389.6–386 Ma.

Tungsenia paradoxa

Lu et al., 2012; **Lu et al., 2019**
Posongchong Formation, Wenshan. Pragian, 410.8–407.6 Ma.

Kenichthys campbelli

Chang and Zhu, 1993; **Zhu and Ahlberg, 2004**
Chuangdong Formation. Late Emsian, 398.1–393.3 Ma.

Osteolepis macrolepidotus

Westoll, 1936; **Thomson, 1965**; **Jarvik, 1980**
Tynet Burn. Late Eifelian, 389.6–387.7 Ma.

Gogonasus andrewsae

Long, 1985; ***Long et al., 1997***; ***Long et al., 2006***; ***Holland, 2013***; ***Holland, 2014***
Gogo Formation. Early Frasnian, 382.7–379.2 Ma.

Eusthenopteron foordi

Jarvik, 1980; ***Porro et al., 2015***
Escuminac Formation. Early Frasnian, 382.7–379.2 Ma.

Deleted taxa from *King et al., 2017*

Wuttagoonaspis fletcheri

The description of the braincase of *Wuttagoonaspis* in ***Ritchie, 1973*** does not match direct observations of specimens (by B. King). Impressions of neurocranial processes can be seen lateral to the sensory grooves in several specimens in the Australia Museum collections. However, since these observations are on unpublished specimens, for reproducibility we elected to remove the taxon.

Gavinaspis convergens

This taxon is known only from an incomplete skull roof, on which the sutures are unclear. Because of the inability to code almost all characters, this specimen was removed from the matrix. *Lehmanosteus* was added as an alternative example of an early arthrodire.

Ramirosuarezia boliviana

This is another taxon for which the vast majority of characters cannot be scored. Although the specimen consists of a braincase, almost all neurocranial features are uncertain, even the position of the optic nerve foramen. The inability to score most characters justifies removal of the taxon a priori. In addition, it is also notable that two of the suggested attributions of *Ramirosuarezia,* a decayed rhenanid braincase, or a holocephalan (***Pradel et al., 2009***), receive no support in phylogenetic analyses (e.g. ***Coates et al., 2018***). Conversely, an acanthodian identity (deemed 'unlikely' by ***Pradel et al., 2009***), receives some support in phylogenetic analysis (***Qiao et al., 2016***).

Osorioichthys marginis

Based on direct observations of the holotype specimen (by B. King), many of the characters scored from the description were unclear or could not be verified. An important character that influences the position of *Osorioichthys* is the described separation of the posterior nostril and orbit by dermal bone. However, observation of the specimen reveals that this is either an artifact of breakage, or represents the postnasal wall of the neurocranium. *Raynerius* was added as an alternative early acinopterygian with better quality preservation of many features.

Appendix 3

Character list

Histology

1. Tessellated calcified cartilage: absent (0); present (1).

Burrow et al., 2016 c1.

2. Tessellated calcified cartilage: single-layered (0); multi-layered (1).

Maisey, 2001, c17.

3. Perichondral bone: present (0); absent (1).

Donoghue et al., 2000, c63.

4. Extensive endochondral ossification: absent (0); present (1).

Zhu et al., 2001 c202; ***Brazeau, 2009*** c3.

5. Extensive pore canal network: absent (0); present (1).

Giles et al., 2015a c8.

6. Three-layered exoskeleton: absent (0); present (1).

Donoghue et al., 2000, c71.

7. Cephalic dermoskeleton bone: cellular (0); acellular (1).

Donoghue et al., 2000 c67; ***Sansom, 2009*** c73.

8. Perforated horizontal lamina in the sensory canals and vascular system: absent (0); present (1).

Sansom, 2009 c85.

9. Galeaspidin: absent (0); present (1).

Sansom, 2009 c87.

10. Dentine: absent (0); present (1).

Brazeau, 2009 c4.

11. Dentine kind: mesodentine (0); semidentine (1); orthodentine (2).

Brazeau, 2009 c5.

12. Bone cell lacunae in body scale bases: present (0); absent (1).

Burrow and Turner, 2010 c61.

13. Main dentinous tissue forming fin spine: osteodentine (0); orthodentine (1).

Burrow and Turner, 2010 c60.

14. Resorption and redeposition of odontodes: absent or partially developed (0); present (1).

Zhu et al., 2006 c122.

15. Enamel(oid) present on dermal bones and scales: absent (0); present (1).

Giles et al., 2015b c5.

16. Enamel: single-layered (0); multi-layered (1).

Giles et al., 2015a c6.

17. Enamel layers: applied directly to one another (ganoine) (0); separated by layers of dentine (1).

Giles et al., 2015b c7.

Braincase proportions

18. Nasal opening(s): dorsal, placed between orbits (0); ventral and anterior to orbits (1).

Friedman, 2007a c142.

19. Nasal capsules in anterlolateral corners of orbit: no (0); yes (1).

King et al., 2017 c96.

20. Elongate preorbital region between orbits and nasal capsules: absent (0); present (1).

King et al., 2017 c22.

21. Ethmoid region elongate with dorsoventrally deep lateral walls: absent (0); present (1).

Davis et al., 2012 c73.

22. Tectum orbitale/supraorbital shelf: absent or very narrow (0); present (1).

Ahlberg and Johanson, 1998b c83; ***King et al., 2017*** c102.

23. Supraorbital shelf broad with convex lateral margin: absent (0); present (1).

Coates and Sequeira, 1998 c17.

24. Orbit dorsal or facing dorsolaterally, surrounded laterally by endocranium: present (0); absent (1).

Brazeau, 2009 c68.

25. Narrow interorbital septum: absent (0); present (1).

Brazeau, 2009 c70.

26. Extended prehypophysial portion of sphenoid: absent (0); present (1).

Brazeau, 2009 c69.

27. Short otico-occipital region of braincase: absent (0); present (1).
Brazeau, 2009 c74.

28. Parachordal shape: broad, flat (0); keeled with sloping lateral margins (1).
Brazeau, 2009 c98.

29. Stalk-shaped parachordal/occipital region: absent (0); present (1).
Giles et al., 2015a c176.

30. Braincase is series of bilateral ossifications: no (0); yes (1).
King et al., 2017 c100.

Braincase processes

31. Median rostral dorsal process of braincase: absent (0); present (1).
King et al., 2017 c101.

32. Rostral processes: absent (0); present (1).
King et al., 2017 c99.

33. Postnasal wall: absent (0); present (1).
Clement et al., 2018 c281.

34. Processus supraorbitalis lateralis: absent (0); present (1).
King et al., 2017 c110.

35. Postorbital process: absent (0); present (1).
Giles et al., 2015b c132.

36. Transverse otic process: present (0); absent (1).
Giles et al., 2015c c125.

37. Transverse otic process: not extending in front of orbits (0); extending in front of orbits (1).
Jia et al., 2010 c95.

38. Branchial ridges: present (0); reduced to vagal process (1); absent (articulation made with bare cranial wall) (2).
Giles et al., 2015c c166.

39. Vagal process: forked (0); unforked (1).
Pan et al., 2015 c14; ***King et al., 2017*** c97.

40. Craniospinal process: absent (0); present (1).
Giles et al., 2015a c167.

41. Paravagal fossa: absent (0); present (1).
Pan et al., 2015 c18.

Braincase fontanelles and fissures

42. Optic fissure: present (0); absent (1).
Dupret et al., 2014 c255.

43. Ventral cranial fissure: absent (0); present (1).
Brazeau, 2009 c92.

44. Anterior margin of ventral fissure: straight (0); sinusoidal (1).
King et al., 2017 c127.

45. Endoskeletal cranial joint: absent (0); present (1).
Brazeau, 2009 c64.

46. Ventral notch between parachordals: absent (0); present or entirely unfused (1).
Brazeau, 2009 c97.

47. Parachordal plates: separated from the otic capsule (0); sutured or fused to otic capsule (1).
Friedman, 2007a c182.

48. Metotic (otic-occipital) fissure: absent (0); present (1).
Brazeau, 2009 c93.

49. Occipital arch wedged in between otic capsules: absent (0); present (1).
Coates and Sequeira, 1998 c9.

50. Precerebral fontanelle: absent (0); present (1).
Coates and Sequeira, 1998 c21.

51. Anterolateral fenestra in roof of otoccipital: absent (0); present (1).
King et al., 2017 c111.

52. Hypophysial foramen in braincase: absent (0); present (1).
King et al., 2017 c114.

53. Posterior dorsal fontanelle: absent (0); present (1).
Brazeau, 2009 c85.

54. Shape of posterior dorsal fontanelle: approximately as long as broad (0); much longer than wide, slot-shaped (1).
Coates and Sequeira, 1998 c10.

55. Perilymphatic fenestra: absent (0); present (1).
Pradel et al., 2011 c16.

56. Vestibular fontanelle: absent (0); present (1).
Friedman, 2007b c180.

57. Ventral cranial fissure connects with vestibular fontanelles: no (0); yes (1).
Coates, 1999 c29; ***King et al., 2017*** c112.

58. Basal fenestra opening into floor of orbit: absent (0); present (1).
King et al., 2017 c129.

59. Subpituitary fenestra: absent (0); present (1).
Goujet and Young, 1995 c12.

60. Basicranial fenestra: absent (0); present (1).
Ahlberg and Johanson, 1998b c76.

Myodomes and articulations

61. Vomeral area with grooves and raised areas: absent (0); present (1).
Zhu and Schultze, 2001 c142.

62. Ethmoidal articulation of palatoquadrate: absent (0); present (1).
King et al., 2017 c122.

63. Ethmoid articulation for palatoquadrate: extends posteriorly to the level of N.II (0); placed on postnasal wall (1); majority of facet anterior to postnasal wall (2).
Friedman, 2007a c172.

64. Eye stalk or unfinished area on neurocranial wall for eye stalk: absent (0); present (1).
Zhu and Schultze, 2001 c36.

65. Position of basal/basipterygoid articulation: same anteroposterior level as hypophysial opening (0); anterior to hypophysial opening (1).
Brazeau, 2009 c81.

66. Basipterygoid process (basal articulation) with vertically oriented component: absent (0); present (1).
Brazeau, 2009 c83.

67. Expanded articular area anterior to basipterygoid process: absent (0); present (1).
King et al., 2017 c103.

68. Orbital/palatobasal articulation: posterior to optic foramen (0); anterior to optic foramen (1).

King et al., 2017 c123.

69. Descending process of sphenoid (with its posterior extremity lacking periostegeal lining): absent (0); present (1).

Ahlberg, 1991 c53.

70. Processus connectens: short (0); elongate (1).

Lu et al., 2016a c66.

71. Articulation between neurocanium and palatoquadrate posterodorsal to orbit (suprapterygoid articulation): absent (0); present (1).

Giles et al., 2015a c147.

72. Division of postorbital palatoquadrate articulation into dorsal and ventral components: absent (0); present (1).

New, adapted from ***King et al., 2017*** c128. Two condyles in the dorsal otic region are found in *Acanthodes* and *Homalacanthus*.

73. Periotic process: absent (0); present (1).

Pradel et al., 2011 c11.

74. Hyomandibula articulating with braincase: yes (0); no (1).

King et al., 2017 c121.

75. Position of hyomandibular articulation on neurocranium: Anterior position, suborbital (0); posterior position, behind orbit (1).

Brazeau, 2009 c89; ***King et al., 2017*** c369.

76. Relative position of jugular groove and hyomandibular articulation: hyomandibula dorsal or same level (0); jugular vein passing dorsal or lateral to hyomandibula (1).

Brazeau and de Winter, 2015 c237.

77. Articulation facet with hyomandibular: single-headed (0); double-headed (1).

Zhu and Schultze, 2001 c128.

78. Hyomandibular facets where they straddle the jugular canal: narrowly separated (0); broadly separated (1).

Friedman, 2007b c176.

79. Articulation surface on ventrolateral surface of otic capsule: absent (0); present (1).

New. There is some uncertainty what articulation surfaces on the otic capsule wall are for (see e.g. ***Chang, 1982***), but they are most commonly assumed to be for the articulation of an infrapharyngobranchial. This character simply codes the presence or absence of an articulation.

80. Paired occipital facets: absent (0); present (1).

Giles et al., 2015b c177.

81. Position of myodome for superior oblique eye muscles: posterior and dorsal to foramen for nerve II (0); anterior and dorsal to foramen for nerve II (1).

Brazeau, 2009 c63.

82. Medial recess of the posteroventral myodome: absent (0); present (1).

Sansom, 2009 c103.

Braincase ridges

83. Pronounced sub-ethmoidal keel: absent (0); present (1).

Coates and Sequeira, 1998 c22; ***Brazeau, 2009*** c62.

84. Subcranial ridges: absent (0); present (1).

Giles et al., 2015a c141.

85. Dorsal ridge: absent (0); present (1).

Coates and Sequeira, 1998 c11; ***Davis et al., 2012*** c91. Includes the unpaired median crista of lungfishes.

86. Shape of median dorsal ridge anterior to endolymphatic fossa: developed as a squared-off ridge or otherwise ungrooved (0); bears a midline groove (1).

Giles et al., 2015a c161.

87. Dorsal otic ridge forming a horizontal crest: absent (0); present (1).

Coates and Sequeira, 1998 c11; ***Pradel et al., 2011*** c12.

88. Hypotic lamina (and dorsally directed glossopharyngeal canal): absent (0); present (1).

Davis et al., 2012 c103.

89. Dorsolateral cristae: absent (0); present (1).

New.

90. Dorsolateral cristae fenestrated: no (0); yes (1).

Friedman, 2007a c16.

91. Lateral (parotic) cristae: absent (0); present (1).

New. The parotic crista of sarcopterygians and the lateral cristae of lungfishes are here considered potential homologues following ***Miles, 1977***. ***Friedman, 2007b*** compares the dorsolateral cristae as homologous to the parotic cristae, but cites Miles, so this is assumed to be erroneous.

Notochord

92. Size of aperture to notochordal canal: much smaller than foramen magnum (0); as large, or larger, than foramen magnum (1).

Giles et al., 2015a c178.

93. Notochord short and stopped by occipital cotylus: absent (0); present (1).

Pradel et al., 2011 c21.

94. Unconstricted cranial notochord: absent (0); present (1).

Ahlberg and Johanson, 1998b c153.

Spiracle

95. Spiracular groove on basicranial surface: absent (0); present (1).

Brazeau, 2009 c65.

96. Spiracular groove on lateral commissure: absent (0); present (1).

Davis et al., 2012 c63.

97. Endoskeletal spiracular enclosure: absent (0); present (1); spiracular canal (2).

Clement et al., 2018 c267.

Endocast

98. Relationship of cranial endocavity to basisphenoid: endocavity occupies full depth of sphenoid (0); endocavity dorsally restricted (1).

Giles et al., 2015b c140.

99. Nasal sacs: unpaired (0); paired (1).

King et al., 2017 c130.

100. Olfactory tracts: separate tracts (0); single anterior division of the cranial cavity (1).

New. In coelacanths there are no separate canals for the olfactory nerves but rather a large anterior division of the endocavity through which the olfactory tracts pass.

101. Rostral organ: absent (0); present (1).

Friedman, 2007b c145.

102. Hypophyseal chamber: projects posteroventrally (0); projects ventrally or anteroventrally (1).

Clement et al., 2018 c270.

103. Paired recesses anterior of hypophysial fossa: absent (0); present, blind (1); present, connect via canals to cranial cavity (2).

New. *Tungsenia* has paired recesses at the anterior of the hypophysial recess (***Lu et al., 2012*** fig. 4b ?PT), interpreted as similar to the pars tuberalis of living urodeles. In *Glyptolepis* there are also extensions of the hypophysial recess that connect anteriorly to the cranial cavity (***Jarvik, 1972*** fig. 17A c.p.tub).

104. Optic lobes: narrower than cerebellum (0); same width or wider than cerebellum (1).

Lu et al., 2017 c271.

105. Lateral cranial canal: absent (0); present (1).

Coates, 1999 c32.

106. Supraotic cavity: absent (0); present (1).

Lu et al., 2017 c275.

107. Endolymphatic ducts: posteriodorsally angled tubes (0); tubes oriented vertically through median endolymphatic fossa (1).

Coates and Sequeira, 2001 c73; ***Brazeau, 2009*** c87.

Inner ear

108. Labyrinth cavity: separated from the main neurocranial cavity by a cartilaginous or ossified capsular wall (0); skeletal capsular wall absent (1).

Davis et al., 2012 c82.

109. External (horizontal) semicircular canal: absent (0); present (1).

Brazeau, 2009 c83.

110. External (horizontal) semicircular canal: joins the vestibular region dorsal to posterior ampulla (0); joins level with posterior ampulla (1).

Davis et al., 2012 c87.

111. Horizontal semicircular canal in dorsal view: medial to path of jugular vein (0); dorsal to jugular vein (1).

Giles et al., 2015b c154.

112. Horizontal semicircular canal: horizontally orientated (0); obliquely orientated (1).

Lu et al., 2017 c274.

113. Crus commune: dorsal to endocranial roof (0); ventral to endocranial roof (1).

Lu et al., 2017 c272.

114. Sinus superior: absent or indistinguishable from union of anterior and posterior canals with saccular chamber (0); present (1).

Davis et al., 2012 c86.

115. Utricular recess: absent (0); present small (1); present large (2).

New. A diverticulum of the labyrinth cavity at the junction of the external semicircular canal and the sacculus, interpreted as housing the utriculus. See ***Brazeau and Friedman, 2014*** p18 for discussion.

116. Lagenar recess: absent (0); present (1).

New. A large recess at the posterior end of the saccular chamber for the lagena is well developed in *Diplocercides* (***Jarvik, 1980***, fig.217 space for lagena). Recently, a similar recess was described for the chondrichthyan *Tristychius* (***Coates et al., 2018***, fig.11).

117. Number of SEL canals: five (0); less than 5 (1).

Sansom, 2009 c91.

118. SEL one canal bifurcation: between orbit and lateral field (0); close to field (1); close to orbit (2).

Sansom, 2009 c110; ***King et al., 2017*** c92.

Blood vessels

119. Canal for efferent pseudobranchial artery within basicranial cartilage: absent (0); present (1).

Brazeau, 2009 c80.

120. Entrance of internal carotids in 'tropibasic' braincase: through basisphenoid pillar (0); through orbits (1).

New. Revised from ***King et al., 2017*** c38 and c125 to remove redundancy. This character is only applicable to taxa with a 'tropibasic' braincase: i.e. it is dependent on character 98.

121. Entrance of internal carotids: through separate openings flanking the hypophyseal opening or recess (0); through a common opening at the central midline of the basicranium (1).

Brazeau, 2009 c79.

122. Canal for lateral dorsal aorta within basicranial cartilage: absent (0); present (1).

Coates and Sequeira, 1998 c4; ***Brazeau, 2009*** c78.

123. Midline canal in basicranium for dorsal aorta: absent (0); present (1).

Zhu et al., 2013 c234.

124. Jugular canal: long (invested in otic region along length of skeletal labyrinth) (0); short (restricted to region anterior of skeletal labyrinth) (1); absent (jugular vein uninvested in otic region) (2).

Giles et al., 2015b c126.

125. Canal for jugular in postorbital process: absent (0); present (1).

Giles et al., 2015c c133.

126. Pituitary vein canal: dorsal to level of basipterygoid process (0); flanked posteriorly by basipterygoid process (1).

Davis et al., 2012 c84.

127. Pituitary vein canal: Discontinuous, enters cranial cavity (0); Discontinuous, enters hypophysial recess (1); Continuous transverse canal (2).

Clement et al., 2018 c282.

128. Marginal vein: absent (0); present (1).

Sansom, 2009 c93.

Cranial nerves

129. Olfactory tracts: short, with olfactory capsules situated close to telencephalon cavity (0); elongate and tubular (much longer than wide) (1).

Brazeau, 2009 c60.

130. Rostral tubuli: absent (0); present (1).

Cloutier and Ahlberg, 1996 c77.

131. Profundus and trigeminal nerves: emerge from cranial cavity separately (0); emerge from cranial cavity together (1).

King et al., 2017 c94.

132. Size of anterior profundus canal: small (0); large (1).

Zhu and Schultze, 2001 c144

Definition revised to remove the postnasal wall, as an anterior profundus foramen can sill be present when the posnasal wall is poorly developed, in particular in '*Ligulalepis*'.

133. Series of perforations for innervation of supraorbital sensory canal in supraorbital shelf: absent (0); present (1).

Giles et al., 2015c c134.

134. Profundus nerve enters orbit with jugular vein: no (0); yes (1).

New. In general, the profundus nerve enters the orbit through a foramen on the posteriodorsal wall. However, in '*Chirodipterus*' the profundus nerve first joins the jugular vein canal (***Henderson and Challands, 2018*** p16).

135. Relative position of trigeminal nerve: behind endoskeletal cranial joint (0); through endoskeletal cranial joint (1); anterior to endoskeletal joint (2).

Zhu and Schultze, 2001 c134. This character is here adapted to include an extra state in when the intracranial joint is behind the trigeminal nerve. It is dependent on the presence of an intracranial joint.

136. Palatine nerve canal: absent (0); present (1).

New. A palatine nerve canal is present in gnathostomes, but is apparently unknown in osteostracans or galeaspids (see discussion in ***King et al., 2017***)

137. Hyoid ramus of facial nerve (N. VII) exits through posterior jugular opening: absent (0); present (1).

Friedman, 2007b c179.

138. Glossopharyngeal nerve (N. IX) exit: foramen situated posteroventral to otic capsule and anterior to metotic fissure (0); through metotic fissure (1).

Coates and Sequeira, 1998 c2; ***Brazeau, 2009*** c73.

139. Spino-occipital nerve foramina: two or more, aligned horizontally (0); one or two, dorsoventrally offset (1).

Coates and Sequeira, 1998 c8; ***Brazeau, 2009*** c95.

Dermal palate bones

140. Median dermal bone of palate (parasphenoid): absent (0); present (1).

Brazeau, 2009 c57.

141. Ascending process of parasphenoid: absent (0); present (1).

Patterson, 1982a c9.

142. Shape of parasphenoid denticulated field: broad rhomboid or lozenge-shaped (0); broad, splint-shaped (1); slender, splint-shaped (2).

Friedman, 2007b c168.

143. Parasphenoid denticulated field with multifid anterior margin: absent (0); present (1).

Friedman, 2007b c167.

144. Parasphenoid: protruding forward into ethmoid region of endocranium (0); behind ethmoid region (1).

Zhu and Schultze, 2001 c124.

145. Denticulated field of parasphenoid: without spiracular groove (0); with spiracular groove (1).

Friedman, 2007b c82.

146. Parasphenoid denticle field: terminates at or anterior to level of foramina for internal carotid arteries (0); extends posterior to foramina for internal carotid arteries (1).

Friedman, 2007b c170.

147. Four carotid foramina in parasphenoid: absent (0); present (1).

Lu et al., 2012 c98; ***King et al., 2017*** c138.

148. Buccohypophysial canal in parasphenoid: single (0); paired (1).

Giles et al., 2015a c114.

149. Posterior stalk of parasphenoid covering otic region: absent (0); present (1).

Friedman, 2007a c63.

150. Parasphenoid posterior stalk furrow: absent (0); present (1).

Schultze, 2001 c51.

151. Prespiracular dental plate: absent (0); present (1).

King et al., 2017 c108.

152. Parotic dental plate: absent (0); present (1).

King et al., 2017 c139.

Skull roof, overall features

153. Dermal skull roof: includes large dermal plates (0); consists of undifferentiated plates or tesserae (1).

Brazeau, 2009 c19.

154. Tesserae morphology: large interlocking polygonal plates (0); microsquamose, not larger than body tesserae (1).

Brazeau, 2009 c20.

155. Extent of dermatocranial cover: complete (0); incomplete (scale-free cheek and elsewhere) (1).

Brazeau, 2009 c21.

156. Series of paired median skull roofing bones that meet at the dorsal midline of the skull (rectilinear skull roof pattern): absent (0); present (1).

Brazeau, 2009 c24.

157. Dermal intracranial joint: absent (0); present (1).

Cloutier and Ahlberg, 1996 c81.

158. Cranial spines: absent (0); present, multicuspid (1); present, monocuspid (2).

Giles et al., 2015c c36.

Skull roof, foramina

159. Pineal opening perforation in dermal skull roof: absent (0); present (1).

Brazeau, 2009 c26.

160. Location of pineal foramen/eminence: level with posterior margin of orbits (0); well posterior of orbits (1).

Ahlberg and Johanson, 1998b c37.

161. Endolymphatic ducts open in dermal skull roof: present (0); absent (1).

Brazeau, 2009 c22.

162. Endolymphatic ducts with oblique course through dermal skull bones: absent (0); present (1).

Goujet and Young, 1995 c8.

163. Endolymphatic duct relationship to median skull roof bone (i.e. nuchal plate): within median bone (0); on bones flanking the median bone (e.g. paranuchals) (1).

Giles et al., 2015c c40.

164. Dermal plate associated with pineal eminence or foramen: contributes to orbital margin (0); plate bordered laterally by skull roofing bones (1).

Giles et al., 2015c c42.

Skull roof, snout

165. Median rostral extension of head shield: absent (0); present (1).

Sansom, 2009 c1.

166. Tooth-bearing median rostral: absent (0); present (1).

Cloutier and Ahlberg, 1996 c22.

167. T-shaped rostral: absent (0); present (1).

Carr and Hlavin, 2010 c5; ***King et al., 2017*** c237.

168. Multiple postrostral bones: no (0); yes (1).

New. Homology of snout bones (i.e. the bones anterior to the parietals) across gnathostomes are difficult to assess. This character simply makes the distinction between the mosaic of small irregular bones (postrostrals, nasals, tectals) found in sarcopterygians with the relatively small number of larger plates in actinopterygians and placoderms.

169. Number of median bones anterior to parietals: none (0); one (1); two (2).

New. This character reformulates a number of previous characters regarding the presence of rostral and premedian plates. In placoderms the first median bone anterior to the patietals (preorbitals) is generally termed the rostral, while the second is called the premedian or internasal. In osteichthyans they are termed as the postrostral and rostral. Here we remove the position of the nasal capsules from the definition of a premedian plate (e.g. Zhu et al. c148) as the position of the nasal capsules is dealt with in other characters. In taxa with a rostral mosaic of bones (character 168), this character is considered inapplicable.

170. Premedian plate: large plate (0); reduced to internasal plate (1).

Zhu et al., 2016 c157, revised. This character is contingent on the presence of a premedian plate. This is covered in character 169 state 2.

171. Paired prenostril trenches on premedian plate: absent (0); present (1).

New. Paired prenostril trenches are present on the premedian/internasal plate of Qilinyu. This character is contingent on the presence of a premedian plate (Character 169 state 2).

172. Unornamented shelf and rostrocaudal groove on premedian: absent (0); present (1).

Jia et al., 2010 c3.

173. Preorbital depression: absent (0); present (1).

Jia et al., 2010 c6.

174. Supraorbital: absent (0); present (1).

Cloutier and Ahlberg, 1996 c28.

175. Lateral plate: absent (0); present (1).

Zhu et al., 2013 c157.

176. Prelateral plate: absent (0); present (1).

King et al., 2017 c251.

177. Submarginal articulation: absent (0); present (1).

Jia et al., 2010 c16.

178. Parietals (preorbitals of placoderms) surround pineal foramentotoeminence: yes (0); no (1).

Ahlberg and Johanson, 1998b c38.

179. Median bone separating parietals: absent (0); present (1); present and separates postparietals as well (2).

King et al., 2017 c271, revised.

180. Paraorbital plate separating suborbital from orbit: absent (0); present (1).

King et al., 2017 c253.

Skull roof, sclerotic ring

181. Sclerotic ring: absent (0); present (1).

Giles et al., 2015a c52.

182. Number of sclerotic plates: four or less (0); more than four (1).

Cloutier and Ahlberg, 1996 c49.

183. Sclerotic ring incorporated into skull: no (0); yes (1).

King et al., 2017 c244.

Skull roof, back half

184. Dermal bone (sarcopt postorbital) between jugal and intertemporal: absent (0); present (1).

King et al., 2017 c279.

185. Complete enclosure of spiracle by skull roof bones: absent (0); present (1).

Friedman, 2007b c148.

186. Suture between paired skull roofing bones (centrals of placoderms postparietals of osteichthyans): straight (0); sinusoidal (1).

Giles et al., 2015a c49.

187. Number of bones bearing otic canal between dermosphenotic and lateral extrascapular: one (0); two (1); more than two (2).

New. These bones are termed the marginal and anterior paranuchal in placoderms and the supratemporal and tabular in osteichthyans.

188. Supratemporal contact with postparietal: present (0); absent due to anterior displacement (1); absent due to lateral displacement (2).

Swartz, 2009 c15; ***King et al., 2017*** c273.

189. Supratemporal contact with nasal: (0); present (1).

Gardiner and Schaeffer, 1989 c26.

190. Contact of tabular or anterior paranuchal with postparietal or central: less than half length of postparietal (0); extends most of the length of postparietal (1).

New.

191. Series of bones lateral to supratemporal series: absent (0); single bone (1); two bones (2).

King et al., 2017 c263.

192. Number of extrascapulars: uneven (0); paired (1).

Cloutier and Ahlberg, 1996 c40.

193. Number of paired extrascapulars: one pair (0); two pairs (1).

Gardiner and Schaeffer, 1989 cA8.

194. Medial processes of paranuchal wrapping posterolateral corners of nuchal plate: absent (0); present (1); paranuchals precluded from nuchal by centrals (2).

Giles et al., 2015a c50. The fourth state of the Giles et al character is not included here (and the taxa are considered inapplicable) as the presence of a median posterior skull roof bone is dealt with by character 192.

195. Nuchal plate: without orbital facets (0); with orbital facets (1).

Jia et al., 2010 c14.

196. Centronuchal plate: absent (0); present (1).

Dupret et al., 2009 c17.

197. Contact of nuchal or centronuchal plate with paired preorbital plates: absent (0); present (1).

Zhu et al., 2013 c164.

198. Postnuchal plate: absent (0); present (1).

Dupret et al., 2009 c45; ***King et al., 2017*** c239.

199. Presupracleithrum: absent (0); present (1).

Patterson, 1982b c13.

200. Fused scale rows on head shield: absent (0); present (1).

Sansom, 2009 c43.

201. Dorsal spinal process on head shield: absent (0); present (1).

Sansom, 2009 c44.

202. Cornual extensions: absent (0); present (1).
Sansom, 2009 c36; ***Zhu and Gai, 2007*** c14.

203. Spines on cornual extension: absent (0); present (1).
Zhu and Gai, 2007 c18.

204. Most posterior bones flanking postparietals: level with posterior margin of postparietals (0); extend posterior to posterior margin of potparietals (1).
Lu et al., 2016b c238.

Skull roof, joint

205. Type of dermal neck-joint: overlap (0); ginglymoid (1).
Zhu et al., 2013 c169; ***Giles et al., 2015a*** c60.

206. Type of ginglymoid neck-joint: conventional (0); reverse (1).
King et al., 2017 c174.

207. Dermal neck-joint between paired main-lateral-line-bearing bones of skull and shoulder girdle: absent (0); present (1).
Zhu et al., 2013 c168.

Skull roof, visceral

208. Broad supraorbital vaults: absent (0); present (1).
Giles et al., 2015a c44.

209. Paired pits on ventral surface of nuchal plate: absent (0); present (1).
Giles et al., 2015b c51.

210. Preorbital recess: absent (0); present (1).
Jia et al., 2010 c8; ***King et al., 2017*** c247.

211. Preorbital recess: restricted to premedian plate (0); extends to lateral plates (1).
Jia et al., 2010 c8; ***King et al., 2017*** c248.

212. Posterior descending lamina of skull roof: absent (0); present (1).
Pan et al., 2015 c6.

213. Mesial lamina of marginal plate: absent (0); present (1).
King et al., 2017 c254.

Skull roof, fields

214. Lateral fields: absent (0); present (1).
Sansom, 2009 c4.

215. Division of lateral fields: absent (0); divided once (1); divided twice (2).
Sansom, 2009 c5-6; ***King et al., 2017*** c220.

216. Lateral fields extend posterior to pectoral sinus: absent (0); present (1).
Sansom, 2009 c10.

217. Lateral field extends to cornua: no (0); yes (1).
Sansom, 2009 c11.

218. Median field: absent (0); present (1).
Sansom, 2009 c13.

219. Median field separation from pineal plate or foramen: absent (0); present (1).
Sansom, 2009 c15.

220. External endolymphatic duct opens within median field: internal (0); external (1).
Sansom, 2009 c17.

221. Median dorsal opening: absent (0); present (1).
Donoghue et al., 2000 c14; ***Zhu and Gai, 2007*** c1.

222. Shape of median dorsal opening: transverse slit-like (0); oval-like (1); slender longitudinal oval (2).
Zhu and Gai, 2007 c6.

Nostrils

223. External nasal opening: single median (0); paired (1).
Donoghue et al., 2000 c14; ***Sansom, 2009*** c25.

224. Nostrils enclosed in dermal skull roof: yes (0); no (1).
King et al., 2017 c256.

225. Nasohypophysial opening shape: unconstricted (0); constricted (1); split (2).
Sansom, 2009 c228; ***King et al., 2017*** c228.

226. Posterior nostril: associated with orbit (0); not associated with orbit (1).
Cloutier and Ahlberg, 1996 c46.

227. Dermintermedial process: absent (0); present (1).
Zhu and Schultze, 2001 c37.

228. Position of posterior nostril: external, far from jaw margin (0); external, close to jaw margin (1); palatal (2).
Zhu and Schultze, 2001 c39.

229. Lacrimal posteriorly enclosing posterior nostril: absent (0); present (1).
Zhu and Schultze, 2001 c28.

230. Premaxilla contributes to posterior nostril: absent (0); present (1).

Friedman and Blom, 2006 c7.

Operculogular

231. Opercular cover of branchial chamber: complete or partial (0); separate gill covers and gill slits (1).

Davis et al., 2012 c32.

232. Branchiostegals: absent (0); present (1).

Brazeau, 2009 c31.

233. Branchiostegal plate series along ventral margin of lower jaw: absent (0); present (1).

Brazeau, 2009 c32.

234. Branchiostegal ossifications: plate-like (0); narrow and ribbon-like (1).

Brazeau, 2009 c33; ***Davis et al., 2012*** c29.

235. Branchiostegal ossifications: ornamented (0); unornamented (1).

Brazeau, 2009 c34.

236. Imbricated branchiostegal ossifications: absent (0); present (1).

Brazeau, 2009 c35.

237. Shape of opercular (submarginal) ossification: broad plate that tapers towards its proximal end (0); narrow, rod-shaped (1).

Brazeau, 2009 c37.

238. Size of lateral gular plates: extending most of length of the lower jaw (0); restricted to the anterior third of the jaw (no longer than the width of three or four branchiostegals (1)).

Brazeau, 2009 c39.

239. Median gular: present (0); absent (1).

Cloutier and Ahlberg, 1996 c66.

240. Number of branchiostegal rays per side: 10 or more (0); 2–7 (1); one (2).

Cloutier and Ahlberg, 1996 c63.

241. Accessory operculum: absent (0); present (1).

Dietze, 2000 c56.

242. Oralobranchial covering: tesserae (0); plates (1).

Sansom, 2009 c60; ***King et al., 2017*** c232.

243. Headshield enclosed posteriorly behind oralobranchial chamber: no (0); yes (1).

King et al., 2017 c235.

Cheek

244. Cheek plate: undivided (0); divided (i.e. squamosal and preopercular) (1).

Giles et al., 2015a c54.

245. Subsquamosals in taxa with divided cheek: absent (0); present (1).

Zhu and Schultze, 2001 c64; ***Giles et al., 2015b*** c54.

246. Preopercular shape: rhombic (0); bar-shaped (1).

Zhu and Schultze, 2001 c71.

247. Consolidated cheek plates: absent (0); present (1).

Brazeau, 2009 c25.

248. Enlarged postorbital tessera separate from orbital series: absent (0); present (1).

Brazeau, 2009 c30.

249. Most posterior major bone of cheek bearing preopercular canal (preopercular) extending forward, close to orbit: absent (0); present (1).

Zhu and Schultze, 2001 c58; ***Zhu et al., 2009*** c59.

250. Contact between most posterior major bone of cheek bearing preopercular canal and maxilla: present (0); absent (1).

Zhu and Schultze, 2001 c66.

251. Bone bearing both quadratojugal pit-line and preopercular canal: absent (0); present (1).

Friedman, 2007b c42.

252. Notch in anterior margin of jugal: absent (0); present (1).

Cloutier and Arratia, 2004 c81.

253. Quadratojugal: present (0); absent (1).

Zhu and Schultze, 2001 c57; ***Dietze, 2000*** c31.

254. Lacrimal: absent (0); present (1).

King et al., 2017 c257.

Premaxilla/maxilla

255. Premaxilla: extends under orbit (0); restricted anterior to orbit (1).

Friedman, 2007b c150.

256. Premaxillae with inturned symphysial processes: absent (0); present (1).

Friedman, 2007b c149.

257. Premaxilla forming part of orbit: absent (0); present (1).

Cloutier and Arratia, 2004 c18.

258. Posterior expansion of maxilla (maxilla cleaver-shaped): present (0); absent (1).

Lund et al., 1995 c52; ***Zhu and Schultze, 2001*** c54.

259. Contribution by maxilla to posterior margin of cheek: present (0); absent (1).

Friedman, 2007b c151.

260. Ventral margin of maxilla: straight (0); curved (1).

Dietze, 2000 c26.

261. Orbital process of maxilla: absent (0); present (1).

King et al., 2017 c282.

Dermal ornament and pores

262. Dermal ornamentation: smooth (0); ridges (1); tuberculate (2).

Giles et al., 2015b c29; ***King et al., 2017*** c205.

263. Size of cosmine pores: small (0); large (1).

Zhu et al., 2001 c149.

264. Pore clusters: absent (0); present (1).

Zhu and Schultze, 2001 c207.

265. Westoll-lines: absent (0); present (1).

Zhu and Schultze, 2001 c207.

266. Transverse external groove behind pineal opening: absent (0); present (1).

King et al., 2017 c255.

267. Sensory foramina on skull roof, behind orbits: absent (0); present (1).

King et al., 2017 c241.

268. Cutaneous pits on cheek bones: absent (0); present (1).

New. Here we combine previous characters dealing with sensory pits on the cheeks of osteichthyans (***Ahlberg and Johanson, 1998b*** 63) and placoderms (***King et al., 2017*** 240, 241). There is no a priori reason to reject homology of these pits.

Teeth

269. Oral dermal tubercles borne on jaw cartilages: absent (0); present (1).

Brazeau, 2009 c41.

270. Oral tubercles in patterned rows (teeth): absent (0); present (1).

Brazeau, 2009 c42.

271. Basal resorption of teeth: absent (0); present (1).

New. This character can be scored based on the presence of replacement pits.

272. Oral dermal tubercles fused to jaw cartilages: absent (0); present (1).

New. *Pucapampella* has the unusual condition in which statodont teeth are fused directly to the jaw cartilage, which extended into the core of the teeth (***Maisey et al., 2018*** p99).

273. Tooth whorls: absent (0); present (1).

Brazeau, 2009 c43.

274. Tooth whorls extent: at symphysis (0); along entire jaw (1).

Giles et al., 2015b c83.

275. Distribution of marginal tooth whorls: upper and lower jaws (0); lower jaws only (1); upper jaws only (2).

Giles et al., 2015b c84.

276. Bases of marginal tooth whorls: single, continuous plate (0); some or all whorls consist of separate tooth units (1).

Brazeau, 2009 c44; ***Davis et al., 2012*** c41.

277. Toothplates: absent (0); present (1).

Coates et al., 2018 c85.

278. Extramandibular dentition: absent (0); present (1).

Lu et al., 2012 c392.

279. Number of tooth rows on outer dental arcade: one (0); two (1).

Friedman, 2007a c157; ***King et al., 2017*** c380.

280. Teeth of dentary: reaching anterior end of dentary (0); not reaching anterior end (1).

Ahlberg and Johanson, 1998b c11.

281. Fangs of coronoids (sensu stricto): absent (0); present (1).

Ahlberg et al., 2000 c15.

282. Number of fang pairs on posterior coronoid: one (0); two (1); none (2).

Ahlberg and Johanson, 1998b c13.

283. Marginal denticle band on coronoids: broad band, at least posteriorly (0); narrow band with 2–4 denticle rows (1).

Ahlberg and Johanson, 1998b c9.

284. Teeth radial rows on prearticular: absent (0); present (1).

Zhu and Schultze, 2001 c95.

285. Core of oral dermal tubercles: open pulp cavity (0); vascular network (osteodentine) (1).

New. We do not differentiate between the absence of a pulp cavity and a secondarily infilled pulp cavity.

286. Enamel(oid) on teeth: absent (0); present (1).

Giles et al., 2015a c79.

287. Plicidentine: absent (0); present (1).

Cloutier and Ahlberg, 1996 c86.

288. Acrodin: absent (0); present (1).

Patterson, 1982b c12.

Jaws, general

289. Jaws: absent (0); present (1).

Dupret et al., 2014 c254.

290. Cosmine-like tissue in oral cavity: absent (0); present (1).

Friedman, 2007a c56.

Dermal lower jaw bones

291. Dermal jaw plates on biting surface of jaw cartilages: absent (0); present (1).

Brazeau, 2009 c48.

292. Dentary: absent (0); present (1).

New.

293. Large ventromesially directed flange of symphysial region of mandible: absent (0); present (1).

Friedman, 2007b c156.

294. Flange like extension of mandible composed of prearticular and Meckelian ossification: absent (0); present (1).

Friedman, 2007b c159.

295. Strong ascending flexion of symphysial region of mandible: absent (0); present (1).

Friedman, 2007b c155.

296. Labial pit: absent (0); present (1).

Cloutier and Ahlberg, 1996 c80.

297. Infradentary: absent (0); present (1).

Zhu et al., 2013 c204.

298. Number of infradentaries: one (0); two (1); more than 2 (2).

Friedman, 2007b c54; ***King et al., 2017*** c381.

299. Extent of infradentaries: along much of ventral margin of dentary (0); restricted to posterior half of dentary (1).

Giles et al., 2015c c93.

300. Infradentary foramina: present (0); absent (1).

Ahlberg and Johanson, 1998b 15; ***King et al., 2017*** 350.

301. Anterior end of prearticular: far from jaw symphysis (0); near jaw symphysis (1).

Zhu and Schultze, 2001 c93.

302. Prearticular - dentary contact: present (0); absent (1).

Cloutier and Ahlberg, 1996, c96.

303. Principal coronoid: absent (0); present (1).

Cloutier, 1996 c95.

304. Coronoids: present (0); absent (1).

Schultze and Cumbaa, 2001 c46.

305. Number of coronoids: more than three (0); three (1).

Ahlberg and Clack, 1998a c4, ***Zhu et al., 2009*** c93.

306. Meckelian bone exposed immediately anterior to first coronoid: yes (0); no (1).

Ahlberg and Clack, 1998a c22.

307. Submandibulars: absent (0); present (1).

Cloutier and Ahlberg, 1996 c104.

Palatoquadrate

308. Large otic process of the palatoquadrate: absent (0); present (1).

Brazeau, 2009 c49.

309. Insertion area for jaw adductor muscles on palatoquadrate: ventral (0); lateral (1).

Brazeau, 2009 c50.

310. Oblique ridge or groove along medial face of palatoquadrate: absent (0); present (1).

Brazeau, 2009 c52.

311. Perforate or fenestrate anterodorsal (metapterygoid) portion of palatoquadrate: absent (0); present (1).

Brazeau, 2009 c54.

312. Processus ascendens of palatoquadrate: absent (0); present (1).

King et al., 2017 c389.

313. Fenestration of palatoquadrate at basipterygoid articulation: absent (0); present (1).

Brazeau, 2009 c53.

314. Metapterygoid with developed medial ventral protrusion: absent (0); present (1).

Zhu et al., 2013 c216.

315. Palatoquadrate fused with neurocranium: absent (0); present (1).

Giles et al., 2015a c101.

316. Jugular vein passes through cranioquadrate passage: absent (0); present (1).

King et al., 2017 c126.

317. Autopalatine and quadrate: comineralized (0); separate mineralizations (1).

Miles and Dennis, 1979 c22, ***Giles et al., 2015b*** c97.

318. Hyosuspensory eminence on quadrate: absent (0); present (1).

Friedman, 2007a, c55.

319. Dermal plates on mesial (lingual) surfaces of Meckels cartilage and palatoquadrate: absent (0); present (1).

Zhu et al., 2013 c213.

320. Contact between palatoquadrate and dermal cheek bones: continuous contact of metapterygoid and autopalatine (0); metapterygoid and autopalatine contacts separated by gap between commissural lamina of palatoquadrate and cheek bones (1).

Zhu et al., 2013 c215.

321. Number of fang pairs on ectopterygoid: one (0); two (1); none (2).

Lu et al., 2012 c103.

322. Proportions of entopterygoid: anterior end level with processus ascendens (0); anterior end considerably anterior to processus ascendens (1).

Lu et al., 2012 c104.

Meckel's cartilage etc

323. Bilateral series of labial cartilages: absent (0); present (1).

King et al., 2017 c393.

324. Pronounced dorsal process on Meckelian bone or cartilage: absent (0); present (1).

Hanke and Wilson, 2004 c11; ***Brazeau, 2009*** c55.

325. Adductor fossa: open (0); reduced to narrow slot (1).

Schultze, 2001 c69; ***Ahlberg et al., 2006*** c41.

326. Preglenoid process: absent (0); present (1).

Davis et al., 2012 c52.

327. Biconcave glenoid on lower jaw: absent (0); present (1).

Friedman and Brazeau, 2010 c17; ***Zhu et al., 2013*** c214.

328. Jaw articulation located on rearmost extremity of mandible: absent (0); present (1).

Davis et al., 2012 c53.

329. Retroarticular process: absent (0); present (1).

Lu et al., 2012 c163.

330. Symplectic articulation: absent (0); present (1).

Friedman, 2007b c160.

Scapulocoracoid

331. Scapular process of shoulder endoskeleton: absent (0); present (1).

Brazeau, 2009 c105.

332. Ventral margin of separate scapular ossification: horizontal (0); deeply angled (1).

Brazeau, 2009 c107.

333. Cross sectional shape of scapular process: flattened or strongly ovate (0); subcircular (1).

Brazeau, 2009 c108.

334. Flange on trailing edge of scapulocoracoid: absent (0); present (1).

Brazeau, 2009 c109.

335. Scapular process with posterodorsal angle: absent (0); present (1).

Davis et al., 2012 c114.

336. Endoskeletal postbranchial lamina on scapular process: present (0); absent (1).

Brazeau, 2009 c110.

337. Mineralization of internal surface of scapular blade: mineralised all around (0); unmineralised on internal face forming a hemicylindrical cross-section (1); unmineralised on lateral face forming a hemicylindrical cross-section (2).

Brazeau, 2009 c111. According to the ***Burrow and Rudkin, 2014*** description, Nerepisacanthus has a scapulocroacoid mineralised only on the medial face. This necessitates a new character state (2).

338. Coracoid process: absent (0); present (1).

Brazeau, 2009 c112.

339. Procoracoid mineralization: absent (0); present (1).

Brazeau, 2009 c114.

340. Fin base articulation on scapulocoracoid: stenobasal (0); eurybasal (1).

Brazeau, 2009 c113.

341. Perforate propterygium: absent (0); present (1).

Patterson, 1982b c15.

342. Endoskeletal supports in pectoral fin: multiple elements articulating with girdle (0); single element ('humerus') articulating with girdle (1).

Zhu and Schultze, 2001 c175.

343. Triradiate scapulocoracoid: absent (0); present (1).

Zhu and Schultze, 2001 c171.

344. Subscapular foramen: absent (0); present (1).

Zhu and Schultze, 2001 c173.

345. Pectoral propterygium: absent (0); present (1).

Zhu and Schultze, 2001 c176.

346. Horizontal plate of scapulocoracoid: absent (0); present (1).

Patterson, 1982b c17; ***Friedman and Blom, 2006*** c40.

Dermal shoulder girdle

347. Macromeric dermal shoulder girdle: present (0); absent (1).

Brazeau, 2009 c99.

348. Dermal shoulder girdle forming a complete ring around the trunk: present (0); absent (1).

Brazeau, 2009 c101.

349. Median dorsal plate: absent (0); present (1).

Brazeau, 2009 c103.

350. Number of MD plates: one (0); two (1); three (2).

Trinajstic and Long, 2009 c445; ***King et al., 2017*** c445.

351. Pronounced internal crista (keel) on median dorsal surface of shoulder girdle: absent (0); present (1).

Brazeau, 2009 c104.

352. Posteriorly spine on MD plate: absent (0); present (1).

Carr and Hlavin, 2010 c37.

353. Anocleithrum: element developed as postcleithrum (0); element developed as anocleithrum sensu stricto (1).

Gardiner and Schaeffer, 1989 cB2.

354. Anocleithrum sensu stricto: exposed (0); subdermal (1).

Cloutier and Ahlberg, 1996 c112.

355. Pectoral fenestra completely encircled by dermal shoulder armour: present (0); absent (1).

Brazeau, 2009 c102.

356. Dermal shoulder girdle composition: ventral and dorsal (scapular) components (0); ventral components only (1).

Brazeau, 2009 c100.

357. Dorsal cleithrum (AL of the Placodermi), ventral cleithrum (AVL of the Placodermi) and pectoral spine (SP of the Placodermi): not fused (0); fused (1).

Cloutier and Ahlberg, 1996 c161.

358. Relationship of clavicle to cleithrum: ascending process of clavicle overlapping cleithrum laterally (0); ascending process of clavicle wrapping round anterior edge of cleithrum, overlapping it both laterally and mesially (1).

Cloutier and Ahlberg, 1996 c116.

359. Shape of dorsal blade of dermal shoulder girdle (either cleithrum or anterolateral plate): spatulate (0); pointed (1).

Cloutier and Ahlberg, 1996 c115.

360. Chang"s apparatus: absent (0); present (1).

King et al., 2017 c444.

361. Clavicles/interolateral plates: large plates, comparable in size to cleithrum (0); reduced to small semilunar plates, paired (1); unpaired semilunar plates (2).

Jia et al., 2010 c44; ***King et al., 2017*** c443.

362. Median ventral trunk plate(s): absent (0); present (1).

King et al., 2017 c447.

363. Extracleithrum: absent (0); present (1).
Forey, 1998 c88.

364. Posterior dorsolateral (PDL) plate or equivalent: absent (0); present (1).
Giles et al., 2015a c187.

365. PL and PDL overlap: simple (0); insertion (1).
Carr and Hlavin, 2010 c42.

366. Left and right PDL contact below MD: absent (0); present (1).
King et al., 2017 c438.

367. PDL plate visible externally: yes (0); no (1).
King et al., 2017 c439.

Dermal pectoral fin

368. Scapular infundibulum: absent (0); present (1).
Giles et al., 2015b c190.

369. Pectoral fin base has large, hemispherical dermal component: absent (0); present (1).
Brazeau, 2009 c121.

370. Pectoral fins covered in macromeric dermal armour: absent (0); present (1).
Brazeau, 2009 c120.

371. Joint in macromeric armoured pectoral fin: unjointed (0); jointed (1).
Jia et al., 2010 c27; ***King et al., 2017*** c441.

372 . Cd1 and Cd2 plates: in contact (0); separated (1).
Jia et al., 2010 c28.

Pectoral fin endoskeleton

373. Number of basals in polybasal pectoral fins: three or more (0); two (1).
Giles et al., 2015b c202.

374. Number of mesomeres in metapterygial axis: five or fewer (0); seven or more (1).
Cloutier and Ahlberg, 1996 123.

375. Biserial pectoral fin endoskeleton: absent (0); present (1).
Giles et al., 2015b c205.

376. Filamentous extension of pectoral fin from axillary region: absent (0); present (1).
Giles et al., 2015b c207.

377. Entepicondyle on humerus: present (0); absent (1).

King et al., 2017 c418.

378. Distal articulation of propterygium: with fin rays (0); with a second enlarged plate (1); no articulation (2).

King et al., 2017 c420.

Pelvic fins and claspers

379. Pelvic fins: absent (0); present (1).

Brazeau, 2009 c117.

380. Pelvic girdle with substantial dermal component: yes (0); no (1).

Zhu et al., 2013 c252.

381. Claspers with large dermal J-shaped element: absent (0); present (1).

Long et al., 2015 c258.

382. Claspers: absent (0); present (1).

Brazeau, 2009 c119. Removed 'pelvic' from the definition, as placoderm claspers may not be associated with the pelvic fins (***Trinajstic et al., 2015***). However, for the purposes of this phylogenetic analysis, the claspers of placoderms and chondrichthyans can be considered primary homologues, as opposed to the coding in ***Long et al., 2015*** and ***King et al., 2017***.

Fin spines

383. Paired fin spines: absent (0); present (1).

Brazeau, 2009 c125.

384. Pectoral fin spine small (bivalve-like): no (0); yes (1).

King et al., 2017 c449.

385. Pelvic fin spine: absent (0); present (1).

Zhu et al., 2013 c253.

386. Dorsal fin spines: absent (0); present (1).

Brazeau, 2009 c123.

387. Anal fin spine: absent (0); present (1).

Brazeau, 2009 c124.

388. Median fin spine insertion: shallow, not greatly deeper than dermal bones/scales (0); deep (1).

Brazeau, 2009 c126.

389. Intermediate fin spines: absent (0); present (1).

Brazeau, 2009 c127.

390. Intermediate spines when present: one pair (0); multiple pairs (1).

Giles et al., 2015c c219.

391. Intermediate spines with finlets: absent (0); present (1).
King et al., 2017 c481.

392. Prepectoral fin spines: absent (0); present (1).
Brazeau, 2009 c128.

393. Prepectoral spines form 'necklace': no (0); yes (1).
King et al., 2017 c483.

394. Median ventral prepectoral spine: absent (0); present (1).
King et al., 2017 c482.

395. Fin spine cross-section: Round or horseshoe shaped (0); Flat-sided, with rectangular profile (1).
Giles et al., 2015c c218.

396. Fin spines with ridges: absent (0); present (1).
Brazeau, 2009 c129.

397. Fin spines with nodes: absent (0); present (1).
Brazeau, 2009 c130.

398. Fin spines with rows of large retrorse denticles: absent (0); present (1).
Davis et al., 2012 c134.

399. Expanded spine rib on leading edge of spine: absent (0); present (1).
Giles et al., 2015c c224.

400. Spine ridges: converging at the distal apex of the spine (0); converging on leading edge of spine (1).
Giles et al., 2015c c225.

Median fins

401. Number of dorsal fins, if present: one (0); two (1).
Coates and Sequeira, 2001 c10.

402. Posterior dorsal fin shape: base approximately as broad as tall, not broader than all of other median fins (0); base much longer than the height of the fin, substantially longer than any of the other dorsal fins (1).
Giles et al., 2015a c229.

403. Basal plate in dorsal fin: absent (0); present (1).
Giles et al., 2015b c230.

404. Branching radial structure articulating with dorsal fin basal plate: absent (0); present (1).
Giles et al., 2015c c231.

405. Anal fin: absent (0); present (1).
Brazeau, 2009 c134.

406. Basal plate in anal fin: absent (0); present (1).
Giles et al., 2015c c233.

407. Spine-brush complex: absent (0); present (1).
King et al., 2017 c479.

Caudal fin

408. Horizontal caudal lobe: absent (0); present (1).
Sansom, 2009 c70.

409. Triphycercal tail: absent (0); present (1).
King et al., 2017 c452.

410. Caudal radials: extend beyond level of body wall and deep into hypochordal lobe (0); restricted to axial lobe (1).
Davis et al., 2012 c138.

411. Supraneurals in axial lobe of caudal fin: absent (0); present (1).
Giles et al., 2015a c235.

412. Fringing fulcra: absent (0); present (1).
Friedman, 2007b c188.

413. Epichordal lepidotrichia in caudal fin: absent (0); present (1).
Cloutier and Ahlberg, 1996 c134.

Axial skeleton

414. Synarcual: absent (0); present (1).
Brazeau, 2009 c132; ***Davis et al., 2012*** c135.

415. Series of thoracic supraneurals: absent (0); present (1).
Cloutier and Ahlberg, 1996 c137.

Fin webs

416. Longitudinal scale alignment in fin webs: present (0); absent (1).
Giles et al., 2015a c13.

417. Differentiated lepidotrichia: absent (0); present (1).
Giles et al., 2013 c14.

418. Interlocking lepidotrichial segments: absent (0); present (1).
Friedman, 2007b c187.

Postcranial plates

419. Scute-like ridge scales (basal fulcra): absent (0); present (1).

Patterson, 1982b c19.

420. Longitudinal rows of enlarged keeled scutes: absent (0); present (1).

King et al., 2017 c484.

421. Series of median hexagonal scutes anterior to first dorsal fin: absent (0); present (1).

King et al., 2017 c480.

Scales

422. Body scale growth pattern: monodontode (0); polyodontode (1).

Brazeau, 2009 c8.

423. Body scale growth concentric: absent (0); present (1).

Brazeau, 2009 c9.

424. Postcranial scales with areal or appositional growth crowns: absent (0); present (1).

Burrow et al., 2016 c260.

425. Body scales with peg-and-socket articulation: absent (0); present (1).

Coates, 1999 c3.

426. Peg on rhomboid scale: narrow (0); broad (1).

Patterson, 1982b c5.

427. Anterodorsal process on scale: absent (0); present (1).

Patterson, 1982b c4.

428. Body scale profile: distinct crown and base demarcated by a constriction (neck) (0); flattened (1).

Brazeau, 2009 c11.

429. Profile of scales with constriction between crown and base: neck similar in width to crown (0); neck greatly constricted, resulting in anvil-like shape (1).

Giles et al., 2015c c22.

430. Body scales with bulging base: absent (0); present (1).

Brazeau, 2009 c12.

431. Body scales with flattened base: present (0); absent (1).

Brazeau, 2009 c13.

432. Scales: macromeric (0); micromeric (1).

Friedman and Blom, 2006 c34.

433. Flank scales alignment: vertical rows (0); oblique rows or hexagonal/rhombic packing (1); disorganised (2).

Davis et al., 2012 c14.

434. Basal pore in scales: absent (0); present (1).

Giles et al., 2015c c25.

435. Scales with well developed pores on ganoine surface: absent (0); present (1).

Friedman and Blom, 2006 c35.

Sensory lines, general

436. Sensory line network: preserved as open grooves (0); pass through canals enclosed within dermal bones (1).

Brazeau, 2009 c40.

437. Sensory canals/grooves: contained within the thickness of dermal bones (0); contained in prominent ridges on visceral surface of bone (1).

Giles et al., 2015c c31.

Sensory lines, snout

438. Course of ethmoid commissure: middle portion through median rostral (0); sutural course (1); through bone center of premaxillary (2).

Zhu and Schultze, 2001 c43.

439. Ethmoid commissure fused into midline canal: absent (0); present (1).

King et al., 2017 c320.

440. Infraorbital canal follows premaxillary suture: no (0); yes (1).

Cloutier and Ahlberg, 1996 c100.

441. Anterior supraorbital canal: absent (0); present (1).

Zhu and Gai, 2007 c38; ***King et al., 2017*** c309.

442. Semicircular pit-line: absent (0); present (1).

Jia et al., 2010 c23.

443. Supraorbital sensory canal: absent (0); present (1).

Zhu and Gai, 2007 c39; ***King et al., 2017*** c307.

444. Course of supraorbital canal: between anterior and posterior nostrils (0); anterior to both nostrils (1).

Cloutier and Ahlberg, 1996 c98.

445. Contact of supraorbital and infraorbital canals: in contact rostrally (0); not in contact rostrally (1).

Zhu et al., 2001 c34.

446. Contact between otic and supraorbital canals: not in contact (0); in contact (1).

Cloutier and Ahlberg, 1996 c102.

447. Branching sensory canal system at posterior of supraorbital canals: absent (0); present (1).

King et al., 2017 c306.

448. Posterior end of supraorbital canal: close to posterior and middle pit-lines (0); anterior to posterior and middle pit-lines (1); extends posterior to middle and posterior pit-lines (2).

King et al., 2017 c292.

449. Anterior pit-line of dermal skull roof: absent (0); present (1).

Giles et al., 2015a c34.

450. Position of anterior pit-line: on paired median skull roofing bones over the otico-occipital division of braincase (0); on paired median skull roofing bones over the sphenoid division of braincase (1).

Cloutier and Ahlberg, 1996 c103.

451. Course of supraorbital canal: straight (0); lyre-shaped (1).

Zhu et al., 2013 c184.

452. Median dorsal canal: absent (0); present (1).

Zhu and Gai, 2007 c43; ***King et al., 2017*** c310.

Sensory lines, skull roof posterior

453. Infra-orbital sensory line: crosses lateral field (0); does not cross lateral field (1).

Sansom, 2009 c31.

454. Festooned pattern of sensory canals: absent (0); present (1).

Zhu and Gai, 2007 c2.

455. Branching of lateral transverse canal: absent (0); present (1).

Zhu and Gai, 2007 c39.

456. Supraorbital canals and posterior pitlines cross as an X: no (0); yes (1).

Long et al., 2015 c256; ***King et al., 2017*** c300.

457. Otic canal: runs through skull roof (0); follows edge of skull roof (1).

Ahlberg and Johanson, 1998b c66.

458. Extension of otic canal beyond infraorbital canal ('P' canal): absent (0); present (1).

King et al., 2017 c319.

459. Otic canal extends through postparietals: absent (0); present (1).
Cloutier and Ahlberg, 1996 c101.

460. Otic canal runs along mesial margin of marginal plate: absent (0); present (1).
Dupret et al., 2009 c16.

461. Central sensory lines: absent (0); present (1).
Dupret et al., 2009 c31.

462. Junction of posterior pitline and main lateral line: far in front of posterior margin of skull roof (0); close to posterior margin of skull roof (1).
Zhu et al., 2013 c166.

463. Middle and posterior pit-lines on postparietal: posteriorly situated (0); mesially situated (1).
Zhu et al., 2001 c39.

464. Position of middle and posterior pit-lines: close to midline (0); near the central portion of each postparietal (1).
Zhu et al., 2006 c41.

465. Posterior pitline and postmarginal canal: staggered (0); confluent (1).
King et al., 2017 c321.

466. Postmarginal canal: absent (0); present (1).
King et al., 2017 c315.

467. Sensory line commissure across extrascapular bones: absent (0); present (1).
King et al., 2017 c323.

Sensory lines, cheek

468. Preopercular canal: absent (0); present (1).
King et al., 2017 c316.

469. Preopercular canal meets main canal: no (0); yes (1).
King et al., 2017 c317.

470. Horizontal sensory canal: absent (0); present (1).
King et al., 2017 c314.

471. Jugal portion of infraorbital canal joins supramaxillary canal: present (0); absent (1).
Davis et al., 2012 c17.

472. Supraoral canal: absent (0); present (1).
King et al., 2017 c318.

473. Sensory canal or pit-line associated with maxilla: absent (0); present (1).

Friedman, 2007b c152.

Sensory lines, jaw

474. Course of mandibular canal: not passing through most posterior infradentary (0); passing through most posterior infradentary (1).

Cloutier and Ahlberg, 1996 c111.

475. Course of mandibular canal: passing through dentary (0); not passing through dentary (1).

Patterson, 1982a c7.

Sensory lines, postcranial

476. Dorsal branch of main lateral line canal on PDL: absent (0); present (1).

King et al., 2017 c325.

477. Sharp downward bend on PDL plate sensory line: absent (0); present (1).

King et al., 2017 c326.

478. Sensory line canal: passes between or beneath scales (0); passes over scales and/or is partially enclosed or surrounded by scales (1); perforates and passes through scales (2).

Friedman and Brazeau, 2010 c26; ***Davis et al., 2012*** c15.

Visceral skeleton

479. Foramen in hyomandibular: absent (0); present (1).

Friedman, 2007b c163.

480. Endoskeletal hyoid rays: absent (0); present (1).

King et al., 2017 c150.

481. Anteriormost unpaired element of branchial skeleton contacted by: one branchial arch only (0); two or more branchial arches (1).

Dearden et al., 2019 c73.

482. Multiple unpaired branchial mineralizations: absent (0); present (1).

Dearden et al., 2019 c74.

483. Interhyal: absent (0); present (1).

Davis et al., 2012 c38.

484. Hypohyal: absent (0); present (1).

Giles et al., 2015c c75.

485. Endoskeletal urohyal: absent (0); present (1).

Friedman, 2007b c164.

486. Gill skeleton extends posteriorly beyond occiput: absent (0); present (1).

Dearden et al., 2019 c67.

487. Sublingual rod: absent (0); present (1).

King et al., 2017 c149.

488. Disposition of the interbranchial ridges of the oralobranchial chamber roof: oligobranchiate (0); orthobranchiate (1); nectaspidiform (2).

Sansom, 2009 c62.

489. Number of branchial fossae: 5–7 (0); 9–17 (1); more than 20 (2).

Zhu and Gai, 2007 c49.

Homology-variable characters

The following characters have variable homology and the data matrix presents two options for their codings in placoderms. Both the marginal jaw bones (characters 490–498) and the palatal bones (characters 599–507) have the same set of dependent characters. Characters regarding the external, facial part of the maxilla and premaxilla are dependent on the presence of a facial lamina, which is absent in placoderms. These characters therefore are coded as inapplicable in placoderms regardless of homology, and do not need to be included in the homology-variable characters.

490. Premaxilla: absent (0); present (1).

New.

491. Maxilla: absent (0); present (1).

Cloutier and Ahlberg, 1996 c19.

492. Facial laminae on (pre)maxilla: absent (0); present (1).

New.

493. Palatal laminae on (pre)maxilla: absent (0); present (1).

New.

494. Premaxilla fused in midline: absent (0); present (1).

King et al., 2017 c372.

495. Pipe-like ridges on (pre)maxilla: absent (0); present (1).

King et al., 2017 c373.

496. Premaxilla posterior process: absent (0); present (1).

New.

497. Fangs on premaxilla palatal lamina: absent (0); present (1).

New.

498. Maxilla fragmented into multiple bones: absent (0); present (1).
New.

499. Vomers: absent (0); present (1).
New.

500. Dermopalatine: absent (0); present (1).
New.

501. Facial laminae on vomer/dermopalatines: absent (0); present (1).
New.

502. Palatal laminae on vomer/dermopalatines: absent (0); present (1).
New

503. Vomers fused in midline: absent (0); present (1).
King et al., 2017 c372.

504. Pipe-like ridges on vomer/dermopalatines: absent (0); present (1).
King et al., 2017 c373.

505. Vomer posterior process: absent (0); present (1).
Lu et al., 2012 c89; ***Carr and Hlavin, 2010*** c68; ***King et al., 2017*** c375.

506. Fangs on vomer palatal lamina: absent (0); present (1).
Adapted from ***Ahlberg and Johanson, 1998b*** c24.

507. Dermopalatine fragmented into multiple bones: absent (0); present (1).
Lu et al., 2012 c106; ***King et al., 2017*** c378.